nature COMMUNICATIONS

ARTICLE

Received 19 Dec 2016 | Accepted 10 May 2017 | Published 23 Jun 2017

DOI: 10.1038/ncomms15892 OPEN

Single-virus genomics reveals hidden cosmopolitan and abundant viruses

Francisco Martinez-Hernandez[1], Oscar Fornas[2,3], Monica Lluesma Gomez[1], Benjamin Bolduc[4], Maria Jose de la Cruz Peña[1], Joaquín Martínez Martínez[5], Josefa Anton[1], Josep M. Gasol[6], Riccardo Rosselli[7], Francisco Rodriguez-Valera[7], Matthew B. Sullivan[4,8], Silvia G. Acinas[6] & Manuel Martinez-Garcia[1]

Microbes drive ecosystems under constraints imposed by viruses. However, a lack of virus genome information hinders our ability to answer fundamental, biological questions concerning microbial communities. Here we apply single-virus genomics (SVGs) to assess whether portions of marine viral communities are missed by current techniques. The majority of the here-identified 44 viral single-amplified genomes (vSAGs) are more abundant in global ocean virome data sets than published metagenome-assembled viral genomes or isolates. This indicates that vSAGs likely best represent the dsDNA viral populations dominating the oceans. Species-specific recruitment patterns and virome simulation data suggest that vSAGs are highly microdiverse and that microdiversity hinders the metagenomic assembly, which could explain why their genomes have not been identified before. Altogether, SVGs enable the discovery of some of the likely most abundant and ecologically relevant marine viral species, such as vSAG 37-F6, which were overlooked by other methodologies.

[1] Department of Physiology, Genetics, and Microbiology, University of Alicante, Carretera San Vicente del Raspeig, San Vicente del Raspeig, Alicante 03690, Spain. [2] Centre for Genomic Regulation (CRG), The Barcelona Institute for Science and Technology (BIST), Carrer del Doctor Aiguader, 88, PRBB Building, Barcelona 08003, Spain. [3] Universitat Pompeu Fabra (UPF), Carrer del Doctor Aiguader, 88, PRBB Building, Barcelona 08003, Spain. [4] Department of Microbiology, The Ohio State University, 105 Biological Sciences Building, 484 West 12th Avenue Columbus, Ohio 43210, USA. [5] Bigelow Laboratory for Ocean Sciences, 60 Bigelow Drive, PO Box 380, East Boothbay, Maine 04544, USA. [6] Department of Marine Biology and Oceanography, Institut de Ciències del Mar (ICM), CSIC, Passeig Marítim, 47, Barcelona 08003, Spain. [7] Evolutionary Genomics Group, Departamento de Producción Vegetal y Microbiología, Universidad Miguel Hernández, Campus San Juan, San Juan, Alicante 03550, Spain. [8] Department of Civil, Environmental and Geodetic Engineering, The Ohio State University, The Ohio State University, 105 Biological Sciences Building, 484 West 12th Avenue Columbus, Ohio 43210, USA. Correspondence and requests for materials should be addressed to M.M.-G. (email: m.martinez@ua.es).

Viruses are the most abundant biological entities on Earth and a major reservoir of genetic diversity[1] that hide an enormous complexity across all habitats[2–5]. Despite the role of viruses in shaping microbial ecosystems[1,4–6], global diversity patterns of viral communities[3,4] are only beginning to be elucidated for certain environments[2,3,5,7,8]. Culture-based methods inefficiently capture naturally occurring viral diversity[1]. As a consequence of the inability to cultivate the majority of microbial hosts, most bacterial and archaeal phyla lack known viruses[4,9]. In turn, culture-independent approaches have provided a wealth of genetic information on environmental viral communities. Metagenomic studies have delivered thousands of viral genomes and large genome fragments. For instance, metagenomic strategies based on capturing viral genomes in fosmids have broaden our knowledge on abundant and widespread viruses in surface waters[10] and in the deep Mediterranean Sea[11]. Broader metagenomic surveys in the context of the *Tara* Oceans expeditions have unveiled ocean viral community patterns at a global scale[3] and provided a map of abundant, double-stranded DNA viruses with a total of 15,222 epipelagic and mesopelagic viral populations, comprising 867 major viral clusters, each corresponding to approximately genus-level groupings[2]. Such studies emphasize the large disparity with cultivation efforts, as $<1\%$ of the observed viral populations are represented in culture[2,3,10,11]. However, even with these greatly augmented reference databases, available reference genomes—cultivated and uncultivated—fail to recruit most ($>80\%$) viral metagenomic reads[2]. Thus, there is an agreement that much viral diversity remains to be discovered in the oceans.

Over the last years, single-cell genomics (SCGs) has enabled sequencing of individual genomes of many abundant and ecologically important prokaryotes in marine and other environments[12–16] by disentangling the genetic complexity of the community to the minimum level, the cell. This powerful approach has opened up new frontiers that overcome some of the metagenomic assembly limitations and culture biases. SCGs also provides the means for a better understanding of the biology, ecology and evolution of microbial communities[14,15]. Currently, a major bottleneck in metagenomics is the reconstruction of genomes from closely related strains. Furthermore, metagenomic assembly 'obscures' the population microdiversity by delivering consensus genome contigs that hide the extant genetic heterogeneity. In many cases such information is crucial for a comprehensive understanding of virus–host interactions and dynamics[17]. Although metagenomics binning of assembled contigs into species clusters has been a major advancement in metagenomics[18], binning at the strain level remains a technical challenge. Albeit not exempt of biases[16], SCGs simplifies the complexity of the puzzle, by assembling individual genomes, one at a time, and therefore captures the natural genetic variability[15]. The feasibility of adapting SCGs methodology to virology has been demonstrated by two previous studies[19,20], yet neither addressed the issue at the level of single viruses in natural viral assemblages. One study sorted and sequenced individual viral particles from a bacteriophage culture of lambda and T4 of *Escherichia coli*[19], and the second study employed fluorescence-activated virus sorting (FAVS) and whole-genome amplification (WGA) to recover the genetic information of a pool of 5,000 sorted uncultured viruses from a marine sample[20]. Oceans have been extensively studied by viral metagenomics and culturing, and thus represent a model scenario to test whether portions of marine viral communities are missed by these techniques. We hypothesize that high intra-population viral diversity could lead to ambiguous sequence metagenomic reconstruction and/or hinder the genome assembly of abundant uncultured viruses.

Here we employ single-virus genomics (SVGs) to natural marine viral assemblages from the Mediterranean Sea (epi- and mesopelagic) and the deep Atlantic Ocean, and demonstrate the power of this approach to uncover the genomics of some of the most abundant marine viruses.

Results

SVGs of marine viruses. First, using FAVS in combination with confocal fluorescence microscopy, we demonstrated the suitability of the used flow cytometer sorter to separate individual viral particles from a culture isolate (Supplementary Fig. 1 and Supplementary Notes 1 and 2). Subsequently, a total of 2,234 virus-like particles were sorted by FAVS from environmental seawater samples collected from the Atlantic Ocean during the Malaspina expedition (bathypelagic, 4,000 m depth) and from the Mediterranean Sea (surface and deep chlorophyll maximum, 60 m depth) (Table 1; Supplementary Figs 2–4). WGA of the sorted single viral particles yielded a total of 392 marine viral single-amplified genomes (vSAGs) (Table 1; Supplementary Fig. 4 and Supplementary Note 1). Forty-four of these vSAGs were selected at random for Illumina sequencing (Table 1; Supplementary Table 1 and Supplementary Figs 5 and 6). For most vSAGs (32 out of 44), a single large genome contig was obtained (from $\approx$10–78 kb, mean $\approx$20 kb, Supplementary Table 1 and Supplementary Note 3). Genome annotation[21] and protein-sharing network[2] analysis confirmed that vSAGs (Fig. 1) were viruses and no other types of biological particles, such as marine vesicles or gene transfer agents[22]. Most of the vSAGs ($n=22$) were tentatively assigned to the Caudovirales (Fig. 1; Supplementary Table 2 and Supplementary Note 3) representing putative novel viral species ($n=37$), and genera ($n=7$) from cosmopolitan oceanic virus clusters (VCs)[2] (Fig. 1; Supplementary Fig. 7 and Supplementary Tables 2–4). Compared to viral genome fragments assembled from the recent Global Oceanic Virome (GOV) metagenomics data set[2], our 37 vSAGs representing putative new viral species were at the 'core' of VCs in the global marine viral network (Fig. 1; Supplementary Fig. 7 and Supplementary Tables 2–4). The centrality of vSAGs within VCs indicated higher frequency of shared proteins with other uncultured viruses ($\sim$11 shared proteins per vSAGs with $\sim$60% of amino-acid identity). However, the remaining seven

Table 1 | Summary of marine samples and viral single-amplified genomes (vSAGs).

Sample	Treatment*	No. of sorted single viruses	No. of vSAGs	No. of sequenced vSAGs
Mediterranean Sea (Barcelona Beach)	A	332	63	8
Mediterranean Sea (Blanes Bay Microbial Observatory)	B	664	149	21
	C	332	41	11
Mediterranean Sea (DCM)	B	332	76	1
North Atlantic Ocean	E	664	63	3
Total		2,324	392	44

*Treatments: A, fixed sample + liquid N_2 and KOH (pH 14) shock; B, unfixed sample + liquid N_2 and KOH (pH 14) shock; C, unfixed sample + KOH (pH 14) shock; E, cryopreserved in GlyTE + treatment.

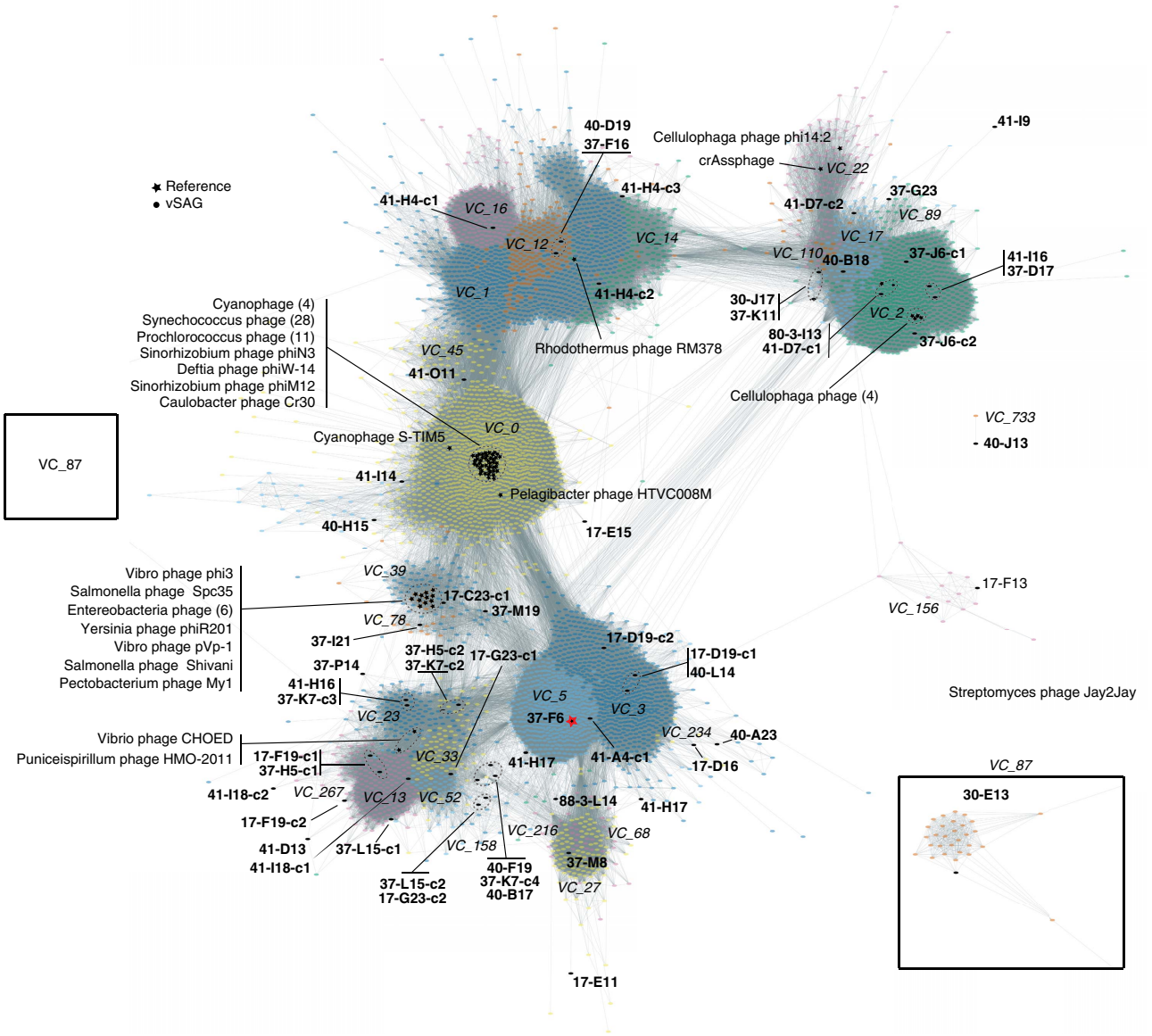

Figure 1 | Global viral protein-sharing network. A total of 5,539 partial and full-length genomes, and 634,497 relationships (edges) from GOV[2], environmental phage from Genbank, archaeal and bacterial viral references (indicated by a black star, *), and vSAGs (this study, indicated by a black dot •, bold font) were included in the analyses. Only viral clusters—with each viral cluster indicated by unique colours—including ≥1 vSAG sequences are represented. Edges between nodes indicate a statistically significant weighted pairwise similarity between the protein profiles of each node (see Methods) with similarity scores ≥1. Viral clusters (italic font) are determined by applying the Markov Cluster Algorithm (MCL) to the edges[2]. vSAG 37-F6 is indicated by a red star.

vSAGs (Supplementary Table 4), such as the autochthonous virus 88-3-L14 from the unexplored massive bathypelagic Atlantic Ocean biome (4,000 m depth) (Fig. 1; Supplementary Figs 7 and 8), had weaker connections within the viral network and were placed on the periphery of VCs, (Supplementary Fig. 7); consequently, they could represent novel genera. Only the surface vSAGs 41-O11, 37-K7 and 37-L15 were distantly related to known phage isolates (cyanophages and Pelagibacter phages; genome average nucleotide identity (gANI) <50%; Supplementary Fig. 9).

Global abundance of single viruses. To assess the global abundance of our vSAGs relative to other approaches (viral metagenomics or viromics and culturing), we analysed fragment recruitment based abundances in viromic[2,3,10,23,24] and microbial metagenomic[25] data sets. For virome recruitment, ≥95% and ≥70% nucleotide identity thresholds were used to target reads from viruses identical to or within the same species[10] than our vSAGs and from the same genus or subfamily viral taxa, respectively[2] (Supplementary Fig. 10; Supplementary Notes 4 and 5). Overall, comparative recruitment of viral genomes obtained by different approaches against available viromes indicated that in all cases but one (Northwest Arabian Sea upwelling virome) the recruitment mean was higher (ANOVA P value <0.001) for our vSAGs followed by other methods as follows: SVGs > virus cloned in fosmids[10] > viruses from single bacterial cells[26] > virome contigs[2,3] (*Tara* Oceans Viromes (TOV)) > virus isolates (Fig. 2; Supplementary Figs 11–13 and Supplementary Note 4). Furthermore, this analysis indicated that our surface vSAGs were highly abundant both at the sampling sites as

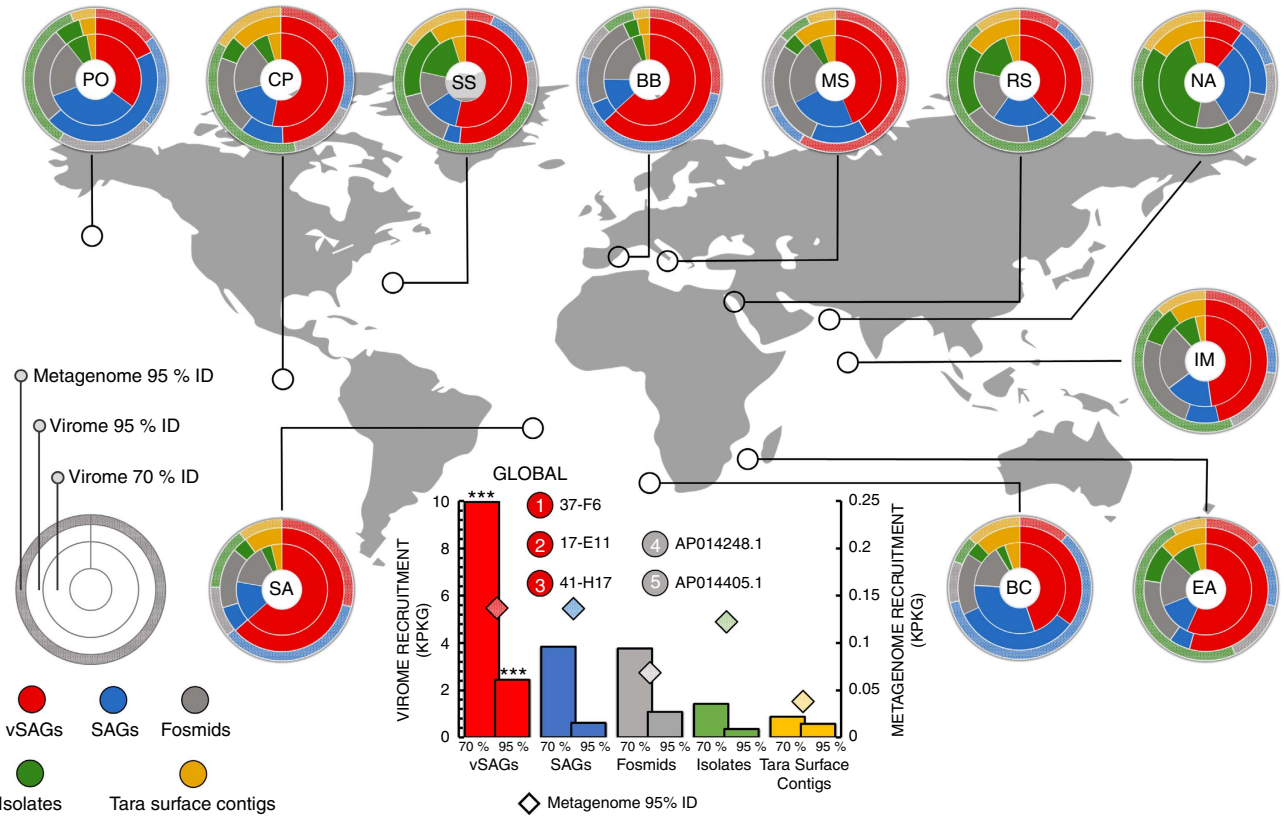

Figure 2 | Relative abundance and distribution of surface marine viruses. Virome and microbiome metagenomic fragment recruitments of marine viruses in each ocean. Rings represent the relative microbiome and virome recruitment frequency for each genomic data set, corresponding to the relative abundance of viral populations. External ring is for the microbiome recruit by using ≥95% nucleotide identity threshold (species level). Inner and medium rings depict the virome recruitment at two different nucleotide identity cut-offs, ≥70% and ≥95%, corresponding to the genus and species levels, respectively (Supplementary Fig. 10 and Supplementary Notes 4 and 5). Viral genomic data sets used were: 40 surface vSAGs (this study), 179 reference virus isolates (Supplementary Table 9), 1,148 viral fosmids[10], 20 viral genomes from uncultured prokaryotic single cells[26] and 3,018 surface viral contigs from the *Tara* expedition[3]. For this calculation: (1) normalized recruitment as the total recruited nucleotides (kb) per kb of viral genome per Gb of virome (KPKG) was estimated for each virus genome, (2) mean normalized recruitment was calculated for each virus genomic data set (see also Supplementary Fig. 11) and (3) mean was normalized by the sum of means from all virus genomic data set expressed as relative recruitment. Statistically significant differences between the recruitment frequency average of the vSAGs versus the rest of viral groups are indicated (***; ANOVA *P* value <0.001). Viromes and microbiomes from previous surveys[3,23–25] used here are abbreviated as: Pacific Ocean (PO), Chile-Peru oceanic region (CP), South Atlantic (SS), Red Sea (RS), Mediterranean Sea (MS), Northwest Arabian Sea upwelling (NA), Indian Monsoon gyre province (IM), Eastern Africa Coastal Province (EA), Benguela Current (BC) and Sargasso Sea (SS). The microbiome and virome from Blanes Bay Microbial Observatory (BB), where surface vSAGs were obtained, was constructed in this study. Global oceanic viromics and microbiome fragment recruitments for each virus genomic data set is represented in the centre of the picture, circles represent overall oceanic top-5 ranking of most abundant viruses at the species level (≥95% of identity).

well as throughout many different surface oceanic regions (Fig. 2; Supplementary Figs 11, 13 and 14; Supplementary Table 5 and Supplementary Note 4). Furthermore, the recovered vSAGs showed the highest relative microbiome recruitment frequency against the *Tara* Oceans microbiome data sets (Fig. 2). Microbiomes are known to contain significant amounts of viral DNA derived from cells undergoing the lytic cycle, and this has been commonly used to determine abundances and diversity of marine viruses in cellular metagenomic libraries[10]. Though it might also be possible that some free virus particles had been retained onto the filters, our microbiome recruitment suggest that those viruses may have been actively infecting the marine bacterioplankton (0.2–3 μm size).

The quantitative analysis of the vSAGs abundance indicated that the virus vSAG 37-F6 along with 17-E11 (distantly related to virus 37-F6; ≈60% gANI) and 41-H17 were more abundant, at the species level, in the global marine surface viriosphere than any extant dsDNA virus in public data sets (Figs 2 and 3; Supplementary Fig. 15), including novel uncultured viruses recently described within cosmopolitan VCs from the GOV data set[2]. For the remaining marine virome data sets, the most abundant viruses for each category were the viruses AAA164-I21 and AAA160-P02, found in two uncultured sorted single cells belonging to Verrucomicrobia and Flavobacteria[26], respectively, a putative cyanophage cloned in the fosmid AP014248.1 (ref. 10), the Pelagibacter phage strain HTVC010P (ref. 27) and the *Tara* contig 34DCM_32712 (ref. 3) (Fig. 3; Supplementary Fig. 15). Estimated abundance of RNA and ssDNA viruses[28] was not considered in this study. In the deep ocean, the vSAG 88-3-L14 from the Atlantic Ocean (4,000 m) representing a potentially novel genus was also fairly cosmopolitan and abundant across distant bathypelagic habitats (Supplementary Fig. 16), with no viral relatives in public databases (Fig. 1; Supplementary Tables 2 and 4).

vSAG 37-F6 is the putative most abundant marine virus. The biogeographic analyses of the vSAG 37-F6 indicated that, at the genus and species level, it was highly abundant in several oceanic regions, such as the Atlantic and Indian oceans; even more

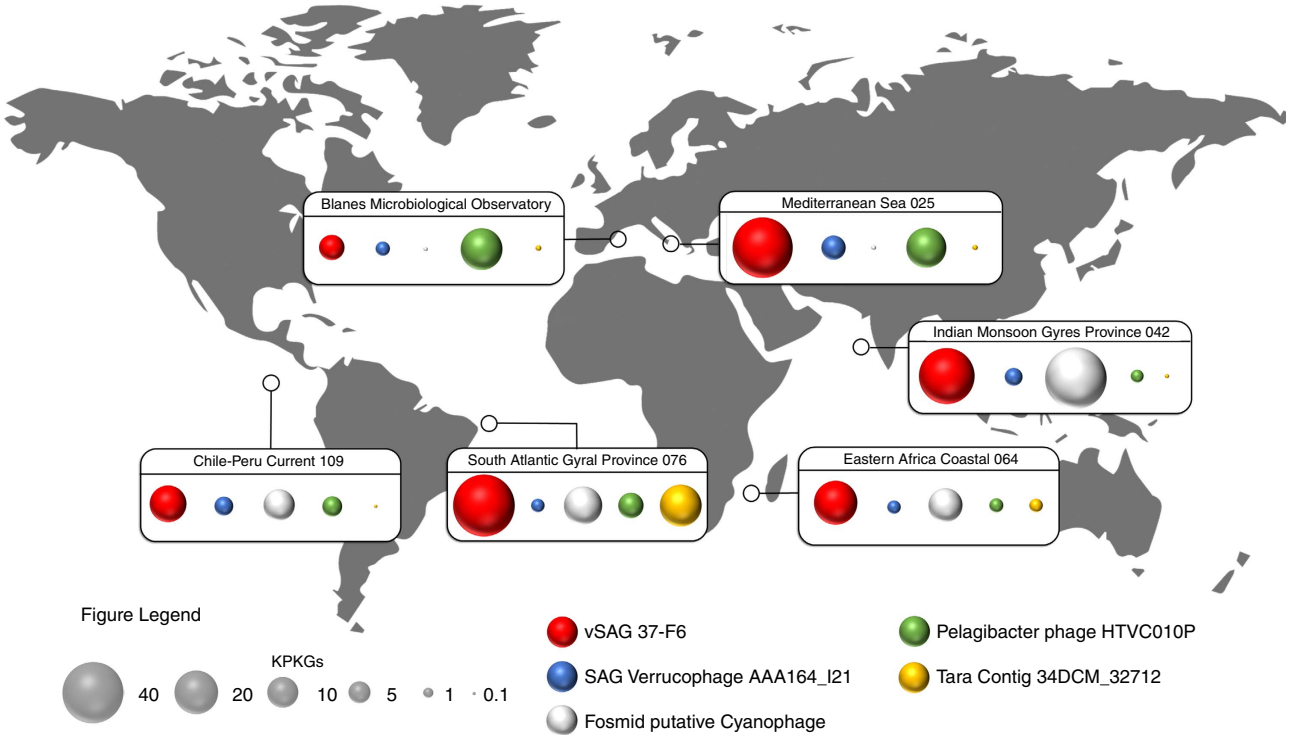

Figure 3 | Biogeography of most abundant marine viruses. The abundance of the most abundant surface dsDNA viruses for each virus genome data set according to the procedure for genome recovering (single-virus genomics (red), viruses from single bacterial cells[26] (blue), virus cloned in fosmids[10] (grey), virus isolates (green) and viromics from *Tara* Oceans data set (yellow)[2,3]. Fragment recruitment data were used to estimate the overall abundance for each region. Bubbles represent the fragment recruitment estimation expressed in KPKG (as in Fig. 2).

abundant than at the sampling point (Blanes Bay Microbial Observatory; Mediterranean Sea) (Figs 2 and 3; Supplementary Fig. 15). When comparing to well-known predominant viral species isolates, such as the Pelagibacter phage HTVC010P28, the vSAG 37-F6 was the most abundant virus in 20 of the 24 metaviromes analysed (Fig. 3; Supplementary Fig. 15). A detailed genomic comparison of the vSAG 37-F6 revealed that it was not genetically similar to any known virus isolates (Fig. 4; Supplementary Figs 10a and 14). Only three uncultured viruses showed genome synteny and relatively low genetic relatedness (<63% nucleotide identity) against vSAG 37-F6: the above-mentioned verrucophage (AAA164-I21) and flavophage (AAA160-P02) from single cells[26,29], and a third virus cloned in a fosmid from a deep Mediterranean Sea water sample (3,000 m depth)[11] (Fig. 4; Supplementary Fig. 17 and Supplementary Table 6). Finding a distant vSAG 37-F6 viral relative at such depths (Fig. 4b) along with a significant fragment recruitment of that virus in the deep ocean virome data sets[11] (Supplementary Fig. 15) suggests that 37-F6-like viruses likely populate the deep ocean as well. We were not able to identify the putative host for the virus 37-F6 based on *in silico* host prediction by using *k-mer* analysis[30], identification of CRISPR host spacers[2], or tRNA signatures (Supplementary Fig. 17).

Mining viral signals of vSAGs in proteomic data. Recently, the most abundant viral marine proteins detected by proteomics in different oceans were identified as capsid proteins of predominantly unknown marine viruses of the cluster CAM_CRCL_773 (ref. 31). The capsid protein encoded by gene 9 of vSAGs 37-F6 was homologous to these unknown abundant capsid proteins (Fig. 5a). The closest capsid protein was that of the phage AAA160-P02 (86% amino-acid identity) recovered in a flavobacterium single cell (Fig. 5b). The predicted three-dimensional (3D) structure of vSAG 37-F6′s gene 9 was nearly identical to the 3D model previously proposed for the capsid proteins of the cluster CAM_CRCL_773 (Fig. 5b)[31].

Furthermore, when comparing the predicted peptide sequences ($n=4{,}871$) obtained by mass spectrometry (MS) from the South Atlantic and Indian Oceans and the Mediterranean Sea viral proteomes[31] against the *in silico* digested capsid protein sequences of virus 37-F6, over 200 peptides from all oceanic regions were a perfect match (100% identity) (Figs 4a and 5). When the comparison of peptide sequences from MS data was extended to the whole viral genome data sets, results showed that predicted capsid proteins of vSAGs accumulated a high number of recruited peptides (Fig. 5; Supplementary Fig. 18). In particular, the capsid proteins of vSAG 37-F6 along with 41-A4, and phage AAA160-P02 showed the highest rate of proteomic recruitment in the *Tara* viral proteome data set. In addition, these capsid proteins of vSAGs were also abundant in a bacterioplankton proteome from the Oregon Coast (Supplementary Fig. 19; Supplementary Table 7). Thus, metagenomic and proteomic data point to the ubiquity and high abundance of some of the uncultured viral species recovered by SVGs.

Microdiversity affects metagenomic assembly. To explain why our discovered abundant viruses have been overlooked by metagenomic assembly[2,3,23], we take advantage of an intriguing empirical observation from the species/genus-specific recruitment pattern of viral populations (hereafter as diversity curve) obtained in the different viromes. In our study, the abundant surface vSAGs populations showed high accumulated microdiversity in the diversity curves against the viromes from the corresponding sampling sites (Fig. 6a; Supplementary Fig. 14 and Supplementary

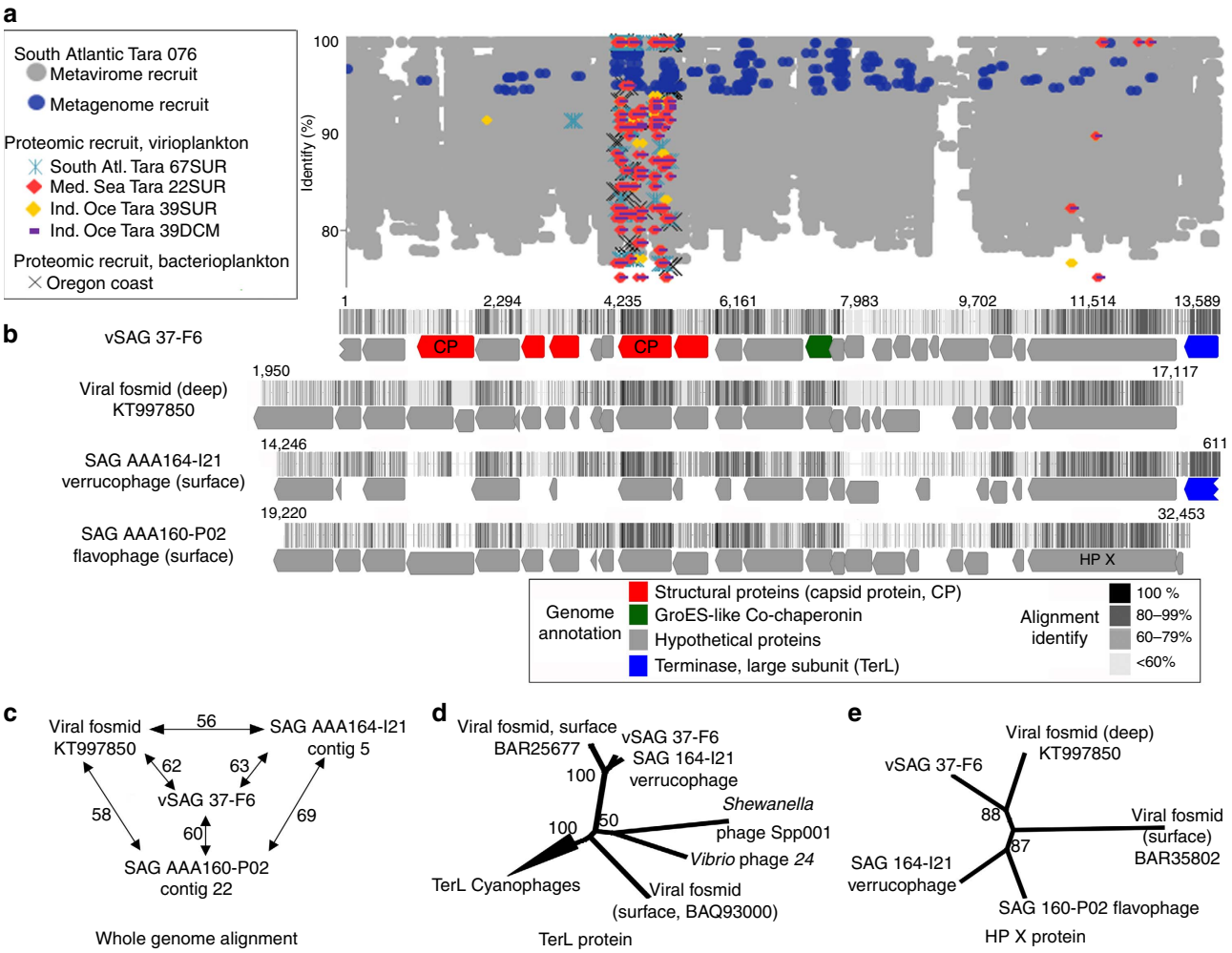

Figure 4 | Ecogenomics of the putative most abundant surface marine virus, the vSAG 37-F6. (**a**) Virome, microbial metagenome and proteome fragment recruitment in different data sets[3,31,62]. A hypervariable genomic island in virus 37-F6 was detected between genomic position 9,000 and 9,700 (unknown protein). (**b**) Genome annotation, synteny and whole-genome alignment of vSAG 37-F6 with closest viral relatives[26,29]. Colour in the alignment (from black to white) denotes identity values among all four genomes for each genome position. (**c**) Whole-genome similarity with closest viral relatives. (**d**,**e**) Phylogeny of large subunit of viral terminases (TerL) and the large conserved hypothetical protein X (HP X) based on maximum-likelihood method. Bootstrap values are indicated in nodes.

Note 5). However, in comparison to viromics for those abundant viral population from *Tara* data set[3], a contrasting population structure lacking microdiversity was observed (Fig. 6a). Furthermore, the frequency of single-nucleotide polymorphisms (SNPs) in the vSAG 37-F6 species population was ~10 to 250-fold higher, depending on the geographical origin of the sample, than in the most abundant viruses recovered by viromics[2,3] (Fig. 6b). Therefore, we hypothesized that population microdiversity would hinder genome reconstruction by metagenomic assembly, which may explain why metagenomics have so far failed to recover some very abundant marine viruses, as is the case for those identified in this study employing SVGs. We tested this hypothesis by creating simulated viromics data sets with variable levels of microdiversity (Supplementary Fig. 20) that we then analysed following standard metagenomics assembly tools. We simulated three different scenarios and introduced viral populations of the vSAG 37-F6 with different degrees of microdiversity (no diversity, low/medium and high) within natural *Tara* viromes from the Mediterranean Sea (for details, see Methods, Supplementary Fig. 20 and Supplementary Note 5). Our results showed that common metagenomic assembly strategies delivered complete reference viral genomes from simulated data sets in the absence of population microdiversity, or when it was very low (Fig. 6c; Supplementary Fig. 20 and Supplementary Note 5).

Discussion

Detection of viral particles by flow cytometry is highly dependent on optimum fluorescence staining of the viral nucleic acids as well as on the equipment sensitivity, since scattered light and fluorescence signals are close to the detection limit of the instrument. Sorting of single viruses at very low flow rate was critical to prevent coincident events of multiple viral particles. In our case, the estimated ratio of putative sorted particle versus generated drops (see Methods for details) ensured sufficient separation between each sorted particle to prevent sorting of doublets (two viruses in the same droplet), which could later obscure the interpretation of SVGs data. The standard protocol commonly used for staining and detecting viruses by flow cytometry employs high concentration of a fixative agent (0.5% glutaraldehyde)[32], which ultimately would prevent the amplification of genetic material. Here the standard procedures for staining viruses were adapted and optimized without

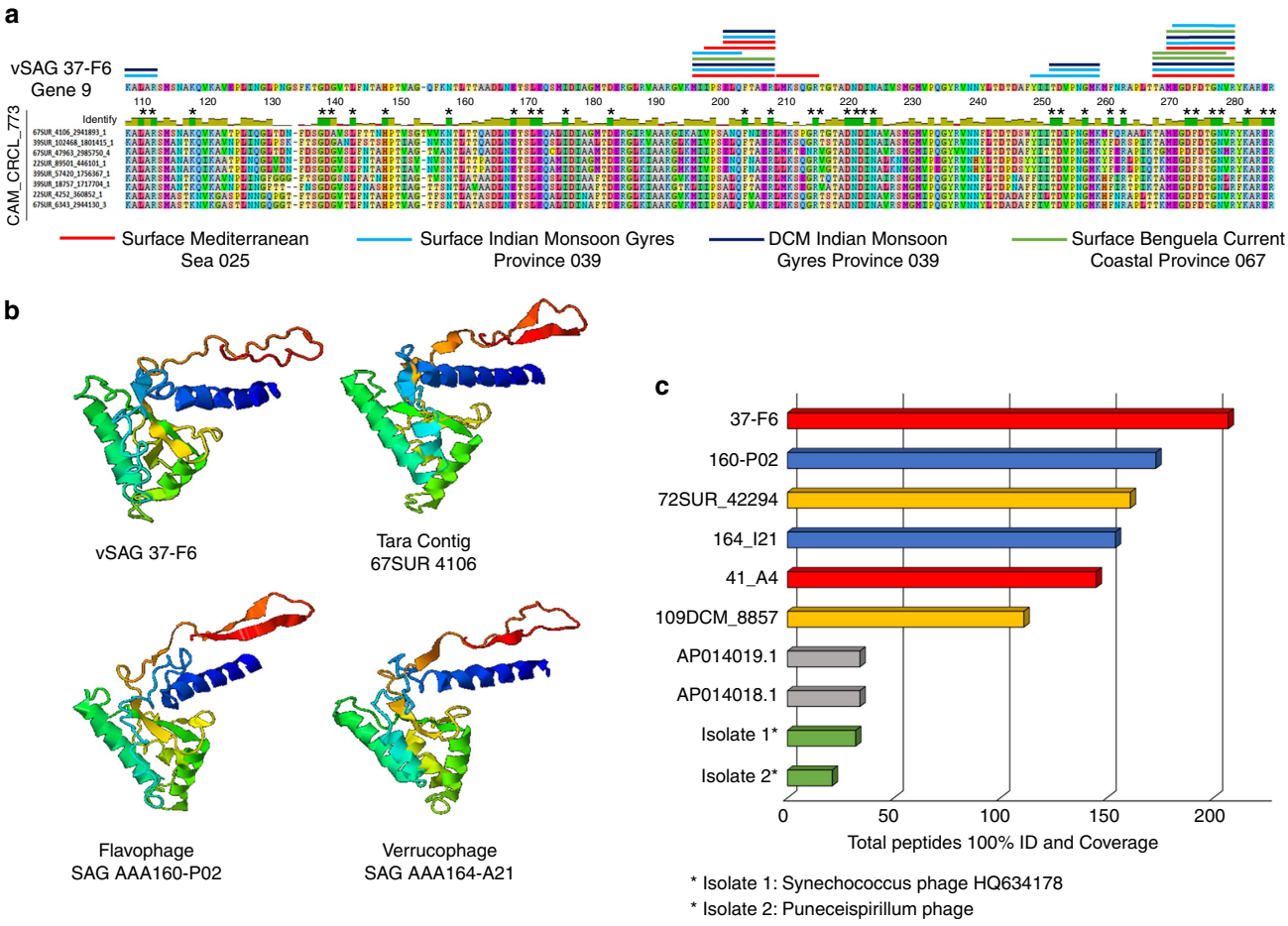

Figure 5 | Capsid protein of vSAG 37-F6 and abundance in proteomic *Tara* viral data set. (**a**) Peptide alignment of vSAG 37-F6 with the capsid proteins of cluster CAM_CRCL_773. For convenience, we only show eight protein sequences out of 152 total capsid proteins. Coloured lines above amino-acid sequence of vSAG 37F6 represent the perfect matches of predicted peptide sequences from *Tara* expedition[31] (100% identity similarity and query coverage). Colour denotes the origin of peptides. Conserved amino-acid positions in the protein alignment are denoted with '*' (**b**) Representative 3D-structural model, using I-TASSER prediction server, of the 37-F6 capsid protein compared with the nearest viral capsid proteins: the *Tara* Contig 67SUR_4106 and viruses from SAGs AAA160-P02 (*Flavobacteria*) and AAA164-I21 (*Verrucomicrobia*). (**c**) Number of total recruited peptides from *Tara* expedition[31] (100% identity and query coverage) for the top two most recruiting viruses from each viral genomic data set[3,10,26].

apparently missing major viral populations (Supplementary Fig. 2). During FAVS, as with SCGs[29], viral stained particles are sorted at random, which means that the more abundant a virus is within a sample, the higher its probability to be sorted. Thus, the uncultured viruses sorted in this study, represent a random subset of, likely, the most abundant dsDNA virus members within natural viral assemblages. Extraction of viral DNA from the capsids of single-sorted viruses without degrading genetic material is critical for the success of WGA. As with SCGs, the proper breakdown of the capsid is paramount to guarantee the success in downstream analyses. A combination of KOH buffer and liquid nitrogen shock proved to be efficient for lysing the viral capsids from marine samples (Supplementary Fig. 4). Although our protocol is promising for a wide range of capsid types, further experiments will need to be conducted to assess the general feasibility of the method. We are aware of the possibility that sub-optimal lysis of some virus groups (either degrading or not releasing the nucleic acids) might have led to underrepresentation of certain virus groups.

Metagenomic fragment recruitment has been widely used to assess the abundance of marine viruses[3,10,11,27] and several programs are available to perform fragment recruitment, such as BLAST[10,11,27] or Bowtie[3]. Here we tested the impact of different recruitment algorithms on our results, and in particular, the reciprocal best-hit approach (each query read assigned only to one viral genome by best-hit score). Our results (Supplementary Fig. 21) indicated no significant differences among the different recruitment strategies. Thus, our data confirmed the overwhelming high relative recruitment rate of our vSAGs and suggest that several of the viruses reported here, in particular vSAG 37-F6, are putatively the most widely distributed, abundant, and likely active virus at the genus- and species-level taxa identified so far in the surface viriosphere (Figs 2 and 3; Supplementary Figs 11–19).

Application of viral taxonomy criteria, such as demarcation of viral genera or species, to uncultured viruses is controversial. The International Committee of Taxonomy of Virus has recently stated[33] that taxonomy is moving to genome-based criteria in the era of metagenomics, but these criteria are currently under debate[2,34,35]. We aimed at targeting and recruiting uncultured viral populations at the species (very closely related) and genus (or subfamily) taxonomic levels by carrying out virome recruitment at 95% (refs 2,10) and 70% cut-off levels, respectively. In our study, nearly all obtained single viruses represented potentially new viral species, and in some cases likely new genera as well, that are highly abundant in nature. It is worth noting that our diversity curves (Fig. 6a) indicate that some of the most abundant and

cosmopolitan vSAGs, such as 37-F6, represent viral populations with an unprecedented diversity and microdiversity at the species and genus level. Although speculative, according to predicted host ranges in the recent GOV data set[2] and taxonomical affiliation of hosts of nearest viruses to our virus 37-F6, we hypothesize that vSAG 37-F6-like populations could infect a broad range of hosts

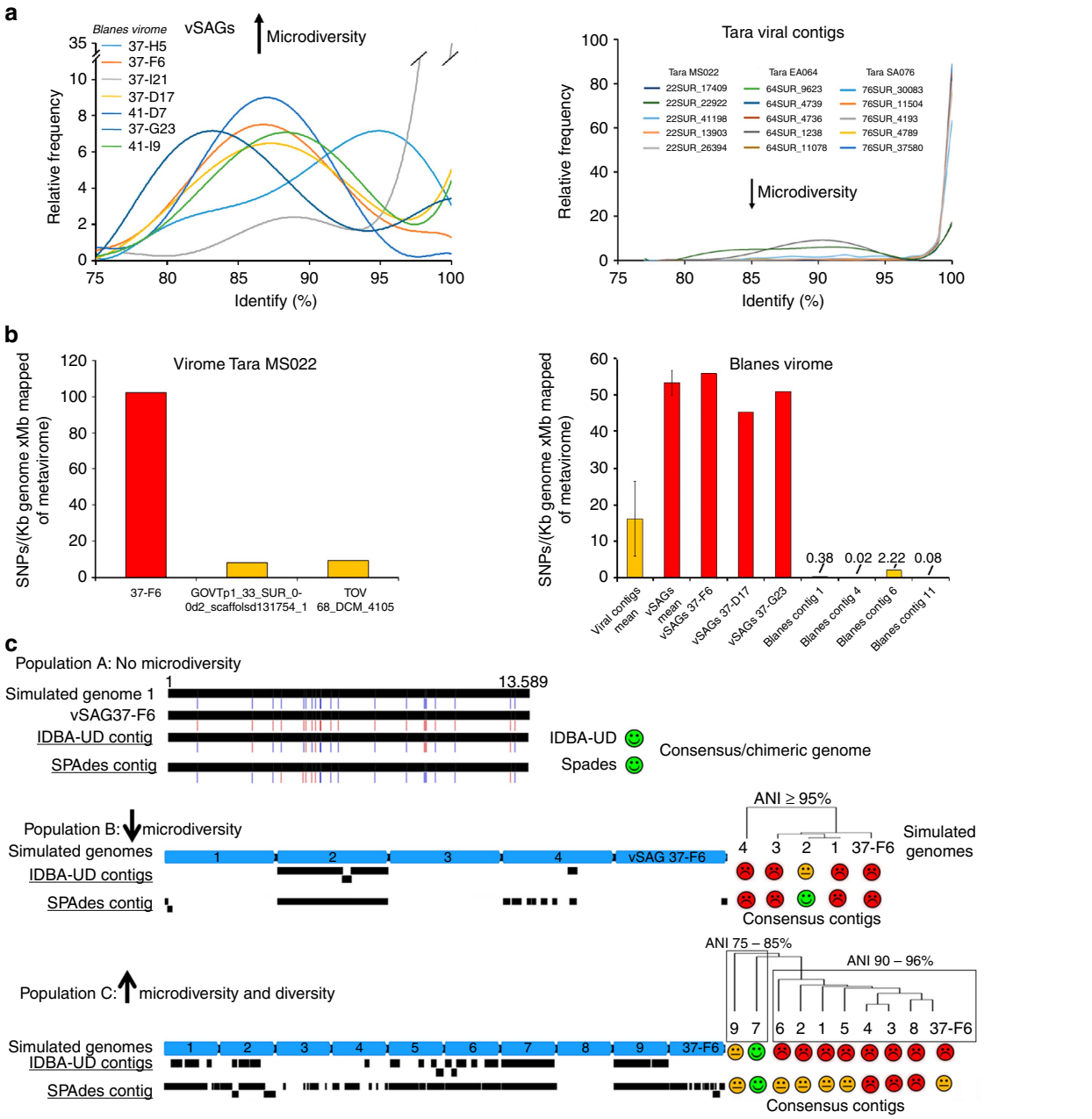

Figure 6 | Assessment of natural vSAGs microdiversity and impact on metagenomic assembly. (**a**) Species-specific recruitment patterns (also referred as diversity curves) for vSAGs and highly abundant viral contigs from viromics. Curves represent the percentage of recruited reads (*Y* axis) at different nucleotide identity values (*X* axis) for vSAGs and *Tara* Oceans contigs[3] in their own viromes. The five most recruiting viruses of each viral data set are shown for convenience. (**b**) SNP frequency for most abundant viral populations at the species level (≥95% nucleotide identity) of vSAGs and viral contigs (within the top 30 ranking in recruitment) recovered by viromics from the Blanes Bay Microbial Observatory (same sampling site of surface vSAGs) and the *Tara* Mediterranean MS022 data set[3]. In Blanes Bay Microbial Observatory, mean ± s.d. of most abundant viral contigs (25 contigs) and vSAGs (4 contigs) are shown. (**c**) Impact of viral diversity and microdiversity on genome reconstruction by metagenomics. Three populations of virus 37-F6 with different (micro)-diversities were simulated within the virome *Tara* MS022 (ref. 3) (see details in Supplementary Fig. 20 and Supplementary Note 5). Population A lacked microdiversity (two simulated nearly identical genomes of 37-F6 with 20 SNPs). A chimeric contig with a mixture of SNPs was obtained (SNPs in blue from simulated genome 1, and in red from vSAG 37-F6). Population B simulated a simplistic scenario with five genomes (ANI≥95%) without high genetic variability in the hypervariable genomic island (Fig. 4; Supplementary Fig. 14). SPAdes assembler reconstructed a consensus contig from only one of the simulated genomes. Population C simulated a more realistic microdiverse scenario than observed in panel A with 10 simulated co-existing viruses (ANI 75-95% and high variability in the genomic island (see details in Supplementary Fig. 20 and Supplementary Note 5). The genome was almost entirely assembled only from those distantly related viruses 7 and 9, while 37-F6 genome could not be assembled. Blue arrows depict the simulated genomes. Black blocks depict the resulting assembled contigs by IDBA_UD and SPAdes assemblers.

from different phyla (Fig. 4), which might partly explain the large genetic diversity within that viral population.

Several models have been proposed to unravel the 'virus–host swinging party' explaining the long-term co-existence of closely related and microdiverse virus and host strains in nature[17,36,37], and metagenomics is a common tool to address these questions[4]. In this study, we show that common metagenomic assembly strategies struggled to reconstruct viral genomes from simulated high-microdiverse populations. Furthermore, when we simulated no microdiversity with only two viral genomes with 20 SNPs of difference along the genome, the metagenomic assemblers unsuccessfully delivered a chimeric contig with a mixture of SNPs from both genomes (Fig. 6c). Accurately determining genetic viral microdiversity is crucial for gaining an understanding of the structure and evolution of microbial population genomics[36]. For instance, a SNP within a viral species population can severely impact on viral fitness, increasing the adhesion to the host and leading to major changes in infection dynamics[38]. Our finding is in agreement with a previous study using simulated viromes from 300 virus isolates that led to similar conclusions[39]. In our study, we demonstrated the impact of microdiversity in a more realistic scenario with natural viromes and considering cosmopolitan and naturally microdiverse viral populations, such as 37-F6-like viruses. Similarly in prokaryotes, the inherent genomic complexity of many microbial populations, such as SAR11, often obfuscates facile generation of whole-genome assemblies from metagenomic data. Our data underlines the power of SVGs to tackle the genetic diversity of the uncultured viruses regardless of the existing microdiversity. We propose a 'marriage of convenience' between single-cell and metagenomics strategies, as it has been recently proposed for prokaryotes[40], to further improve the assembly of (more) complete environmental viral genomes.

Culture-based approaches are inefficient at recovering the uncultured viral majority[1,3]. In turn, shot-gun virome sequencing[2,3] is identified as the preferable tool in viral ecology. However, as we demonstrated here, virome assembly remains complicated and in many cases it yields chimeric contigs, which hide natural microdiversity (Fig. 6). Alternatively, cloning of viral genomes in fosmids has been successfully used for obtaining complete marine viral genomes[10,11], but this approach is limited by the maximum insert size that is allowed by the cloning vectors (genomes <40 kb). Furthermore, current standard virome protocols often exclude large viruses, RNA[28] and ssDNA viruses. SVGs are already able to target ds- and ssDNA viruses. An additional benefit of SVGs is the low sample volume requirement (typically ≤ 1 ml) to unveil the genomics of biologically relevant viruses, which is particularly advantageous for the investigation of the viral community in environments where it is technologically difficult or unfeasible, to collect large sample volumes. On the other hand, one could argue that the small sample volume may not capture the breath of a viral community (for example, due to patchy distribution). However, our results and those of a prior study using a similar approach to investigate the dsDNA viral community by bulk sorting from a single 1 ml seawater sample are comparable in diversity with viromic studies with large sample volumes[20]. Nonetheless, certain steps of the SVGs pipeline remain a challenge. For instance, the detection of viral particles with very small genomes, in particular those with ssDNA and RNA genomes, is difficult due to the low levels of fluorescence signal per viral particle achieved with commercially available fluorescence dyes. Additional stumbling blocks include complete prevention/elimination of minute amounts of contaminant DNA, which may be amplified by WGA, as well as current biases inherent to the available WGA methods[16]. Furthermore, as it is the case with viromics, linking individual viruses to their hosts remain a major challenge.

Altogether, our results provide evidence of SVGs enormous potential, albeit in its incipient development, to aid in unveiling the true extent of viral genetic diversity and microdiversity within natural populations and for complementing current culture and metagenomic methods for addressing key questions in environmental viral ecology. Data from this study support that vSAGs best represent uncultured dsDNA viruses in nature. Nevertheless, though not completely free of bias, recent advances on microfluidics and single-cell genome-sequencing methods[16] bode a promising road for SVGs to fill existing gaps between viromics and culture in virology.

Methods

Culture of bacteriophage P1. The bacteriophage P1 of *Escherichia coli* strain LB21 (provided by Francisco Juan Martínez Mojica, Molecular Microbiology Laboratory, University of Alicante) was used to assess the performance of the Influx sorter (Becton Dickinson) to separate single viruses from a viral culture before working with natural viral samples. To prepare bacteriophage cultures, P1 was grown as previously described[41] and then, the culture was centrifuged at 6,000*g* for 15 min, and the supernatant filtered through 0.22 µm syringe polyethersulfone (PES) membrane filters (ref. SLGP033RS, Millipore, Milford, MA, USA) to purify the viral fraction. The presence of bacteriophage P1 was confirmed by nucleic-acid staining and epifluorescence microscopy[42] before flow cytometry analyses and sorting.

Virus staining optimization for flow cytometry analyses. Standard protocols for detecting viruses by flow cytometry are performed typically on fixed samples with 0.5% of glutaraldehyde[32], which ultimately for our purpose would prevent the amplification of genetic material by multiple displacement amplification (MDA). In this work, we carried out SVGs with unfixed and fixed samples. For fixed viral samples, they were first 0.2 µm-filtered and then fixed with 0.1% of glutaraldehyde final concentration and processed as described in detail[20] with the exception that the used dye was SYBR Gold to 0.5 × final concentration (Invitrogen catalogue no. S11494). For staining unfixed viral samples, the protocol was as follows. SYBR Gold commercial stock with a concentration of 10,000 × was diluted to 1,000 × in sterile MilliQ water, filtered through 0.02 µm Anotop filters (Whatman, ref. 6809–1002) and stored at −20 °C in the dark. Viral samples (typically 1 ml), previously filtered through 0.22 µm syringe PES membrane filters, were concentrated to 50 µl with Nanosep 10 kDa (OMEGA, Pall Life Sciences) and washed with 500 µl of sterile 0.02 µm-filtered TE buffer (10 mM Tris, 1 mM EDTA; pH 8.0) to remove free DNA. The viruses in sterile TE buffer were then stained with SYBR Gold (final concentration of 4 ×) at room temperature for 20 min in the dark and washed three times with 500 µl of sterile 0.02 µm-filtered TE buffer in the ultracentrifugal devices. Finally, 500 µl of sterile 0.02 µm-filtered TE buffer were added to the column and recovered for flow cytometry analyses and sorting. The whole staining procedure was applied to blanks for flow cytometry analyses as per recommendation of reference viral staining protocols[32] to identify the correct viral gates for analyses and sorting. A similar staining protocol for fresh unfixed samples has been successfully used for flow cytometry to stain *Synechococcus* phages[34]. We noted that SYBR Gold provided better resolution than SYBR Green for unfixed samples.

Optimization of virus staining previous to flow cytometry sorting was performed with a FACS Canto II cytometer (BD Biosciences) equipped with a 488-nm laser. A threshold was set on green fluorescence at a value of 200, and samples were analysed using a flow rate below 1,000 events per second to avoid coincidence of viral particles[32]. Green fluorescence, total counts and side scatter were recorded for 1 min for each analysed sample and blank.

Fluorescence-activated virus sorting. BD Influx sorter (Becton Dickinson, San Jose, CA), reagents and disposable material for sterile FAVS were DNA decontaminated as described in detail[43] with some modifications. Sterile TE buffer used for staining viruses was previously ultraviolet-treated for 16 h in a UVP Ultraviolet CL-1000 Crosslinker. 384-well plates (ref. 4ti-0384; 4titude Limited, UK) were autoclaved and then 0.6 µl of ultraviolet-treated 1 × TE buffer was added per well. Plates were then ultraviolet-treated for 10 min without a cover ($\approx$10 cm distance from ultraviolet lamps) in a laminar PCR hood (Alpina K1000) equipped with three ultraviolet lamps (18 W × 3) that sterilize the incoming flow air. Finally, once the plate was set in the Computerized Cell Deposition Unit (CCDU) of Influx sorter was again ultraviolet-irradiated for at least 2 min. Before virus sorting, stained samples were pre-screened through a 35-µm mesh-size cell strainer (BD Biosciences). BD Influx jet-in-air cell sorter was selected for FAVS because of the fine-tuning and high-resolution capabilities. The instrument was equipped with a high-power blue 488-nm laser at 200 mW that was set to 100% power to improve nano-particle detection such as viruses with very low fluorescence emission signal.

In addition, the Influx sorter is equipped with a small-particle detector in which a forward scatter detector is replaced for a high-performance photomultiplier tube (PMT). Furthermore, a mechanical diaphragm, working as a pinhole, was used for fine laser alignment to maximize fluorochrome excitation and fluorescence collection. Before virus sorting, instrument setup was performed using standard 8-peaks Rainbow beads (Sphero Rainbow Calibration Particles 3.0–3.4 μm, BD Biosciences, ref. 559123) for laser alignment. In addition, 220 nm 1-peak yellow beads (Sphero Nano Fluorescent Particles, Yellow 0.22 μm, Spherotech Inc., ref. NFPPS-0252-5) were used for instrument fine-tuning to obtain highest resolution of nano-particle detection. For virus sorting, instrument was set to 'Single' sort mode, which is the most rigorous setting to sort single particles. For sorting, threshold on green fluorescence was set at 1.0 for detecting SYBR Gold fluorescence through a light line passing a 505 LP filter and collected by 530/40 nm band-pass filter. The 100 μm nozzle was chosen because of the best piezoelectric-frequency/electronic-noise ratio with the piezoelectric frequency adjusted at 38.7 kHz. In addition, 100 μm nozzle can work at relative low pressure (20 p.s.i.) compared with 70 μm nozzle (40 p.s.i), reducing particle speed with a consequent increase of exposition time of a particle passing through a laser beam (time-of-flight), which ultimately allowed to collect more fluorescence signal per stained viral particle. Initially, electronic noise without sample acquisition was detected to set the baseline for fluorescence signal detection. For that, green fluorescence PMT voltage and trigger was adjusted to 20–30 events per second with a low sample differential of 1.0 p.s.i. approximately. Then, blanks as described above were analysed to aid in gate selection for virus sorting with a similar sample rate (20–30 events per second) as that of electronic noise. Since very low sample flow rate is mandatory for single-virus sorting to prevent doublets, virus sample flow rate was adjusted to 40–50 events per second. Considering that 20–30 events could come from electronic noise and that a total of 38,700 drops per second were generated (piezoelectric at 38.7 kHz), the estimated ratio of putative-sorted particle versus generated drops was 1/1,300, which ensured a separation enough between each sorted particle to prevent sorting of doublets. All parameters (forward scatter, side scatter and green fluorescence) were collected in logarithmic mode and analysed with BD FACS Software, version 1.0.0.0.650 (Becton Dickinson, San Jose, CA). Fine alignment of 384-well plates in the CCDU was performed by visually inspecting the colour change of small disks (1 mm size) of litmus paper placed at the bottom of the wells, caused by the deposition of sorted droplets. Layout of 384-well plates for viral samples was as follows: 332 were dedicated for single viruses, 44 were used as negative controls (no droplet deposition), 2 received 10 viruses each, 2 received 20 viruses each, and 4 wells were used as positive controls with 1 ng of genomic lambda DNA (New England Biolab). Plates were then covered with sterile film and stored at −80 °C until used.

Confocal microscopy of single viruses. Imaging of sorted P1 bacteriophages was performed on a TCS SP5 II CW-STED Leica microscope equipped with a Leica Confocal Software (LasAF 2.5.1) at the Centre for Genomic Regulation (CRG) (Barcelona). For imaging of single viruses, individual viral particles were sorted directly on a slide and scanned using a HC PL APO ×100/1.40 oil objective with a 488 nm argon laser line (power to 33%), high-disk adjusted to 200% and the PMT 2 gain to 700 V.

Marine sample collection and processing. SVGs was performed for the following collected samples: (i) surface seawater from the Blanes Bay Microbial Observatory (BBMO) in the north-western Mediterranean Sea (41°40′13.5" N 2°48′00.6" E; 2.7 miles offshore) collected on 15 April 2015 (chlorophyll a concentration 0.32 μg l^{-1} and temperature 14.6 °C), (ii) surface seawater samples from the Barcelona Beach (Barcelona, Spain, 41°23′01.7" N 2°11′50.0" E) collected on 19 November 2014 (iii) mesopelagic seawater sample taken in the South-Western Mediterranean Sea (37°21′12.96" N 0°1710.32" W) from the deep chlorophyll maximum (DCM), 60 m depth, on 15 October 2015 and (iv) deep water samples collected in the North Atlantic Sea with the Malaspina expedition, at stations 131 (17°25′39"N 59°49′43" W) and 134 (18°19′38" N 52°38′20.15" W), on 26 November 2011 and 29 November 2011, respectively, both from 4,000 m depth. Metadata for station 131 is: $T\Delta$. 2.31 °C, prokaryote abundance of 2.8E^4 cells per ml and virus-like particle abundance of 1.3E^5 VLP per ml. Metadata for station 134 is: $T\Delta = 2.26$ °C, prokaryote abundance of 2.41E^4 cells per ml and virus-like particle abundance of 1.14E^5 VLP per ml.

Surface and DCM seawater samples were immediately filtered through 0.22 μm syringe PES membrane filters (ref. SLGP033RS, Millipore, Milford, MA, USA). Surface samples were processed for FAVS (see above) within the same day, while the DCM sample was conserved at 4 °C until the sorting on 5 November 2015. The Malaspina expedition samples were cryopreserved as described[12] until sorting.

BBMO metavirome and microbial metagenome were constructed in this study as follows. For microbial metagenomics, 100 ml of seawater was filtered through 0.2 μm filter (ref. SLGP033RS, Millipore, Milford, MA, USA) and nucleic acids extracted with MasterPure Complete DNA and RNA Purification Kit '(Epibio, Illumina) according to the manufacturer's protocol.

For seawater viromics, 28 l of seawater was sieved through a 20-μm mesh, filtered through a 0.2 μm filter (ref. SLGP033RS, Millipore, Milford, MA, USA), and then viruses were concentrated to 20 ml from the filtrate using tangential flow filtration with a 30 kDa polyethersulfone Vivaflow 200 membrane (Sartorius). The virus concentrate was again 0.2 μm-filtered to ensure that no cells remained, which was later confirmed by SYBR Gold staining by epifluorescence microscopy as described[42]. Then, the viral fraction was concentrated to 1.5 ml with Amicon Ultra-15 (Millipore), washed with 10 ml of sterile TE buffer to remove free small DNA fragments, and then 1.5 ml of viral concentrate was treated with 2.5U of Turbo DNase I (Ambion) at 37 °C for 1 h to remove the remaining free DNA. Finally, the viral fraction was ultra-concentrated to 150 μl with Amicon Ultra-50 (10 kDa-cut off, Millipore) and nucleic acids extracted with MasterPure Complete DNA and RNA Purification Kit (Epibio, Illumina) according to the manufacturer's protocol. PCR amplification for 16S rRNA gene with primers 341F and 907R (ref. 44) with the cycling conditions as described[45] was not obtained from the extracted viral DNA, which indicated that contamination with bacterial DNA is negligent.

Whole-genome amplification of single viruses. MDA procedure and DNA decontamination of reagents prior to MDA set up was done as described[43] with some modifications. Single-virus 'lysis' was done by a combination of liquid N_2 shock and/or cold KOH lysis. First, upon thawing 384-well plates at 4 °C, plates were carefully immersed in liquid N_2 for 30–60 s. avoiding contact of liquid N_2 with the film covering the plate. Then a quick thawing shock was applied in a 45 °C water bath for ≈1–2 min. This cycle was repeated two to four times. Next, to each well, 0.7 μl of lysis buffer D2 (see details for preparation and composition in ref. 43) was added and incubated for 5 min at 4 °C. KOH lysis reaction was stopped either with 0.7 μl of Tris-HCl pH 4 or 0.7 μl of Stop solution (Qiagen, ref. 1032393) per well. Then, genomic DNA from the lysed single viruses was amplified by MDA in a 10 μl final volume reaction. The master mix MDA reaction contained 0.26 μl of phi29 DNA polymerase (ref. M0269L; 10 U μl^{-1}; New England Biolab), 1 μl of Phi29 10 × reaction buffer (ref. M0269L; New England Biolab), 1 μl of hexamers (0.5 mM; IDT), 0.1 μl of DTT (1 M; Sigma), 0.4 μl of dNTPs (10 mM each; ref. N0447L, New England Biolab), 0.002 μl of SYTO 9 (Invitrogen) and 5.2 μl of sterile ultraviolet 16 h-treated mQ water. The MDA master mix, except SYTO 9, was ultraviolet decontaminated for 15 min at 4 °C in a UVP Ultraviolet CL-1000 Crosslinker as described in detail[43]. After ultraviolet treatment, SYTO 9 was added to the master mix. Finally, 0.6 ng of genomic lambda DNA (ref. N3011S, New England Biolab) was added to wells A1, A24, P1 and P24 of the plate as positive control. MDA reactions were incubated at 30 °C for 16 h in a CLARIOstar plate reader (BMG Labtech) to monitor the whole-genome amplification. The MDA reaction was stopped by heat-inactivation of the phi 29 at 65 °C for 10 min and the MDA product was diluted 50-fold in sterile TE buffer. Overall 0.5 μl aliquots of the dilute MDA products were served as templates for PCR screening of 16S rRNA gene to assess exogenous bacterial contamination. PCR amplification was performed with primers Prok_340F and Prok_806R as described[46]. No amplification was obtained for the single amplified viral genomes. The MDA Cp values indicated time (hours) required to reach half of the maximal fluorescence in each well. Mean Cp values for positive controls with 0.6 ng of total DNA per well was ≈4–6 h, while Cp MDA values for positive single amplified viral genomes was ≈10–11 h.

Subtle variation of phi29 polymerase activity (ref. M0269L; 10 U μl^{-1}; New England Biolab) has been detected during this study across different batch numbers of enzyme that affect Cp MDA values. As the amount of DNA template from single viruses is significantly less than for single bacterial cells, we recommend to test the activity of phi29 ahead with 0.6 ng of lambda DNA (positive control) template to obtain the above mentioned Cp values to guarantee enough *a priori* activity to amplify genetic material from single viruses. At the same time, ultraviolet decontamination step has to ensure little or no background amplification in the negative controls. The concentration of enzyme used in this study has been 0.26 μl per well, but notice that, the amount of enzyme and ultraviolet decontamination should be adjusted accordingly to obtain the above-mentioned Cp values for positive controls as described[43].

Evaluation of free DNA in sorted seawater microdroplets. Seawater sample from BBMO was sequentially filtered through 0.2 and 0.02 μm filter. The elute, free of viruses, was then stained as above, with the exception that no fixation and liquid nitrogen shock was applied to avoid degradation of putative-free DNA. Flow cytometry sorting of single sorted events from the positive-stained fraction and MDA reactions were performed to evaluate the putative presence of free DNA in the seawater volume co-ocurring with single sorted viruses in the microdroplet.

Sequencing and genome analyses of single-viruses. Single-amplified viral genomes, microbial metagenomes and viromes were sequenced by Illumina technology using the Nextera XT DNA library (ref. FC-131-1024, Illumina) in a MiSeq sequencer (2 × 250, pair-end) according to the manufacturer's protocol. In addition, four vSAGs (37-I21, 17-E11, 37-F6 and 37-L15) were also sequenced by using TruSeq DNA PCR-Free library (ref. FC-121-3001) in a MiSeq sequencer (2 × 150, pair-end) according to the manufacturer's protocol. The reads were quality-filtered using prinseq-lite program[47] with the following parameters: min_length: 50, trim_qual_right: 20, trim_qual_type: mean and trim_qual_window: 20. Genome assembly was performed with SPAdes version 3.6.1 (ref. 48) by applying the following parameters: --sc, -k 33,55,77,99,127, --

careful. Generated contigs were subjected to another round of assembly using Geneious R8 bioinformatic program[49] with stringent conditions (100% sequence identity in the alignment, no gap and a minimum of 200 bp of overlapping). Then, a thorough manual inspection was done for all resulting contigs to ensure a non-chimeric assembly. Specifically, we reviewed those merged contigs resulted from Geneious post-assembly, one at a time, to corroborate that no mismatches were presented in these contigs. Contigs $<1{,}000$ bp and contigs matching to human DNA or common bacterial contaminants in SCGs and sequencing[50,51] were removed from the analyses. Contamination screening was done by using a combination of ProDeGe program and a comparison with the database nr/nt using the stand alone BLAST version 2.2.31+. Finally, prediction of open reading frames (ORFs) from the curated viral genomes and genome annotation were done in Metavir platform by using the default parameters as described[21]. In addition, in parallel predicted ORFs from Metavir were also compared in house by BLASTp with version 2.2.31+ against the non redundant (nr) database (date 28 October 2015) with the following parameters: e-value $<1e-5$. We obtained similar annotation than that from the Metavir platform.

For vSAG 37-F6, five specific primer (Supplementary Table 8) sets covering different genomic regions were designed and successfully tested for the corresponding MDA product of that single viruses, which validate the results from genome assembly. Prediction of structural viral proteins was conducted with an artificial neural network algorithm[52]. The Metavirome from BMMO was assembled by IDBA-UD using option '-precreation'[53], while the BBMO metagenome with SPAdes 3.8.1 using metaspades options with parameters -k 33,55,77,99,127. Contigs were annotated as above. Microbial taxonomy profiling for the metagenome from BBMO was carried out with riboFrame[54]. Whole-genome alignment was first performed with Mauve program[55] and polished with CLUSTAL W aligner and finally manually inspected. Alignment identity values for each nucleotide position was calculated in Geneious bioinformatics software[49]. Calculation of average genome nucleotide identity (ANI) among viral genomes was calculated with the Gegenees software with the following parameters: fragment size = 100 and step size = 50 (refs 56,57). Alignment of large subunit of terminase (TerL) and phylogeny was carried out as described[10,11]. Protein alignment was done with CLUSTAL W implemented in Geneious bioinformatics package. Prediction of 3D structure of capsid proteins was carried out as described[31] with the online server i.-Tasser. *In silico* digestion of predicted proteins from vSAGs was performed with the on-line bioinformatics tool PeptideMass in ExPASy resource portal (http://web.expasy.org/peptide_mass/). Parameters used for searching the predicted proteins of vSAGs was as previously described[31]: parent mass tolerance, 3.0; fragment ion tolerance, 0.5; up to four missed cleavages allowed, variable modification of carboxymethyl cysteine (+57.021 Da) and tryptic peptides only.

Gene-content-based network analysis. Proteins were predicted from the marine vSAGs (61 sequences, 1,192 proteins, respectively) using metagene annotator[58], and added to all proteins from bacterial and archaeal viruses from NCBI RefSeq (2,010 sequences, 198,102 proteins, v75), from predicted proteins from the GOV data set (370,165 proteins[59]), and from environmental phage from Genbank (40,803 proteins). This resulted in 610,262 proteins from 17,744 sequences. Proteins were compared through all-verses-all BLASTP with an E-value threshold of 10^{-5} and 50 for bit score. Protein clusters (PCs) were then defined using Markov Clustering Algorithm (MCL)[60], using default parameters and 2 for an inflation value. vContact (https://bitbucket.org/MAVERICLab/vcontact)[61,62] was then used to calculate a similar score between every pair of genomes based on the number of PCs shared between two sequences and all pairs using the hypergeometric similarity, as previous[2,59]. MCL was applied to the similarity scores using a threshold of 1 and MCL inflation of 2 to generate viral clusters (VCs, ≥ 2 sequences). A total of 933 VCs (17,149 sequences) were obtained, with 31 containing at least one vSAG. Sequences were post-vContact analysed using custom python scripts that performed the following functions: identification of highly similar VCs from the GOV data set using the Jaccard similarity (with the highest similarity values used to associate VC members of vSAG-VCs and GOV-VCs), predicted taxonomy using reference sequences present within the VCs (below), and constructed a network (the python package network[63]) using the similarity scores generated by vContact between each genome pair. Taxonomy predictions were based on the presence of reference sequences within each VC, with either (1) a 'majority-rules approach' where the most abundant ($\geq$ 50%) reference sequence taxonomy being applied to all VC members (that is, if 60% of reference sequences were *Caudovirales*, then the entire VC was classified as such) or (2) using a 'lowest common ancestor' approach among the reference sequences, where taxonomic lineages for each reference within the VC were compared to identify the lowest taxonomic rank (order, family, genus and so on) that contains all the reference sequences. To reduce the complexity of visualizing 17,149 sequences, network components (node groups disconnected from other node groups) not including at least one vSAG were excluded. The final data set (sequences) was exported to Cytoscape (v3.3.0)[63] and images were post-processed using Adobe Illustrator CC 2015.

Metagenomics and metaproteome fragment recruitment. To estimate the abundance and distribution of marine vSAGs, we performed a comprehensive fragment recruitment using different marine metagenome and virome data sets from the *Tara* Oceans expedition[3], Pacific Ocean Virome[23], the Sargasso Sea[24] besides those generated in this study from the Mediterranean Sea. Viromes from the deep ocean were from the *Malaspina Expedition* and are publicly available at the Joint Genome Institute (see ref. 31 for details). In addition, to compare the *in silico* abundance of our vSAG, the following reference marine viruses were included in the analyses: 5,468 viral contigs from surface and DCM (≥ 10 kb) from the *Tara* expedition[3], viral genomes obtained from single cells (the longest contig for each virus)[26], 179 marine virus isolates available at IMG database (Supplementary Table 9) and marine viral genomes reconstructed from fosmids[10,11]. Fragment recruitment analyses were carried out with stand alone BLAST version 2.2.31+ similarly as described for viruses[10] but with an e-value $<1e-5$, and a query coverage $>80\%$. The used commands were as follow: 'blastn -db *Viral_data_base.fasta* -outfmt "6 qseqid sseqid salltitles sallseqid pident bitscore evalue length qstart qend sstart send" -out *recruit_name*.txt -query *Virome.fasta* -evalue 0.00001 -perc_identity 50 -num_threads 6'. Then, by using R software, two different identity percentage cut-offs were applied, 'perc_identity 95' and 'perc_identity 70' (Supplementary Note 5), to recruit only reads from putative closely related viruses or reads from distantly related viruses as well. R software was also used to remove hits with query coverage $<80\%$ and normalize according to genome and metagenome size,as in the previous studies[3,10] to estimate the kb recruited per kb of genome per Gb of metagenome (KPKG). One-way ANOVA was calculated in R package by using the viral data set as factor. Alternatively, reciprocal best-hit fragment recruitment with the viral data set was done as described[27] but employing the Enveomics bioinformatics package (https://peerj.com/preprints/1900/). For the metaproteomic recruitment analyses, peptides obtained from the Oregon coast[64] and *Tara Oceans* Expedition[31] were compared with the vSAG and the above-mentioned viral genomes from different data sets by using BLASTx and BLASTp with the optimized parameters for short sequences as manual describes. Recruitment data were normalized according to viral genome size. Those peptide signatures matching 100% sequence identity and coverage with translated ORFs of vSAG were also screened to assess geographical distribution along the different metavirome data sets.

SNPs of vSAGs in viromes. To estimate the frequency of SNPs of vSAGs at the level of viral species, first we mapped the virome reads from the Mediterranean Sea MS022 and the BBMO, which was the sampling site where vSAGs were obtained. As sequencing errors could bias the SNPs analyses, it is important to remark that only those raw reads from BBMO and *Tara* viromes passing the quality filtering were considered. For *Tara* viromes, parameters for quality filtering[3] were similar to those used here for BBMO virome (see above) since as previously described[3], reads were removed when the median quality score was <20 and bases were trimmed at the 3′ end of reads if the quality score was <20. For the *Tara* MS022 virome, the two most abundant TOV and GOV viral contigs were used. For the BBMO virome, the 25 best viral contig recruiters that ranked within the top 30 in the recruitment were considered. For vSAGs, a total of five best recruited, within the top 30 best recruiters, were considered. For SNP calculation, first virome reads were mapped by using Geneious bioinformatic program[49] against the reference viral contigs and vSAGs with the following parameters: $\geq 95\%$ nucleotide identity, $\geq 70\%$ of read coverage and sensitivity 'fast/read mapping'. SNP calculation with the mapped reads was carried out with Geneious bioinformatics program with the default parameters except for the coverage, that a minimum coverage of $5\times$ was considered. In fact, for most of the obtained SNPs the observed coverage was $>20\times$. In all cases, the detected SNPs had a P value <0.000001 (binominal coefficient implemented in Geneious bioinformatic package under tool 'Find Variations/SNPs'), which also considered the probability of a nucleotide variant because of sequencing errors. The 'effective' genome fraction (kb) with a minimum of $5\times$ coverage was considered for the normalization of SNPs frequency. Thus, the estimation of frequency of SNPs for vSAGs and viral contigs was number of SNPs per kb of effective mapped viral genome per 1 Mb of mapped virome reads.

Simulation of viromes with different microdiversity degrees. The genome assembly performance of the assemblers IDBA_UD[53] and SPAdes[48] for natural virome data sets with populations with different degrees of diversity and microdiversity was assessed. While recently, IDBA_UD has been commonly used for metagenomic assembly.

SPAdes, with the new version optimized for metagenomics (option 'metaspades') is currently considered as one of the most powerful assemblers to address uneven sequencing genome coverages typically obtained in a metagenome (see link: arXiv:1604.03071). The general method for simulation of natural viromes with different degrees of microdiversity for vSAG 37-F6 is depicted in Supplementary Fig. 20 and explained in detail in Supplementary Methods.

Data availability. Raw sequences of metagenome and metavirome from BBMO sample have been deposited in the European Nucleotide Archive under the accession number PRJEB12379. Genomes of vSAGs have been deposited in Genbank under accession numbers KY052794–KY052854. Genome annotations are in JGI-IMG under GOLD ID projects Gp0155348–Gp0155387, and Gp0155393–Gp0155396. Genomes of vSAGs and annotations, as well as metagenome viral contigs assembled from the BBMO virome have been

deposited in Cyverse and are publicly accessible with the following link: http://de.iplantcollaborative.org/dl/d/288CCEA1-7C16-47FA-9E60-5628B695D842/vSAGs_Data.zip. Data of simulated genomes and *Tara* MS22 virome with vSAG 37-F6 populations with different degrees of microdiversity are publicly available with the following links: http://de.iplantcollaborative.org/dl/d/0D119B9B-D912-4D1A-8554-F27FCF3F6E8A/SIMULATION_VIROME_TARA22.zip and http://de.iplantcollaborative.org/dl/d/5D6E8373-6864-4303-8073-8A7A25B4ADDB/Simulated_genomes.zip. Data on relative recruitment frequencies for each viral data set and relatedness of vSAGs with nearest viruses within VCs from GOV data set at the protein level is available in Cyverse with the following link: http://de.iplantcollaborative.org/dl/d/0BA309BE-980E-42AC-A935-2CB564E1F91C/Virome_Recruitment.xlsx. All other data are available from the authors upon request.

References

1. Suttle, C. A. Marine viruses-major players in the global ecosystem. *Nat. Rev. Microbiol.* **5,** 801–812 (2007).
2. Roux, S. *et al.* Ecogenomics and potential biogeochemical impacts of globally abundant ocean viruses. *Nature* **537,** 689–693 (2016).
3. Brum, J. R. *et al.* Ocean plankton. Patterns and ecological drivers of ocean viral communities. *Science* **348,** 1261498 (2015).
4. Paez-Espino, D. *et al.* Uncovering Earth's virome. *Nature* **536,** 425–430 (2016).
5. Manrique, P. *et al.* Healthy human gut phageome. *Proc. Natl Acad. Sci. USA* **113,** 10400–10405 (2016).
6. Dutilh, B. E. *et al.* A highly abundant bacteriophage discovered in the unknown sequences of human faecal metagenomes. *Nat. Commun.* **5,** 1–11 (2014).
7. Abeles, S. R. *et al.* Human oral viruses are personal, persistent and gender-consistent. *ISME J.* **8,** 1753–1767 (2014).
8. Minot, S. *et al.* The human gut virome: inter-individual variation and dynamic response to diet. *Genome Res.* **21,** 1616–1625 (2011).
9. Roux, S., Hallam, S. J., Woyke, T. & Sullivan, M. B. Viral dark matter and virus–host interactions resolved from publicly available microbial genomes. *Elife* **4,** 1–20 (2015).
10. Mizuno, C. M., Rodriguez-Valera, F., Kimes, N. E. & Ghai, R. Expanding the marine virosphere using metagenomics. *PLoS Genet.* **9,** e1003987 (2013).
11. Mizuno, C. M., Ghai, R., Saghaï, A., López-García, P. & Rodriguez-Valera, F. Genomes of abundant and widespread viruses from the deep ocean. *MBio* **7,** e00805–e00816 (2016).
12. Swan, B. K. *et al.* Potential for chemolithoautotrophy among ubiquitous bacteria lineages in the dark ocean. *Science* **333,** 1296–1300 (2011).
13. Swan, B. K. *et al.* Prevalent genome streamlining and latitudinal divergence of planktonic bacteria in the surface ocean. *Proc. Natl Acad. Sci. USA* **110,** 11463–11468 (2013).
14. Rinke, C. *et al.* Insights into the phylogeny and coding potential of microbial dark matter. *Nature* **499,** 431–437 (2013).
15. Kashtan, N. *et al.* Single-cell genomics reveals hundreds of coexisting subpopulations in wild Prochlorococcus. *Science* **344,** 416–420 (2014).
16. Gawad, C., Koh, W. & Quake, S. R. Single-cell genome sequencing: current state of the science. *Nat. Rev. Genet.* **17,** 175–188 (2016).
17. Avrani, S., Wurtzel, O., Sharon, I., Sorek, R. & Lindell, D. Genomic island variability facilitates Prochlorococcus-virus coexistence. *Nature* **474,** 604–608 (2011).
18. Albertsen, M. *et al.* Genome sequences of rare, uncultured bacteria obtained by differential coverage binning of multiple metagenomes. *Nat. Biotechnol.* **31,** 533–538 (2013).
19. Allen, L. Z. *et al.* Single virus genomics: a new tool for virus discovery. *PLoS ONE* **6,** e17722 (2011).
20. Martínez Martínez, J., Swan, B. K. & Wilson, W. H. Marine viruses, a genetic reservoir revealed by targeted viromics. *ISME J.* **8,** 1079–1088 (2014).
21. Roux, S., Tournayre, J., Mahul, A., Debroas, D. & Enault, F. Metavir 2: new tools for viral metagenome comparison and assembled virome analysis. *BMC Bioinformatics* **15,** 76 (2014).
22. Biller, S. J. *et al.* Bacterial vesicles in marine ecosystems. *Science* **343,** 183–186 (2014).
23. Hurwitz, B. L. & Sullivan, M. B. The Pacific Ocean Virome (POV): a marine viral metagenomic dataset and associated protein clusters for quantitative viral ecology. *PLoS ONE* **8,** e57355 (2013).
24. Angly, F. E. *et al.* The marine viromes of four oceanic regions. *PLoS Biol.* **4,** e368 (2006).
25. Sunagawa, S. *et al.* Structure and function of the global ocean microbiome. *Science* **348,** 1–9 (2015).
26. Labonté, J. M. *et al.* Single-cell genomics-based analysis of virus-host interactions in marine surface bacterioplankton. *ISME J.* **9,** 2386–2399 (2015).
27. Zhao, Y. *et al.* Abundant SAR11 viruses in the ocean. *Nature* **494,** 357–360 (2013).
28. Steward, G. F. *et al.* Are we missing half of the viruses in the ocean? *ISME J.* **7,** 672–679 (2013).
29. Martinez-Garcia, M. *et al.* Capturing single cell genomes of active polysaccharide degraders: an unexpected contribution of verrucomicrobia. *PLoS ONE* **7,** e35314 (2012).
30. Ahlgren, N. A., Ren, J., Lu, Y. Y., Fuhrman, J. A. & Sun, F. Alignment-free d2* oligonucleotide frequency dissimilarity measure improves prediction of hosts from metagenomically-derived viral sequences. *Nucleic Acids Res.* **45,** 39–53 (2017).
31. Brum, J. R. *et al.* Illuminating structural proteins in viral 'dark matter' with metaproteomics. *Proc. Natl Acad. Sci. USA* **113,** 2436–2441 (2016).
32. Brussaard, C. P. D. Optimization of procedures for counting viruses by flow cytometry. *Appl. Environ. Microbiol.* **70,** 1506–1513 (2004).
33. Simmonds, P. *et al.* Consensus statement: virus taxonomy in the age of metagenomics. *Nat. Rev. Microbiol.* **15,** 161–168 (2017).
34. Deng, L. *et al.* Viral tagging reveals discrete populations in Synechococcus viral genome sequence space. *Nature* **513,** 242–245 (2014).
35. Gregory, A. C. *et al.* Genomic differentiation among wild cyanophages despite widespread horizontal gene transfer. *BMC Genomics* **17,** 930 (2016).
36. Rodriguez-Valera, F. *et al.* Explaining microbial population genomics through phage predation. *Nat. Rev. Microbiol.* **7,** 828–836 (2009).
37. Avrani, S., Schwartz, D. A. & Lindell, D. Virus-host swinging party in the oceans: incorporating biological complexity into paradigms of antagonistic coexistence. *Mob. Genet. Elements* **2,** 88–95 (2012).
38. Van de Walle, G. R. R. *et al.* A single-nucleotide polymorphism in a herpesvirus DNA polymerase is sufficient to cause lethal neurological disease. *J. Infect. Dis.* **200,** 20–25 (2009).
39. Aguirre de Cárcer, D. *et al.* Evaluation of viral genome assembly and diversity estimation in deep metagenomes. *BMC Genomics* **15,** 989 (2014).
40. Mende, D. R., Aylward, F. O., Eppley, J. M., Nielsen, T. N. & DeLong, E. F. Improved environmental genomes via integration of metagenomic and single-cell assemblies. *Front. Microbiol.* **7,** 143 (2016).
41. Liu, J., Chen, C.-Y., Shiomi, D., Niki, H. & Margolin, W. Visualization of bacteriophage P1 infection by cryo-electron tomography of tiny *Escherichia coli*. *Virology* **417,** 304–311 (2011).
42. Patel, A. *et al.* Virus and prokaryote enumeration from planktonic aquatic environments by epifluorescence microscopy with SYBR Green I. *Nat. Protoc.* **2,** 269–276 (2007).
43. Rinke, C. *et al.* Obtaining genomes from uncultivated environmental microorganisms using FACS-based single-cell genomics. *Nat. Protoc.* **9,** 1038–1048 (2014).
44. Schäfer, H. *et al.* Microbial community dynamics in Mediterranean nutrient-enriched seawater mesocosms: changes in the genetic diversity of bacterial populations. *FEMS Microbiol. Ecol.* **34,** 243–253 (2001).
45. Martínez-García, M., Díaz-Valdés, M., Wanner, G., Ramos-Esplá, A. & Antón, J. Microbial community associated with the colonial ascidian *Cystodytes dellechiajei*. *Environ. Microbiol.* **9,** 521–534 (2007).
46. Martinez-Garcia, M. *et al.* High-throughput single-cell sequencing identifies photoheterotrophs and chemoautotrophs in freshwater bacterioplankton. *ISME J.* **6,** 113–123 (2012).
47. Schmieder, R. & Edwards, R. Quality control and preprocessing of metagenomic datasets. *Bioinformatics.* **27,** 863–864 (2011).
48. Bankevich, A. *et al.* SPAdes: a new genome assembly algorithm and its applications to single-cell sequencing. *J. Comput. Biol.* **19,** 455–477 (2012).
49. Kearse, M. *et al.* Geneious basic: an integrated and extendable desktop software platform for the organization and analysis of sequence data. *Bioinformatics* **28,** 1647–1649 (2012).
50. Laurence, M., Hatzis, C. & Brash, D. E. Common contaminants in next-generation sequencing that hinder discovery of low-abundance microbes. *PLoS ONE* **9,** e97876 (2014).
51. Tennessen, K. *et al.* ProDeGe: a computational protocol for fully automated decontamination of genomes. *ISME J.* **10,** 269–272 (2015).
52. Seguritan, V. *et al.* Artificial neural networks trained to detect viral and phage structural proteins. *PLoS Comput. Biol.* **8,** e1002657 (2012).
53. Peng, Y., Leung, H. C. M., Yiu, S. M. & Chin, F. Y. L. IDBA-UD: a *de novo* assembler for single-cell and metagenomic sequencing data with highly uneven depth. *Bioinformatics* **28,** 1420–1428 (2012).
54. Ramazzotti, M., Berná, L., Donati, C. & Cavalieri, D. riboFrame: an improved method for microbial taxonomy profiling from non-targeted metagenomics. *Front. Genet.* **6,** 329 (2015).
55. Darling, A. C. E., Mau, B., Blattner, F. R. & Perna, N. T. Mauve: multiple alignment of conserved genomic sequence with rearrangements. *Genome Res.* **14,** 1394–1403 (2004).
56. Barylski, J., Nowicki, G. & Godzicka-Jzefiak, A. The discovery of phiAGATE, a novel phage infecting *Bacillus pumilus*, leads to new insights into the phylogeny of the subfamily Spounavirinae. *PLoS ONE* **9,** e86632 (2014).
57. Ågren, J., Sundström, A., Håfström, T. & Segerman, B. Gegenees: fragmented alignment of multiple genomes for determining phylogenomic distances and genetic signatures unique for specified target groups. *PLoS ONE* **7,** e39107 (2012).

58. Noguchi, H., Park, J. & Takagi, T. MetaGene: prokaryotic gene finding from environmental genome shotgun sequences. *Nucleic Acids Res.* **34,** 5623–5630 (2006).
59. Lima-Mendez, G., Van Helden, J., Toussaint, A. & Leplae, R. Reticulate representation of evolutionary and functional relationships between phage genomes. *Mol. Biol. Evol.* **25,** 762–777 (2008).
60. Enright, A. J., Van Dongen, S. & Ouzounis, C. A. An efficient algorithm for large-scale detection of protein families. *Nucleic Acids Res.* **30,** 1575–1584 (2002).
61. Bolduc, B. *et al.* vConTACT: an iVirus tool to classify double-stranded DNA viruses that infect Archaea and Bacteria. *Peer J.* **5,** e3243 (2017).
62. Bolduc, B., Youens-Clark, K., Roux, S., Hurwitz, B. L. & Sullivan, M. B. iVirus: facilitating new insights in viral ecology with software and community data sets imbedded in a cyberinfrastructure. *ISME J.* **11,** 7–14 (2017).
63. Shannon, P. *et al.* Cytoscape: a software environment for integrated models of biomolecular interaction networks. *Genome Res.* **13,** 2498–2504 (2003).
64. Sowell, S. M. *et al.* Environmental proteomics of microbial plankton in a highly productive coastal upwelling system. *ISME J.* **5,** 856–865 (2011).

Acknowledgements

This work has been supported by Spanish Ministry of Economy and Competitiveness (refs CGL2013-40564-R and SAF2013-49267-EXP), Generalitat Valenciana (ref. ACOM/2015/133 and ACIF/2015/332), the USA National Science Foundation (OCE#1536989), the USA Department of Energy (DE-SC0010580), and Gordon and Betty Moore Foundation (grants 3305, 3790, and 5334). The Ohio Supercomputer supported gene-sharing network high performance compute time. Work at BBMO was funded by Spanish project CT2015-70340-R. Work at CRG, BIST and UPF was in part funded by the Spanish Ministry of Economy and Competitiveness, 'Centro de Excelencia Severo Ochoa 2013-2017' and the Spanish Ministry of Economy and Competitiveness, 'Centro de Excelencia Maria de Maeztu 2016-2019'.

Author contributions

M.M.-G. conceived and led the study. F.M.-H. led the analyses and interpretation of data. M.M.-G., F.M.-H., O.F., M.L.G., B.B., M.J.d.l.C.P., J.M.M., J.A., J.M.G., R.R., F.R.-V., M.B.S. and S.G.A. participated in the analyses and interpretation of data. M.M.-G. and F.M.-H. wrote the paper.

Additional information

Supplementary Information accompanies this paper at http://www.nature.com/naturecommunications

Competing interests: The authors declare no competing financial interests.

Reprints and permission information is available online at http://npg.nature.com/reprintsandpermissions/

How to cite this article: Martinez-Hernandez, F. *et al.* Single-virus genomics reveals hidden cosmopolitan and abundant viruses. *Nat. Commun.* **8,** 15892 doi: 10.1038/ncomms15892 (2017).

Publisher's note: Springer Nature remains neutral with regard to jurisdictional claims in published maps and institutional affiliations.

Supplementary Information

Supplementary Figures

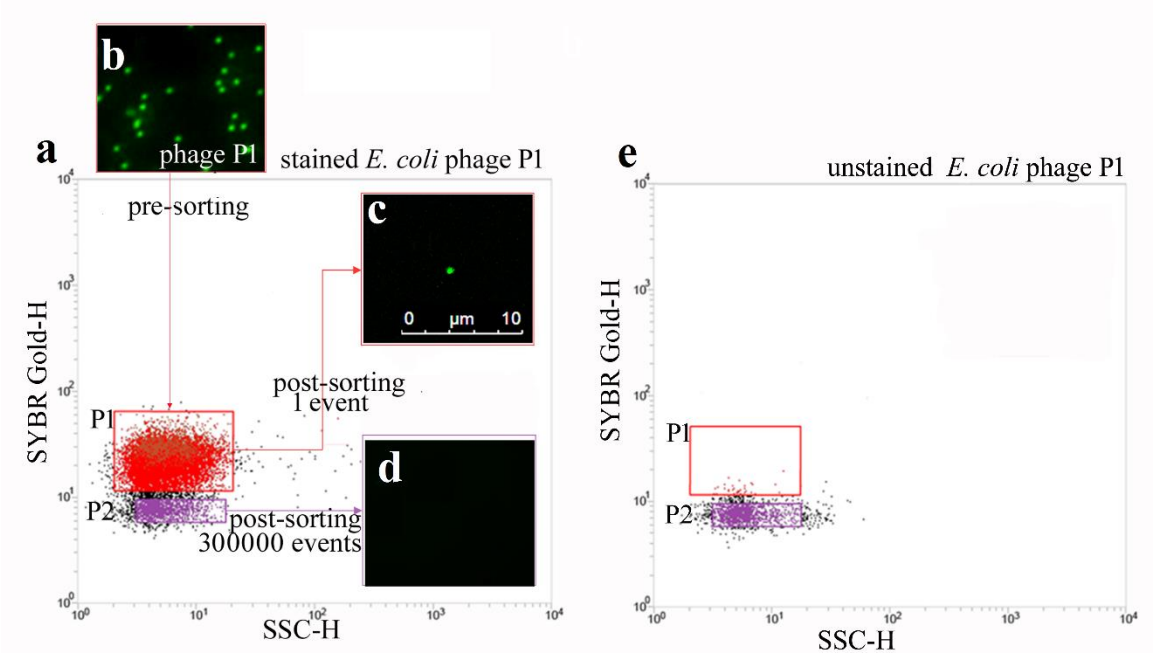

Supplementary Fig. 1. Fluorescence-activated virus sorting (FAVS) of bacteriophage P1 of *Escherichia coli*. (**a**) Flow cytometric plot of 90° light (side) scatter (SSC-H; height value) vs. green fluorescence after staining with SYBR Gold, (SYBR Gold-H; height value, relative units) of *E. coli* phage P1. Selected sorting gate of individual viral particles is indicated in red (gate P1). Background noise, gate P2. **(b)** Epifluorescence microscopy image of phage P1 culture used for sorting (pre-FAVS). **(c)** Confocal laser scanning microscopy of 1 sorted individual virus (post-sorting). A thorough scan was performed to rule out the presence of doublets or more coincident events. The experiment was repeated five times with identical results. **(d)** Epifluorescence image of 300,000 sorted events from background noise (gate P2). No stained viruses were detected in this area. **(e)** Flow cytometric plot of the unstained phage P1 (blank control).

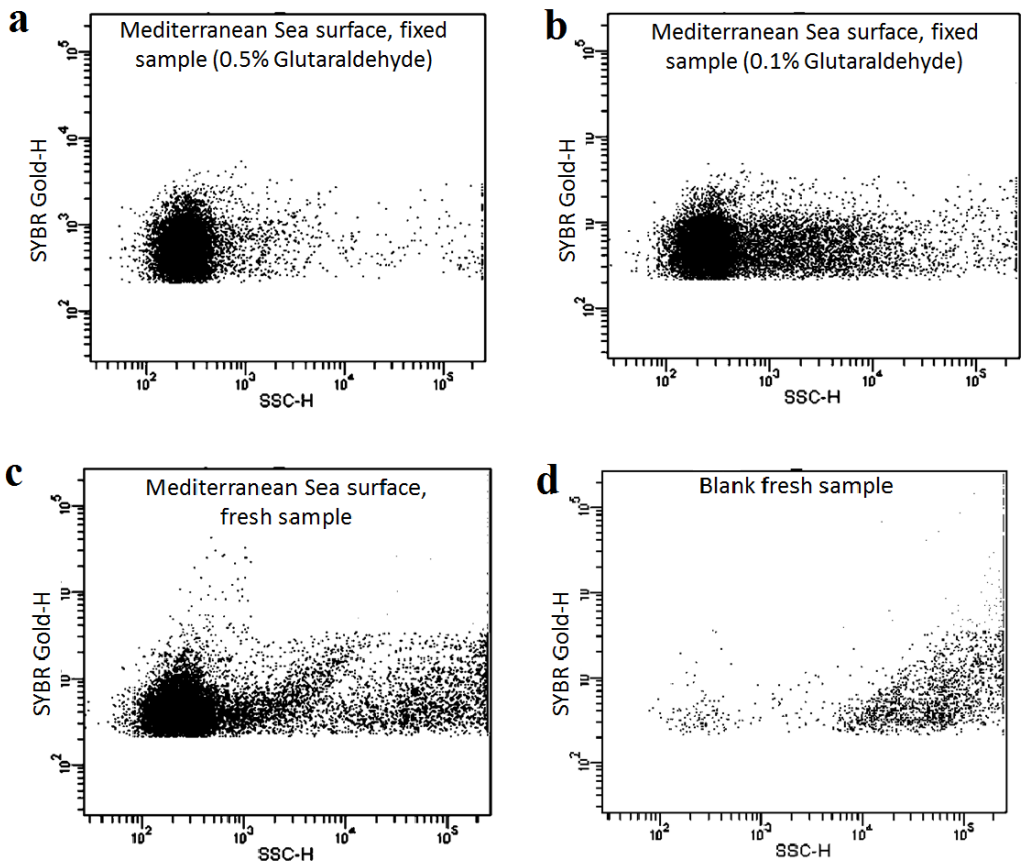

Supplementary Fig. 2. Virus staining optimization for fluorescence-activated virus sorting (FAVS). The standard and reference protocol used for staining and detection of viruses by flow cytometry for aquatic samples was that previously published by Corina Brussard[1]. However, the amount of fixative (0.5% glutaraldehyde) used in that protocol prevent the amplification of genetic material by multiple displacement amplification (MDA) and consequently subtle variations on that protocol were performed (see methods). Comparison of the staining of same marine viral samples with different fixation treatments (see Methods for details): fixed with 0.5% (panel **a;** reference protocol by Corina Brussard[1]), with 0.1% glutaraldehyde **(b)**, and fresh (unfixed) sample (**c**). Samples were stained with SYBR Gold 0.5X final concentration (see Methods for details). Flow cytometry was performed using FACS Canto II (see Methods). Our results indicated that the staining procedures used in this study showed similar results than the reference protocol traditionally used in viral ecology to count and detect viruses from natural marine samples.

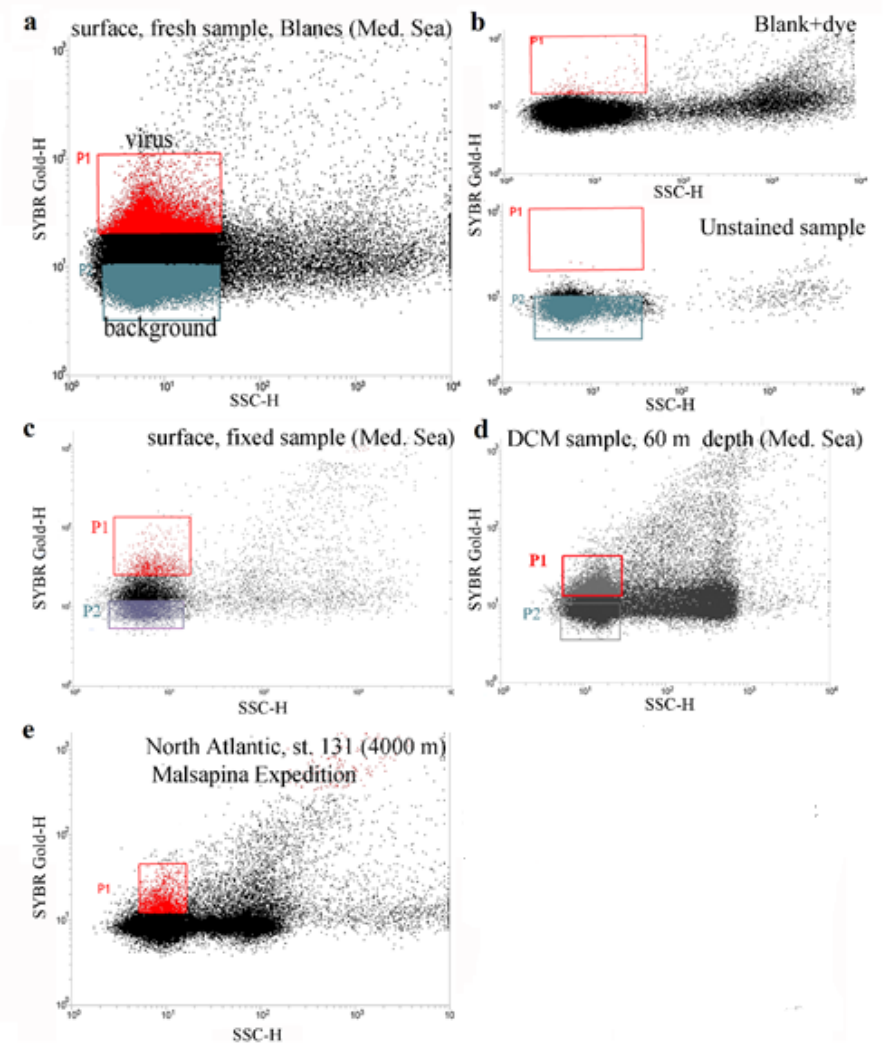

Supplementary Fig. 3. Fluorescence-activated virus sorting (FAVS) of marine and human salivary samples. For each sample, flow cytometric plot of 90° light scatter (SSC-H; height value) and green fluorescence, (SYBR Gold-H; height value, relative units) is shown. Gate P1 was used for sorting of single-viruses. **(a)** Surface seawater sample from the Blanes Bay Microbial Observatory (BBMO, Spain) in the Mediterranean Sea. **(b)** Blank and unstained viral fraction for the BBMO sample. No fluorescence signal was observed in gate P1. For all marine samples data from negatives were very similar. For convenience only negative and blank data are shown for BBMO. **(c)** Surface seawater sample from the Barcelona Beach (Barcelona, Spain) from the Mediterranean Sea. **(d)** Seawater sample from the deep chlorophyll maximum zone in the Mediterranean Sea (depth 60 m). **(e)** Deep seawater samples from the North Atlantic (4,000 m depth). Station 131 from the Malaspina Expedition. The deep seawater sample from station 134 showed a similar flow cytometric pattern.

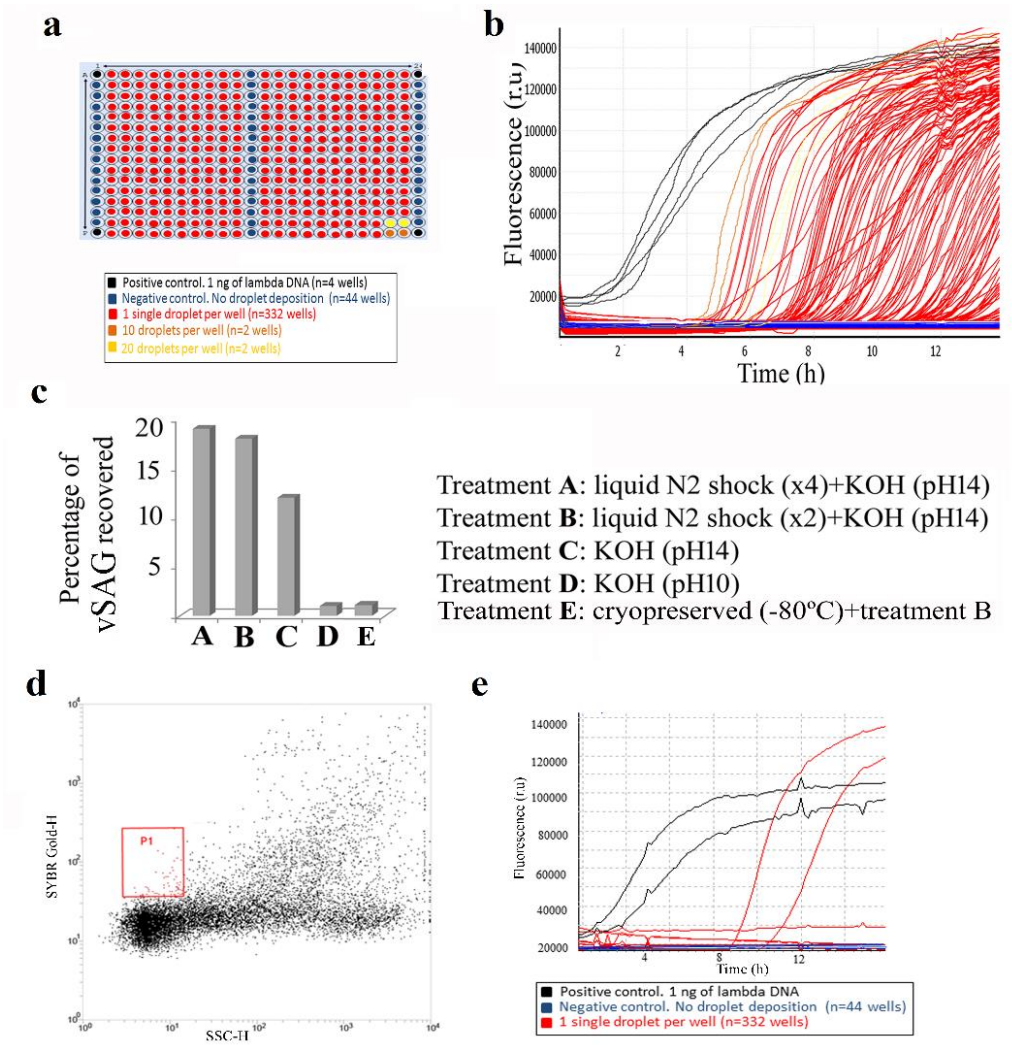

Supplementary Fig. 4. Whole genome amplification (WGA) of marine single-viruses and assessment of effect of free DNA in seawater on WGA. (a) Layout of a 384-well plate indicating the wells distribution. **(b)** Real-time multiple displacement amplification (MDA) of the genome of sorted single-viruses from the Blanes Bay Microbial Observatory (BBMO). **(c)** Efficiency of vSAGs recovery according to the various methods employed to break the capsid, with different cycles of freezing in liquid nitrogen followed by a shock in buffer KOH (pH 10 or 14). **(d** and **e)** Assessment of contribution of free DNA in to whole genome amplification of sorted single-viruses. **(d)** Flow cytometric plot of 90° light scatter (SSC-H; height value) and green SYBR Gold-H fluorescence (relative units, height values) of a stained seawater sample (Barcelona Beach in the Mediterranean Sea) previously filtered through 0.02 µm pore size to remove viruses. Putative free DNA was stained with SYBR Gold and processed as a fresh sample (see methods for details). Note that, as expected, stained putative free DNA were not detected in gate P1 used previously for virus sorting. Gate P1 was restricted for those events with higher fluorescence signals, which in theory would represent large stained free DNA fragments. **(e)** Real-time MDA results of sorted events with putative free DNA molecules deposited in a 384-well plate.

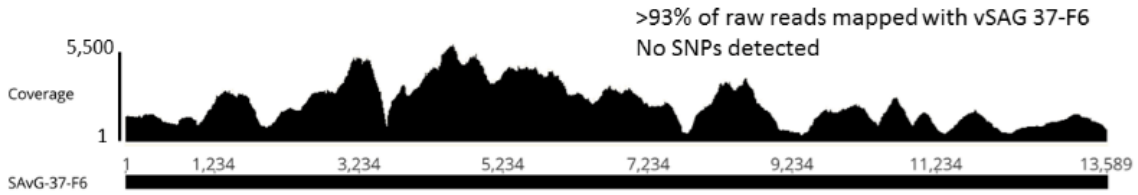

Supplementary Figure 5: **Raw Illumina reads mapping against the assembled genome of vSAG 37-F6**. Nearly all obtained reads for vSAG 37-F6 mapped perfectly without SNPs with the reconstructed genome indicating that the MDA did not generated chimeric artifacts. Only in two vSAGs, the 17-D19 and 41-A4, we observed that for each one, two assembled genome fragments with similar size were obtained with a similarity between 85 and 71%, respectively. We speculate that in this case, two viral particles from same population could be co-sorted. In the case of vSAG 17-D19, both genome fragments belonged to same viral cluster (see Supplementary Table 3).

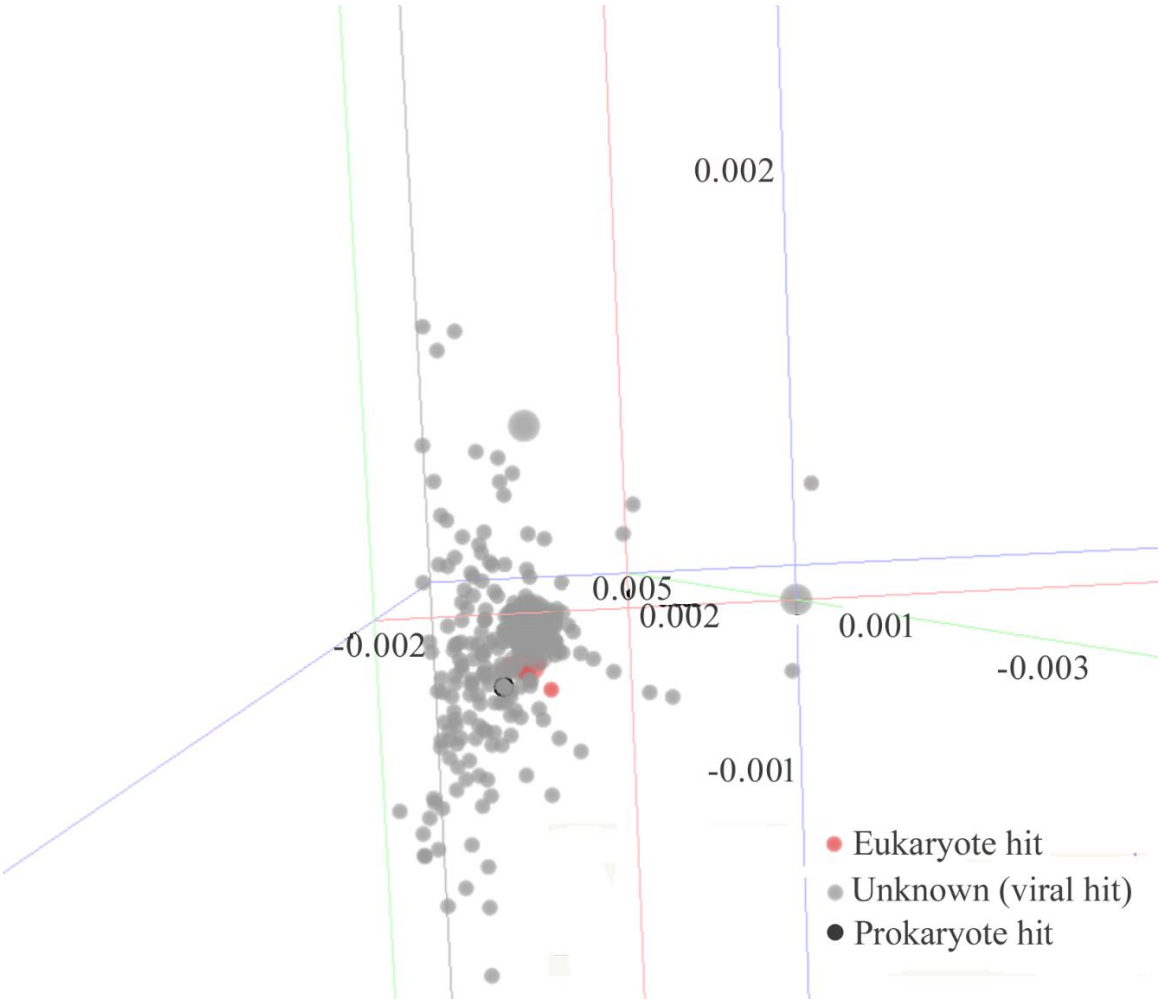

Supplementary Figure 6: Decontamination of genomic data of single amplified viral genomes. Decontamination was done by a semi-automatic approach by combining the use of the ProDeGe pipeline[2] and a thorough manual decontamination by BLASTx and BLASTn against the nr database. Detected contaminant contigs (typically <1kb length) were removed and the remained putative viral genome fragments were screened with ProDeGe pipeline and the results of the principal component analyses is shown. ProDeGe bins kmers (5-mers and 9-mers) generated from cleaned vSAGs and compare them by BLAST against nr Genbank database. Nearly all cleaned putative viral genome fragments were of unknown origin, taxonomically not related to prokaryotes. Each dot is a putative viral genome fragment. Color of dot indicates the putative taxonomic affiliation of the best hit kmers generated from vSAGS with the nr Genbank database.

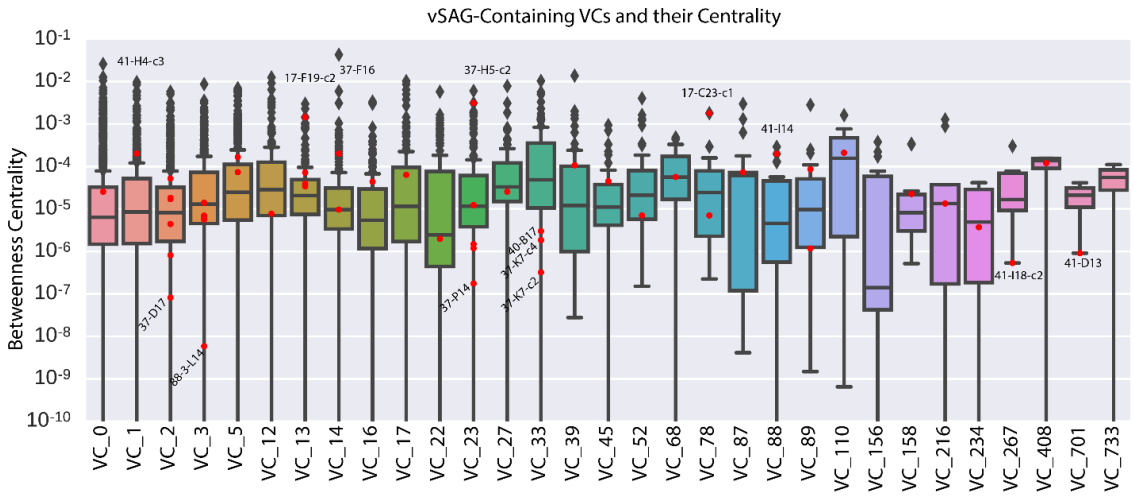

Supplementary Fig. 7. Relatedness of vSAGs with the Global Oceanic Virome clusters described in this study (Supplementary Table 3). Figure illustrates the centrality and frequency of connections between vSAGs and viral clusters (VCs, X-axis). Low betweenness values (Y-axis) correspond to fewer/weaker connections with VCs, with higher values being more-connected sequences. Each box represents 95% confidence intervals, with average score centrality within VCs denoted by a line in the box. vSAGs outliers (in red) below average score centrality could represent new genera. Although application of viral taxonomy criteria to define viral species and genera remains complicated to uncultured viruses, in this study we have used the following criteria based on a previous study by Roix and colleagues[4]. New genera are defined when the vSAGs presented weaker connections with closest viral relatives within the global marine viral network, as previously described[4]. New viral species are defined when ≤95% of nucleotide identity was obtained with the closest viral relative.

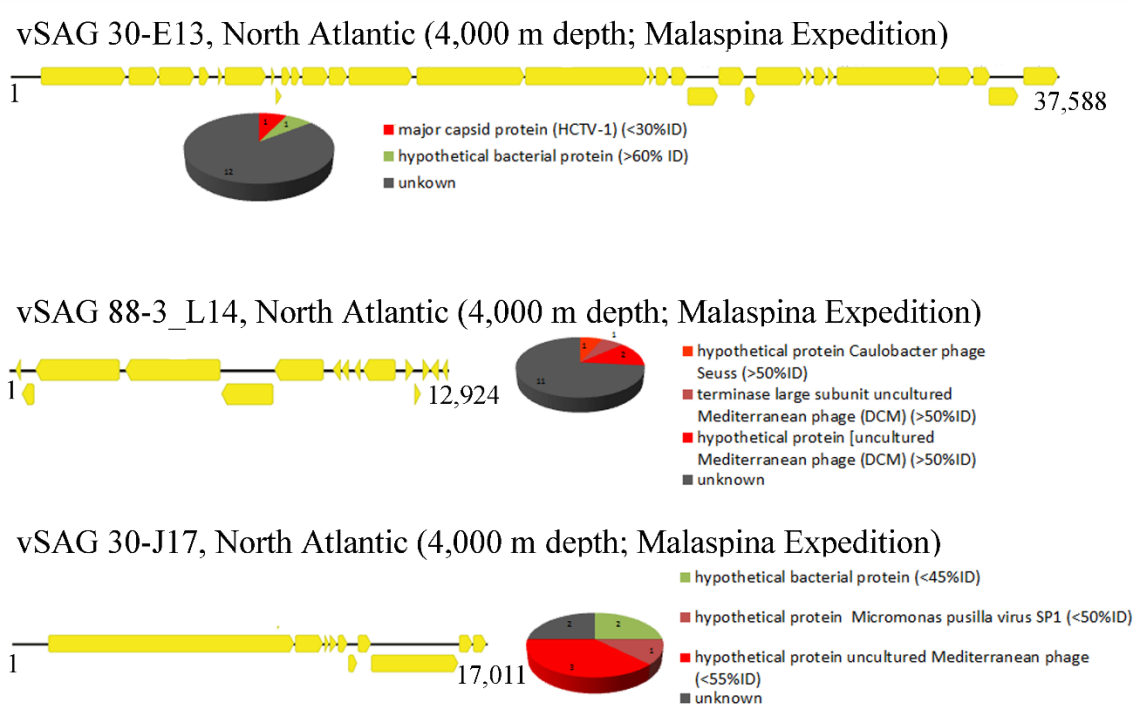

Supplementary Figure 8: Single amplified viral genomes obtained from the deep ocean. Genome annotation of three vSAGs from the North Atlantic. Prediction of open reading frames (ORFs) were done with Genmark with heuristic model optimized for viruses[3,4]. Comparison with BLASTp of predicted ORFs was carried out with non-redundant Genbank and viral fosmids from mesopelagic and bathypelagic samples of the Mediterranean Sea[5]. Conserved domains of predicted proteins were searched[6].

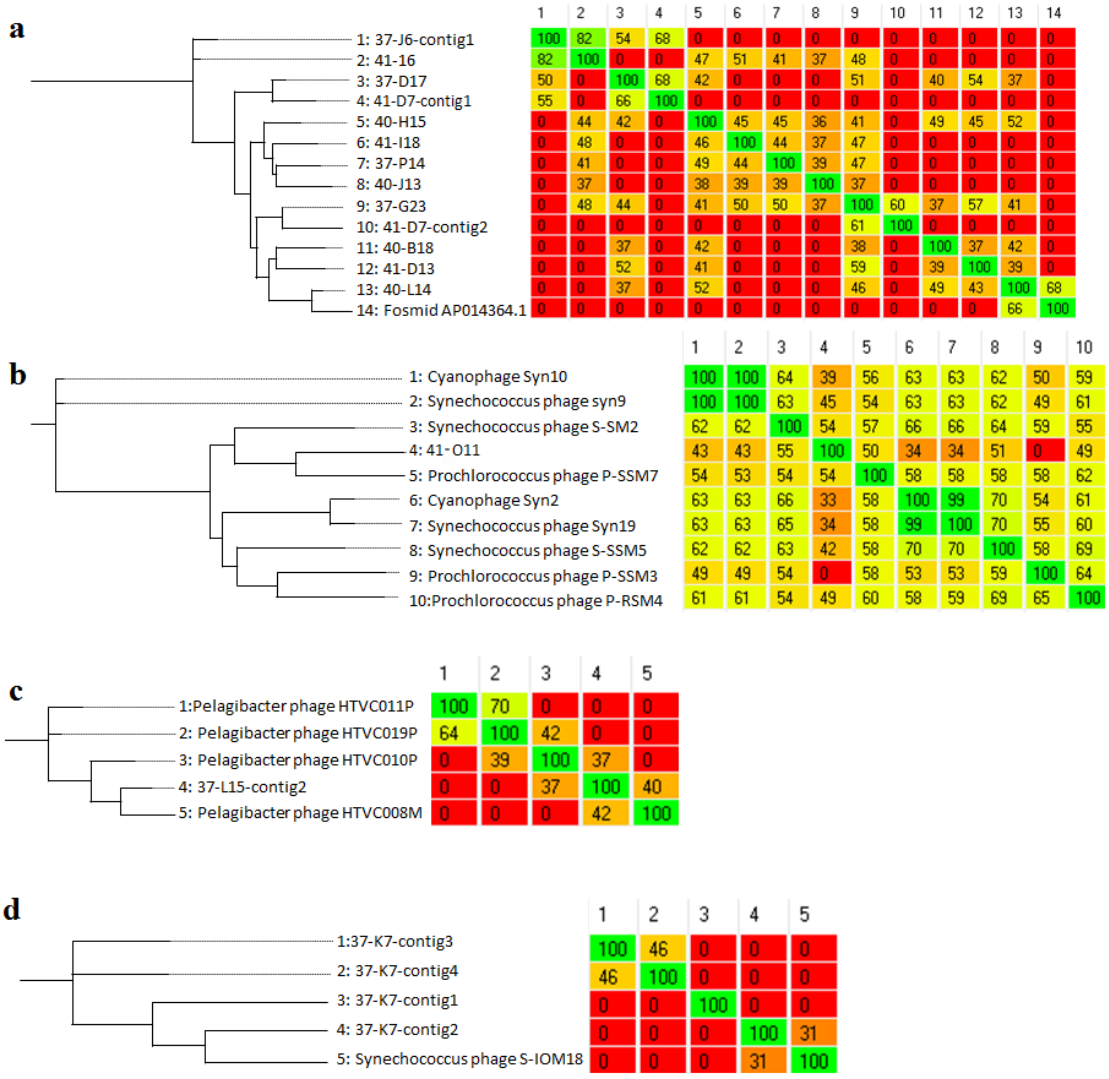

Supplementary Figure 9: Comparative genome analyses based on average nucleotide identity (ANI). (a-d) Different heat maps calculated using Gegenees 2.2.1 software showing the genetic relatedness (ANI values) within the obtained vSAGs **(a)**, and with other marine viral groups **(b-d)**. The trees were constructed with SplitsTree using the neighbor joining method.

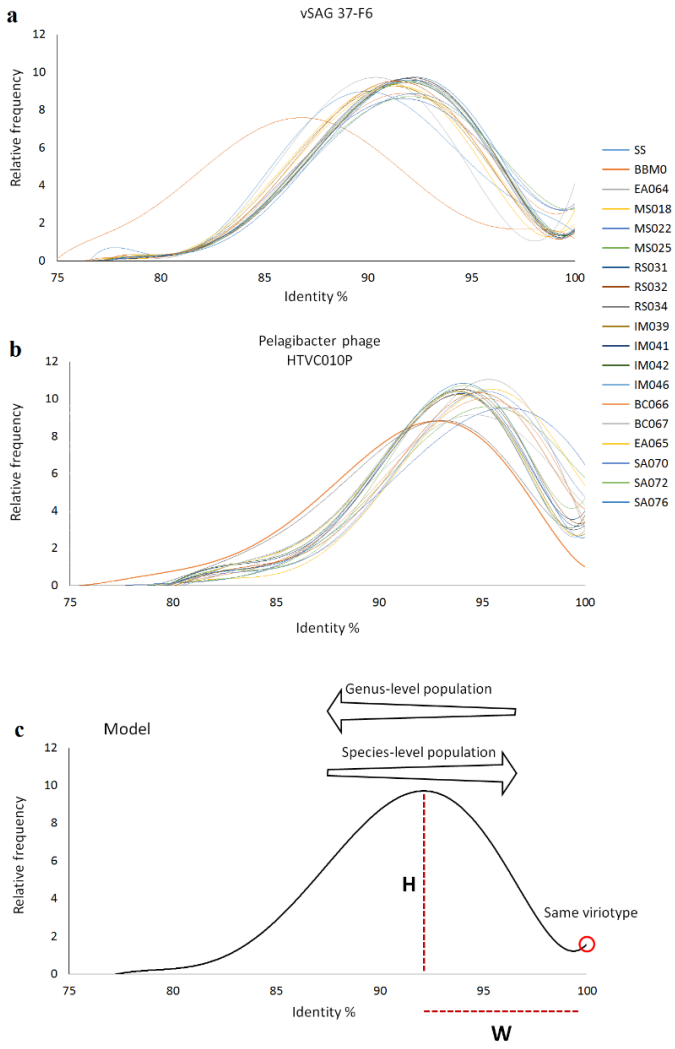

Supplementary Figure 10: Specific-species pattern of viral population of reference viruses in marine environments. (a) Viral population structure of the virus 37-F6 and **(b)** the reference abundant *Pelagibacter* phage in over twenty viromes spanning nearly all oceanic regions. List of abbreviations of viromes as in Fig. 2. Appended numbers refer to the *Tara* metavirome sample nomenclature previously used[7]. Notice that the structure of viral population of virus 37-F6 from the same sampling point (Blanes, Mediterranean Sea) is slightly different than the rest of oceanic regions and based on our proposed model depicted in panel **C** and supplementary text, it is likely more (micro-)diverse in the sampling point than in other regions. **(c)** Proposed model of viral population structure based on metagenomics recruitment inspired by that previously described for prokaryotes[8]. Notice that in contrast to prokaryotes, a genetic discontinuity is not observed between 90-95% of identity but is rather a continuous line with a clear peak precisely in that identity range. None of vSAGs, virus isolates, fosmids and viral contigs recruited reads below 75% identity. Furthermore, a secondary peak observed in prokaryotes at the level of <90% identity is not observed either. Red arrows and dots

depict the biological meaning of recruited viromic reads. H, height of the curve. W, half of the width of the curve.

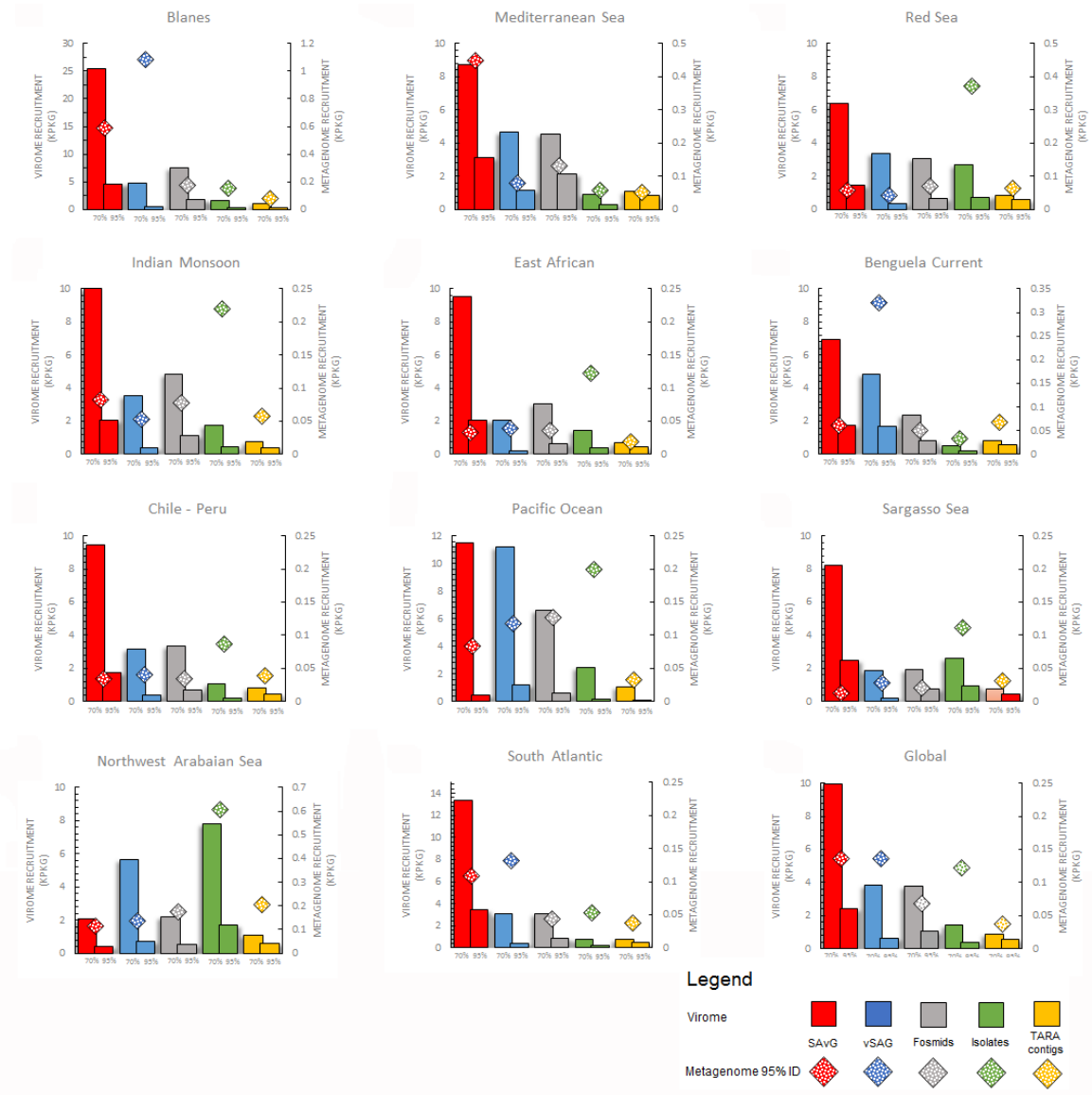

Supplementary Fig. 11. Abundance of viral genome datasets in the different analyzed regions. Virome recruitment (in columns) with different identity thresholds (≥70 and ≥95%). Microbial metagenomic recruitment rate (diamonds) results with an identity threshold of ≥95%. The vSAG dataset showed the highest recruitment rate expressed in recruited kb per kb viral genome per Gb of virome (KPKG) in most of the analyzed viromes, but no significant differences in the microbial metagenomics recruitment were observed among the viral genome datasets.

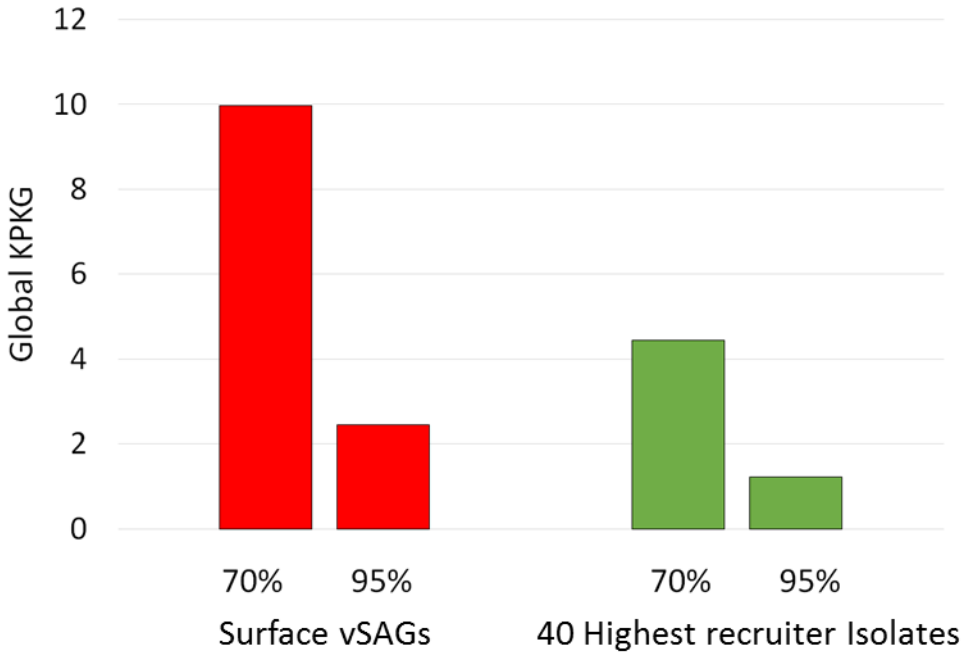

Supplementary Figure 12: Virome recruitment rate of vSAGs compared to the 40 most abundant virus isolates at the global scale. We used two identity thresholds (≥70 and ≥95%**).** In this analysis, we biased in purpose the comparison by considering only those 40 virus isolates with the highest recruitment rate in the surface viriosphere. Even in that scenario, the relative recruitment rate of vSAG was higher.

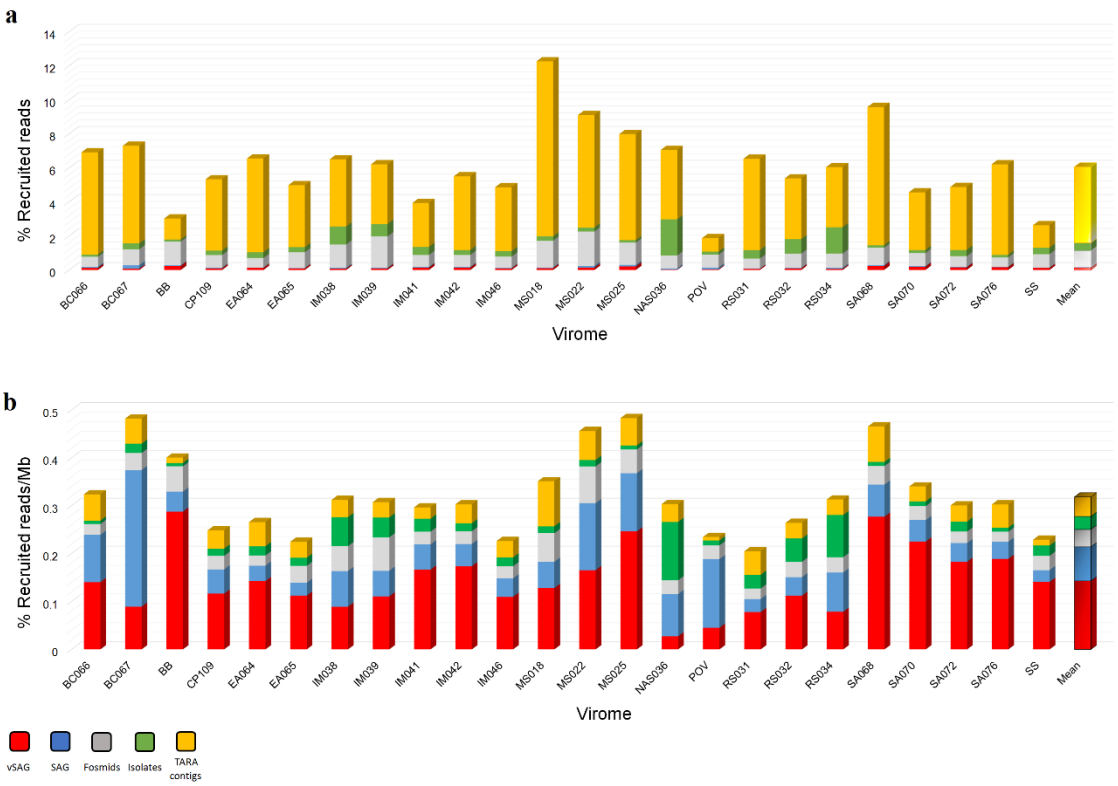

Supplementary Figure 13: Reads recruited for each viral genomic dataset (≥95% cut-off identity). **(a)** Non-normalized viromic recruitment results. **(b)** Normalized viromic recruitment results considering the size of the viral genomic dataset.

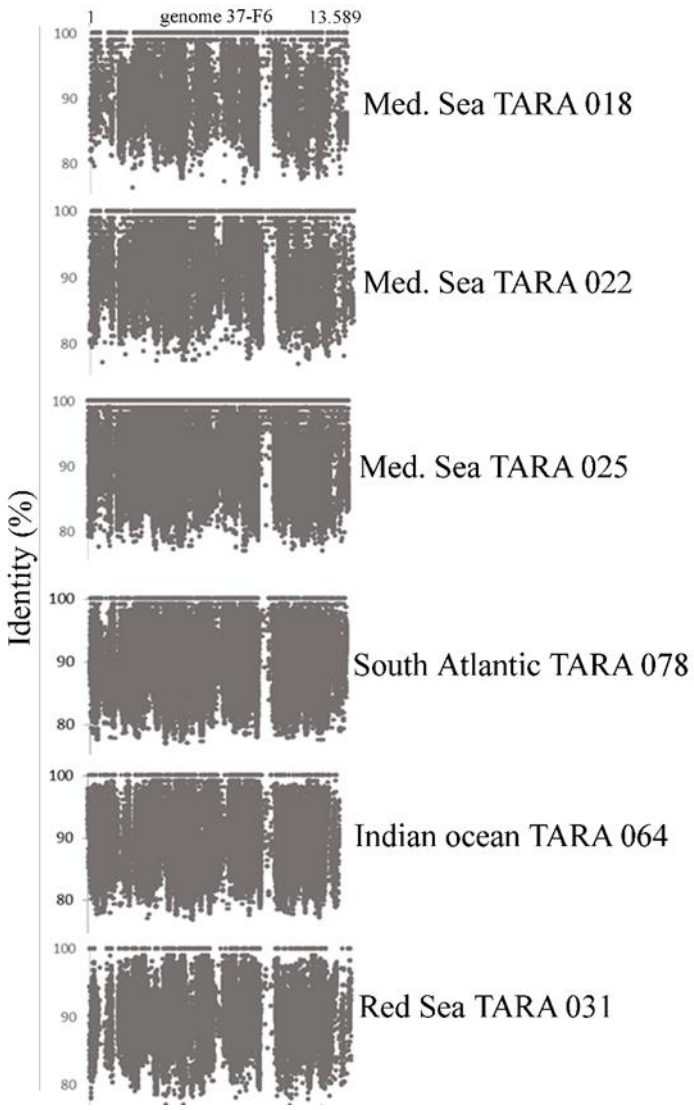

Supplementary Fig. 14. Virome fragment recruitment of the vSAG 37-F6. Virome fragment recruitment in the Indian and the South Atlantic oceans and the Red Sea from *Tara* expedition samples collected several thousand kilometers away from the sampling point of the vSAG 37-F6 (NW Mediterranean, Blanes Bay Microbial Observatory). Note that the genomic island of viruses is almost fully covered in *Tara* Mediterranean viromes from the Western Mediterranean Sea, geographically near to Blanes Bay Microbial Observatory.

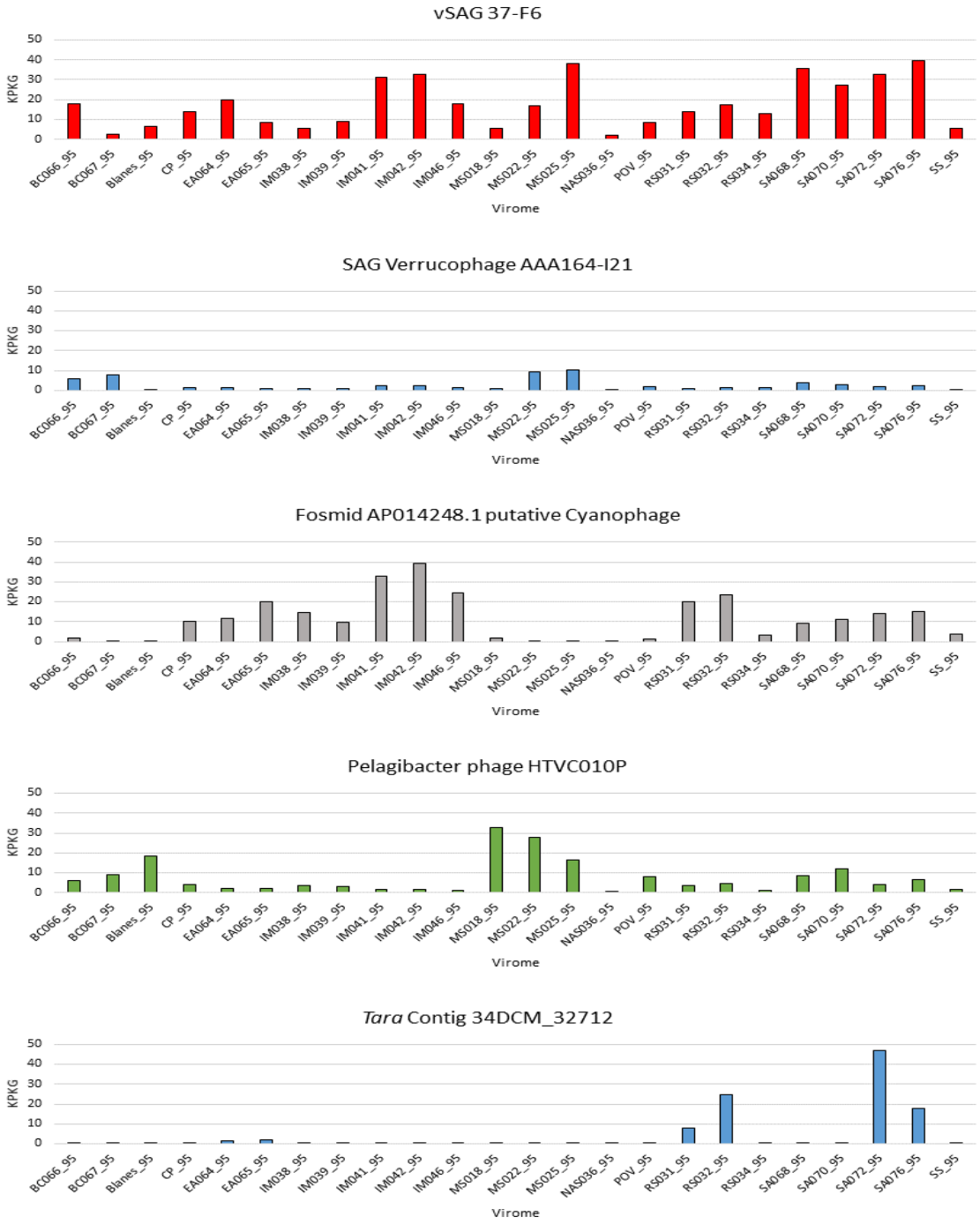

Supplementary Figure 15: Abundance distribution of the most abundant marine viruses. The abundance of the most abundant surface dsDNA viruses for each virus genome datasets according to the procedure for genome recovering (single-virus genomics (37-F6), viruses from single bacterial cells[9] (Verrucophage AAA164-I21), virus cloned in fosmids[10] (AP014248. putative Cyanophage), virus isolates (Pelagibacter phage HTVC010P) and viromics from *Tara* Oceans dataset[11,7] (34DCM_32712), in all viromes. Fragment recruitment data was used to stimate the overall abundance for each region. Abundance is represented in KPKG (as in Fig. 2).

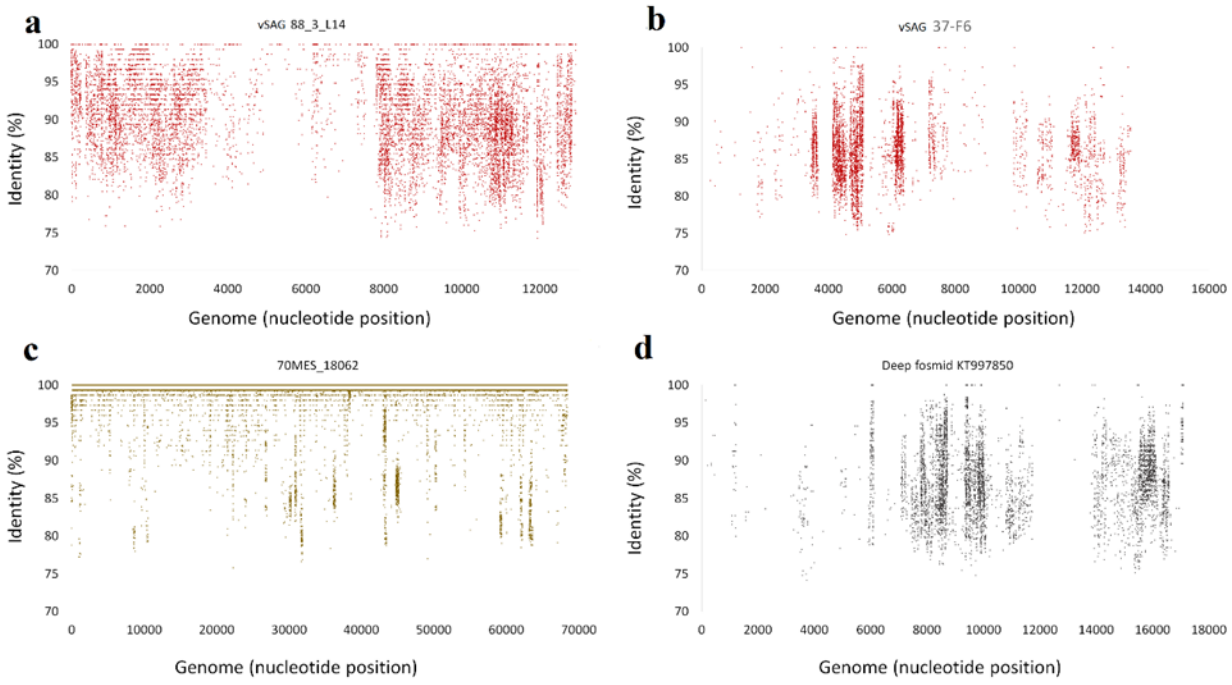

Supplementary Fig. 16. Deep viromic fragment recruitment. Fragment virome recruitment plots from the North Atlantic bathypelagic region (4000 m depth; sample MSP131 from the *Malaspina* Expedition[11]). (**a-d**) Recruitment of the deep vSAG 88-3-L14 was compared with the abundant surface vSAG 37-F6 and those most abundant genome fragments recovered by viromics and cloning in fosmids: *Tara* contig 70_MES_18062 and viral fosmid KT997850[5].

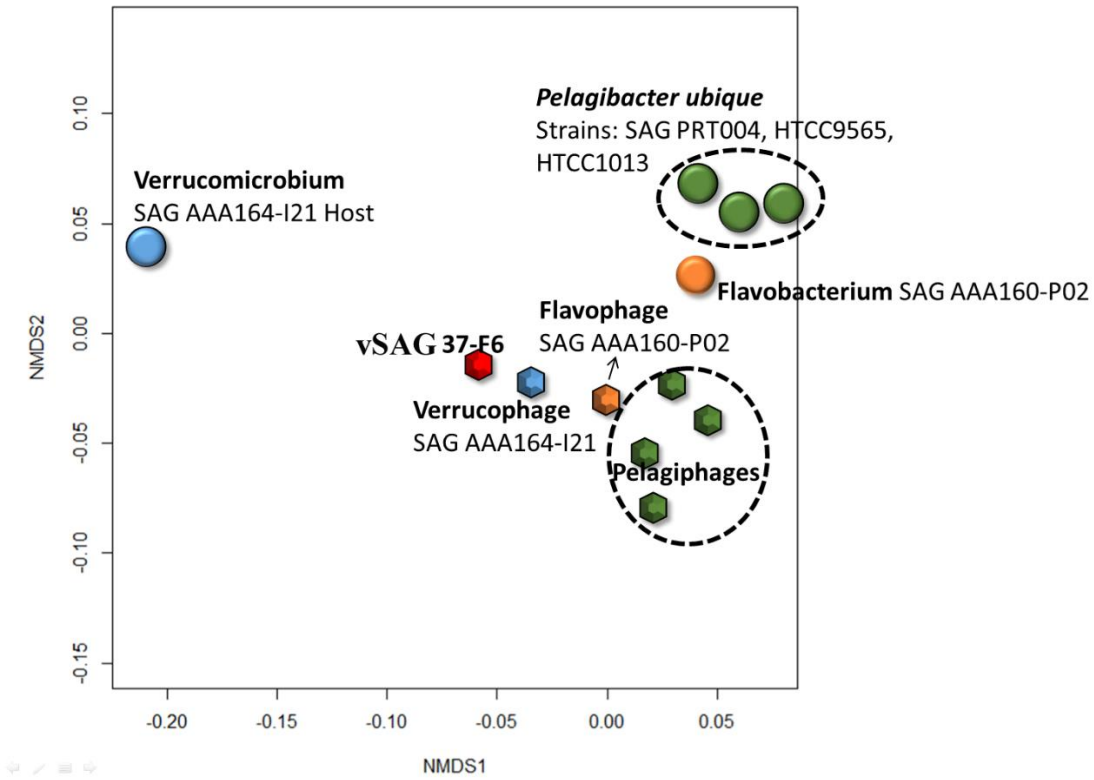

Supplementary Figure 17: Tentative assignation of viruses to hosts according to tetranucleotide frequency signatures. Non-metric MDA of tetranucleotide frequency show the degree of similarity between the different phages and their host with the vSAG 37-F6. Tetranucleotide frequency were calculated with the publicly available bioinformatics tool at the following link: http://mobyle.pasteur.fr/cgi-bin/portal.py#forms::compseq

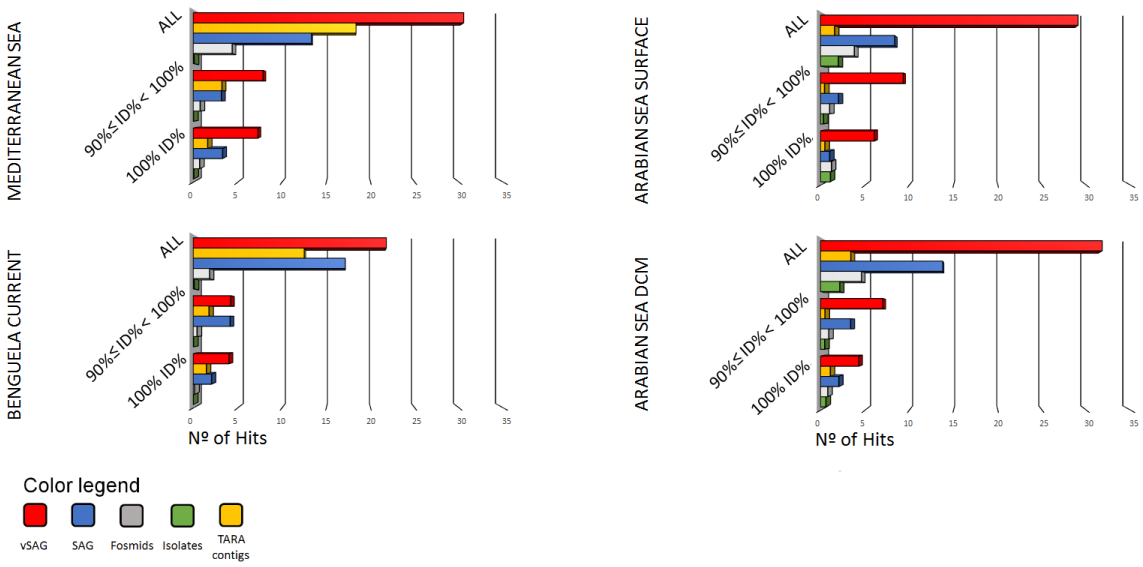

Supplementary Fig. 18. Peptide recruitment for each viral genomic dataset using predicted peptide sequences obtained from *Tara* expedition[12]. Different cut-off identities were used (no cut off, ≥90 but <100%, and 100%). In all four metaproteomes, vSAGs are the most peptide recruiters.

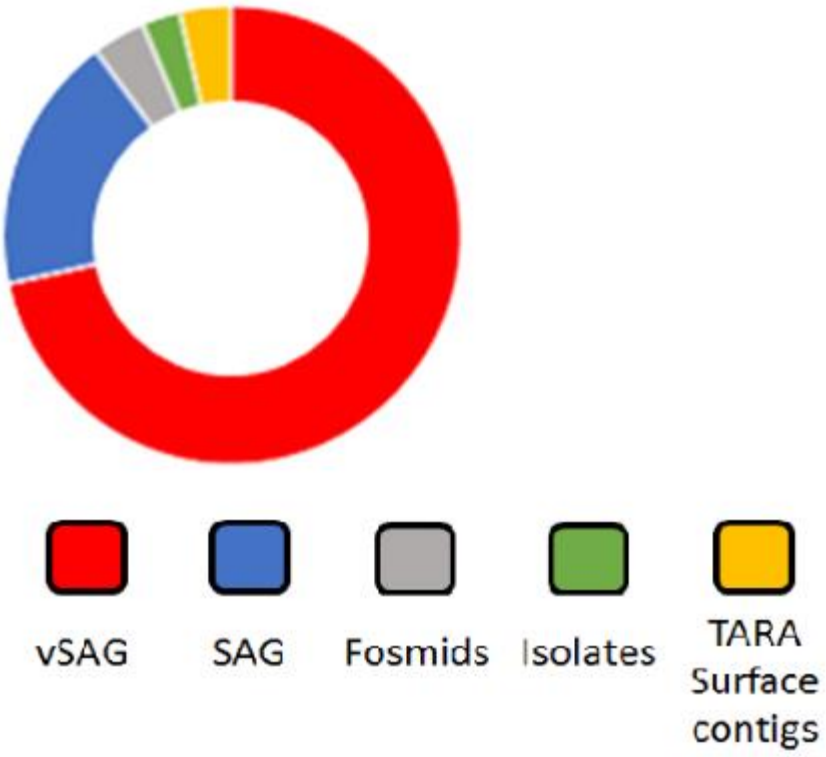

Supplementary Fig. 19. Peptide recruitment (100% identity) for each viral genomic dataset using the predicted peptide sequences obtained in the Oregon Coast[13].

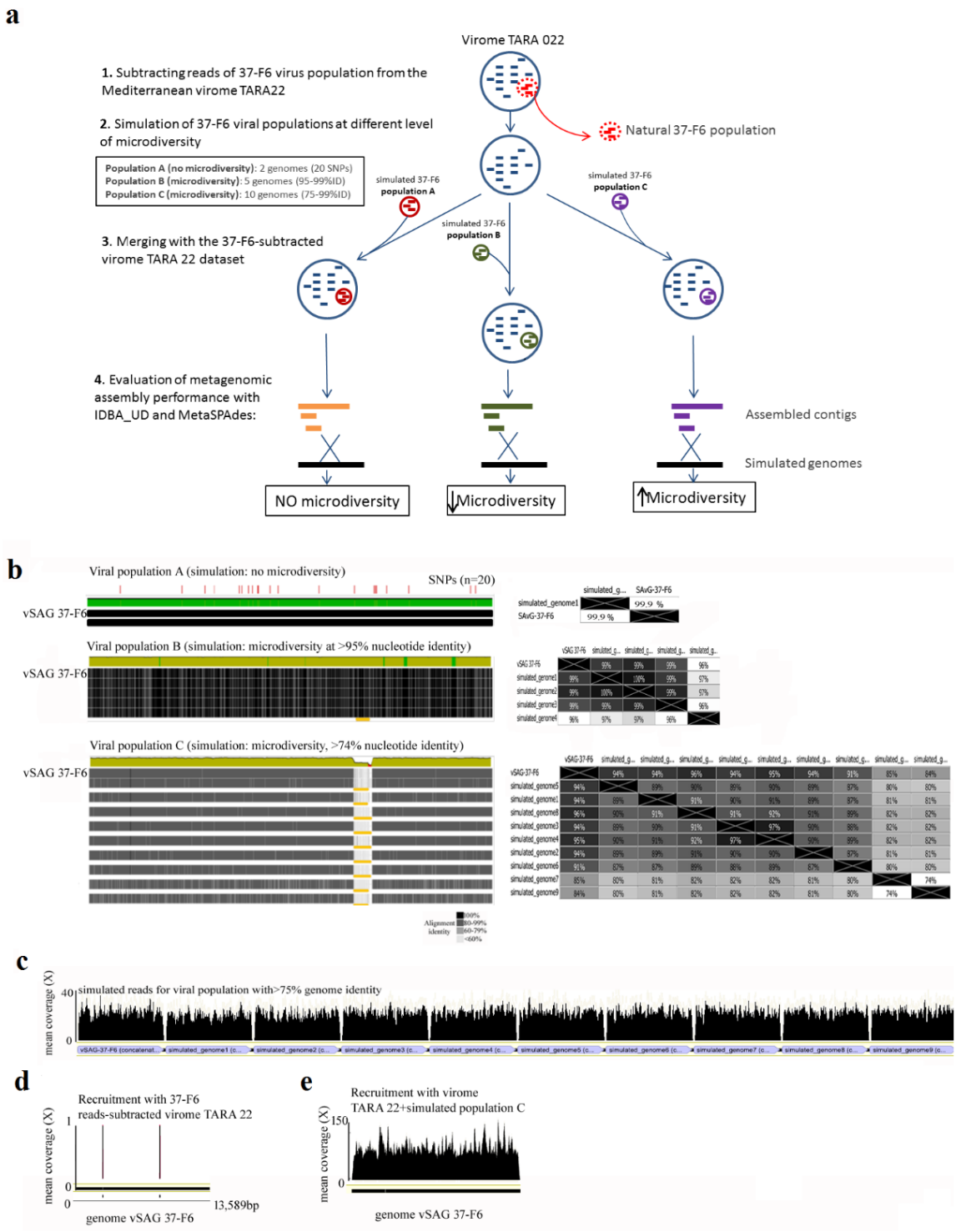

Supplementary Fig. 20. Employed methodology to assess the effect of (micro)-diversity on the metagenomics viral assembly (a) Schematic diagram illustrating the employed methodology to evaluate the metagenomic assembly performance of assemblers to reconstruct the viral genome from populations with different degrees of diversity and microdiversity within a natural virome. First, raw reads from vSAG 37-F6 were removed from *Tara* virome MS022 (see panel d). Then, simulated reads from the

three populations with different level of microdiversity were introduced within *Tara* virome MS022 (see panels b and c). **(b)** Three viral populations of vSAG 37-F6 were simulated (see Methods for details). Population A: no microdiversity; population B: low microdiverse; and population C: medium-high microdiverse. **(c)** For each population**,** Illumina raw reads were generated (see Methods) to simulate the viral populations. Read mapping of those simulated reads against the reference simulated genomes of vSAG at different microdiversity degrees confirmed that all genomes had at least a genome coverage of 40X. For convenience, only the simulation and mapping of reads is shown for the population C. **(d)** Reads corresponding for the vSAG population 37-F6 were removed from virome *Tara* MS022. **(e)** Mapping of simulated virome *Tara* MS022 with the introduced population C of vSAG 37-F6 confirmed that raw reads mapped with high coverage against the reference simulated genomes. For convenience, only data is shown for the population C.

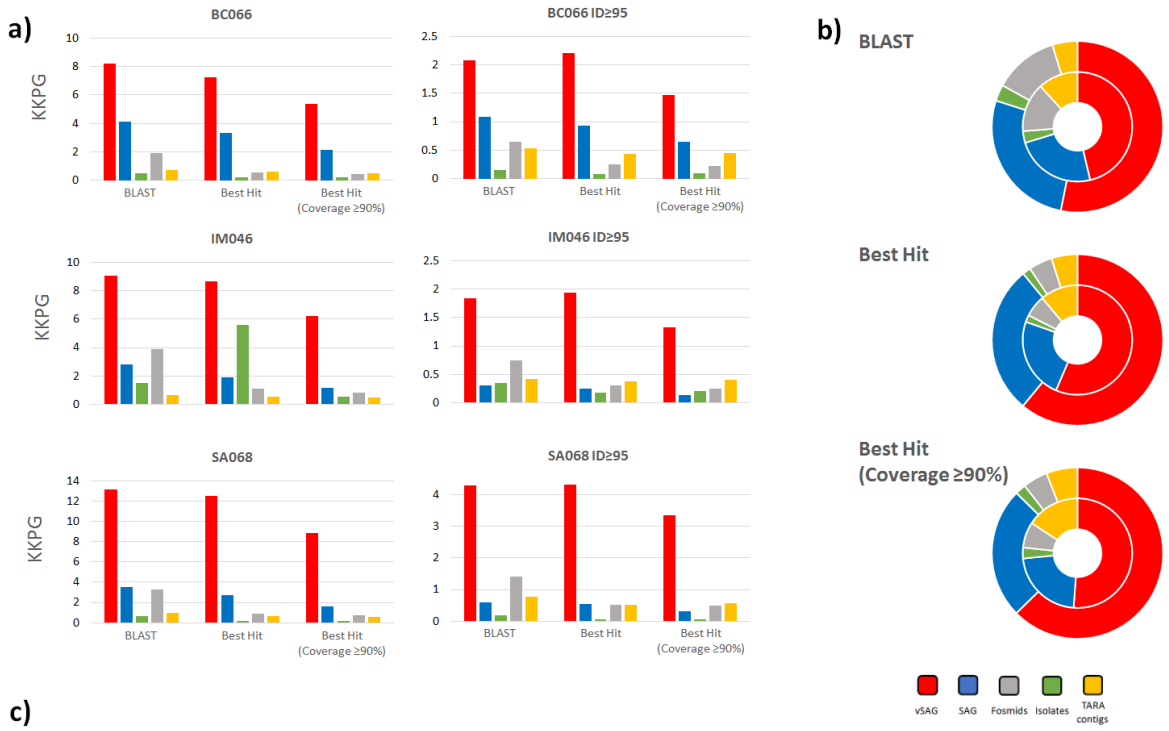

c)

	BC066			BC066 ID ≥ 95%		
	BLAST	Best Hit	Best Hit Cov ≥ 90%	BLAST	Best Hit	Best Hit Cov ≥ 90%
vSAG	8.223	7.221	5.39	2.085	2.206	1.473
SAG	4.148	3.323	2.127	1.08	0.935	0.642
Isolates	0.475	0.186	0.174	0.155	0.081	0.093
Fosmids	1.894	0.525	0.405	0.653	0.251	0.219
Tara Contigs	0.733	0.581	0.506	0.531	0.435	0.453

	IM046			IM046 ID ≥ 95%		
	BLAST	Best Hit	Best Hit Cov ≥ 90%	BLAST	Best Hit	Best Hit Cov ≥ 90%
vSAG	9.086	8.656	6.243	1.833	1.941	1.331
SAG	2.824	1.908	1.139	0.305	0.245	0.128
Isolates	1.518	5.571	0.543	0.343	0.183	0.202
Fosmids	3.862	1.081	0.822	0.751	0.304	0.25
Tara Contigs	0.663	0.55	0.469	0.413	0.375	0.403

	SA068			SA068 ID ≥ 95%		
	BLAST	Best Hit	Best Hit Cov ≥ 90%	BLAST	Best Hit	Best Hit Cov ≥ 90%
vSAG	13.166	12.519	8.839	4.297	4.322	3.362
SAG	3.499	2.729	1.627	0.602	0.543	0.312
Isolates	0.681	0.195	0.158	0.177	0.062	0.059
Fosmids	3.302	0.891	0.736	1.414	0.507	0.479
Tara Contigs	0.986	0.664	0.598	0.781	0.516	0.564

Supplementary Fig. 21. Comparison of different algorithms for matagenomic fragment recruitment. We compared the method that we used in our metagenomic fragment recruitment (**Fig. 2**) previously used by other authors[10] with the reciprocal-best hit fragment recruitment employed in the study of Pelagibacter phages[14]. Best-hit fragment recruitment was carried out with the Enveomics bioinformatic package (https://peerj.com/preprints/1900/) as described. Two fragment recruitment variants were also tested: without query coverage filtering and applying 90% of query coverage cut-off. **a)** Fragment recruitment with three different viromes are shown, Benguela Current (BC066), Indian Monsoon (IM046), and Southern Atlantic (SA068), using a 70% and 95% Identity cut-off. **b)** Relative fragment recruitment with Benguela Current virome (BC066). **c)** Data of the three recruitments. Overall, data indicate that no differences were observed among recruiter strategies.

Supplementary Tables

Supplementary Table 1. Sequencing results and assembly for the marine vSAGs

vSAG	Sample[α]	Treatment[β]	Contigs	GC%	Sequence Length (bp)
17-C23	1	A	17-C23-contig1	35.10	78,637
			17-C23-contig2	39.00	7,850
17-D16	1	A	17-D16	30.30	12,025
17-D19	1	A	17-D19-contig1	34.10	7,108
			17-D19-contig20	35.00	14,151
17-E11*	1	A	17-E11	36.30	6,957
17-E15	1	A	17-E15	34.60	33,035
17-F13	1	A	17-F13	38.40	33,869
17-F19	1	A	17-F19-contig1	36.30	15,706
			17-F19-contig2	35.80	2,525
			17-F19-contig3	35.90	2,236
17-G23	1	A	17-G23-contig1	32.40	7,276
			17-G23-contig2	32.60	11,351
37-D17	2	B	37-D17	34.20	8,248
37-F6*	2	B	37-F6	38.20	13,589
37-F16	2	B	37-F16	30.90	58,722
37-G23	2	B	37-G23	36.00	11,565
37-H5	2	B	37-H5-contig1	37.60	25,858
			37-H5-contig2	39.50	18,835
37-I21*	2	B	37-I21	36.10	31,959
37-J6	2	B	37-J6-contig1	33.70	23,751
			37-J6-contig2	32.80	6,530
37-K7	2	B	37-K7-contig1	35.10	2,871
			37-K7-contig2	35.90	10,586
			37-K7-contig3	37.80	8,957
			37-K7-contig4	35.00	8,189
37-K11	2	B	37-K11	34.50	13,098
37-L15*	2	B	37-L15-contig1	31.70	16,494
			37-L15-contig2	34.00	13,846
			37-L15-contig3	30.20	2,160
37-M8	2	B	37-M8	36.50	10,162
37-M19	2	B	37-M19	35.20	20,541
37-P14	2	B	37-P14	35.90	7,161
40-A23	2	B	40-A23	36.90	4,388
40-B17	2	B	40-B17	33.50	5,502
40-B18	2	B	40-B18	38.20	20,323
40-D19	2	B	40-D19	33.50	23,628
40-H15	2	B	40-H15	33.70	7,577
40-J13	2	B	40-J13	44.50	4,380

40-L14	2	B	40-L14	37.70	8,282
40-P19	2	B	40-P19	31.20	6,640
41-A4	2	C	41-A4-contig1	36.80	13,834
			41-A4-contig2	37.80	18,697
41-D7*	2	C	41-D7-contig1	32.60	24,030
			41-D7-contig2	34.00	14,432
41-D13	2	C	41-D13	32.80	6,045
41-H4	2	C	41-H4-contig1	28.50	36,279
			41-H4-contig2	29.60	17,198
			41-H4-contig3	29.20	10,721
41-H16	2	C	41-H16	39.20	11,145
41-H17	2	C	41-H17	35.50	6,664
41-I9	2	C	41-I9	31.20	4,913
41-I14	2	C	41-I14	36.20	28,554
41-I16	2	C	41-I16	34.10	7,028
41-I18	2	C	41-I18-contig1	36.30	8,360
			41-I18-contig2	34.20	8,389
41-O11	2	C	41-O11	37.20	14,512
80-3-I13	3	B	80-3-I13	36.60	22,966
30-E13	4	E	30-E13	44.50	37,588
30-J17	4	E	30-J17	32.90	17,011
88-3-L14	5	E	88-3-L14	37.20	12,924

*Two different sequencing were done, using Nextera and True Seq;

[α]Sample: 1=Mediterranean Sea, Barceloneta Beach; 2=Mediterranean Sea, Blanes Bay Microbial Observatory; 3=Mediterranean Sea DCM; 4=North Atlantic Ocean, Malaspina expedition sample 134; 5=North Atlantic Ocean, Malaspina expedition sample 131Treatment[β]: A=fixed sample+liquid N_2 and KOH (pH14) shock; B=unfixed sample+liquid N_2 and KOH (pH=14) shock; C=unfixed sample+KOH (pH=14) shock.; E=cryopreserved in GlyTE+treatment B

Supplementary Table 2: Relatedness of vSAGs with the Global Oceanic Viral Clusters [11] and tentative taxonomy prediction based on gene-content network analysis (see methods for details)

Sequence	vSAG	Closest VC (this study)	VC Size	GOV VC (Roux et al, 2016)	No. of GOV	No. of vSAGs	References	Order*	Family*	Genus*
17-C23-contig1	17-C23	VC_0078	34	VC_0434	20	2	12	Caudovirales (12)	Siphoviridae (12)	T5 like virus (8)
17-C23-contig2	17-C23									
17-D16	17-D16	VC_0234	8	VC_0446	7	1	0			
17-D19-contig1	17-D19	VC_0003	626	VC_0006	616	6	0			
17-D19-contig2	17-D19	VC_0003	626	VC_0006	616	6	0			
17-E11	17-E11	VC_0005	467	VC_0008	461	3	0			
17-E15	17-E15	VC_0408	4	VC_1116	3	1	0			
17-F13	17-F13	VC_0156	14	VC_0303	13	1	0			
17-F19-contig1	17-F19	VC_0013	205	VC_0019	199	5	1	Caudovirales (1)	Podoviridae (1)	
17-F19-contig2	17-F19	VC_0013	205	VC_0019	199	5	1			
17-F19-contig3	17-F19									
17-G23-contig1	17-G23	VC_0052	58	VC_0095	57	1	0			
17-G23-contig2	17-G23	VC_0158	14	VC_0281	13	1	0			
30-E13	30-E13	VC_0087	30	VC_0165	28	1	1	Caudovirales (1)	Siphoviridae (1)	
30-J17	30-J17	VC_0110	23	VC_0143	22	1	0			
37-D17	37-D17	VC_0002	678	VC_0005	665	7	5	Caudovirales (5)	Podoviridae (5)	
37-F16	37-F16	VC_0014	195	VC_0031	190	2	1	Caudovirales (1)	Myoviridae (1)	
37-F6	37-F6	VC_0005	467	VC_0008	461	3	0			
37-G23	37-G23	VC_0089	29	VC_0176	27	2	0			
37-H5-contig1	37-H5	VC_0013	205	VC_0019	199	5	1	Caudovirales (1)	Podoviridae (1)	
37-H5-contig2	37-H5	VC_0023	136	VC_0019	125	5	1	Caudovirales (1)	Podoviridae (1)	

37-I21	37-I21	VC_0078	34	VC_0434	20	2	12	Caudovirales (12)	Siphoviridae (12)	T5 like virus (8)
37-J6-contig1	37-J6	VC_0002	678	VC_0005	665	7	5	Caudovirales (5)	Podoviridae (5)	
37-J6-contig2	37-J6	VC_0002	678	VC_0005	665	7	5			
37-K11	37-K11	VC_0022	141	VC_0047	138	1	2	Caudovirales (1)	Podoviridae (1)	
37-K7-contig1	37-K7									
37-K7-contig2	37-K7	VC_0033	102	VC_0060	98	3	0			
37-K7-contig3	37-K7	VC_0023	136	VC_0019	125	5	1	Caudovirales (1)	Podoviridae (1)	
37-K7-contig4	37-K7	VC_0033	102	VC_0060	98	3	0			
37-L15-contig1	37-L15	VC_0013	205	VC_0019	199	5	1	Caudovirales (1)	Podoviridae (1)	
37-L15-contig2	37-L15	VC_0068	39	VC_0155	12	1	0			
37-L15-contig3	37-L15									
37-M19	37-M19	VC_0039	83	VC_0054	82	1	0			
37-M8	37-M8	VC_0027	123	VC_0067	80	1	0			
37-P14	37-P14	VC_0023	136	VC_0019	125	5	1	Caudovirales (1)	Podoviridae (1)	
40-A23	40-A23	VC_0003	626	VC_0006	616	6	0			
40-B17	40-B17	VC_0033	102	VC_0060	98	3	0			
40-B18	40-B18	VC_0017	168	VC_0029	167	1	0			
40-D19	40-D19	VC_0012	210	VC_0027	208	1	0			
40-H15	40-H15	VC_0000	1090	VC_0002	970	1	49	Caudovirales (48)	Myoviridae (45)	T4 like virus (18)
40-J13	40-J13	VC_0733	2		1	1	0			
40-L14	40-L14	VC_0003	626	VC_0006	616	6	0			
40-P19	40-P19	VC_0023	136	VC_0019	125	5	1	Caudovirales (1)	Podoviridae (1)	
41-A4-contig1	41-A4	VC_0005	467	VC_0008	461	3	0			
41-A4-contig2	41-A4	VC_0216	9	VC_0384	8	1	0			
41-D13	41-D13	VC_0701	2		1	1	0			

41-D7-contig1	41-D7	VC_0002	678	VC_0005	665	7	5	Caudovirales (5)	Podoviridae (5)
41-D7-contig2	41-D7	VC_0089	29	VC_0176	27	2	0		
41-H16	41-H16	VC_0023	136	VC_0019	125	5	1	Caudovirales (1)	Podoviridae (1)
41-H17	41-H17	VC_0003	626	VC_0006	616	6	0		
41-H4-contig1	41-H4	VC_0016	193	VC_0033	191	1	0		
41-H4-contig2	41-H4	VC_0014	195	VC_0031	190	2	1	Caudovirales (1)	Myoviridae (1)
41-H4-contig3	41-H4	VC_0001	751	VC_0003	750	1	0		
41-I14	41-I14	VC_0088	30	VC_0171	29	1	0		
41-I16	41-I16	VC_0002	678	VC_0005	665	7	5	Caudovirales (5)	Podoviridae (5)
41-I18-contig1	41-I18	VC_0013	205	VC_0019	199	5	1	Caudovirales (1)	Podoviridae (1)
41-I18-contig2	41-I18	VC_0267	7	VC_0525	6	1	0		
41-I9	41-I9	VC_0002	678	VC_0005	665	7	5	Caudovirales (5)	Podoviridae (5)
41-O11	41-O11	VC_0045	68	VC_0090	67	1	0		
80-3-I13	80-3-I13	VC_0002	678	VC_0005	665	7	5	Caudovirales (5)	Podoviridae (5)
88-3-L14	88-3-L14	VC_0003	626	VC_0006	616	6	0		

*Taxonomic affiliation of vSAG at the level of Family or Order is tentative and has to be taken very cautious since there is no experimental proof

Supplementary Table 3. Comparison at the population level of the single-viruses with viral clusters obtained in the Global Ocean Virome (GOV) dataset[11]

vSAG	Putative assignment[α]	VC_2	VC_3	VC_5	VC_6	VC_8	VC_9
17-D16	VC6				**52**		
17-D19	VC6				**184**	11	
17-E11	VC8				35	**236**	
37-D17	VC5			345			
37-J6	VC5			**1041**			
37-K11	VC5	9		**121**	4	4	19
37-F6	VC8				59	**413**	
40-A23	VC6				**10**		
40-B18	VC5			**15**			
40-H15	VC2	**10**					
40_L14	VC6				**89**		
41-A4	VC8				89	**566**	
41-D7	VC5		37	**1162**			
41-H17	VC6				**11**	1	
41-H4	VC3	2	**40**	8			
41-I14	VC2	171	1				
41-I16	VC5			**236**			
41-I9	VC5			**146**			
41-O11	VC2	92	9	1			

[α]Assignment was done based on genomic comparison by BLASTn against all bins and viral contigs in the GOV dataset. Only hits with GOV dataset with the following criteria were considered for assignment: bitscore threshold hit>100, sequence alignment length>500 bp, >10 hits spanning the genome and ≥80% of hits accumulated within the same VC. Alignment mean identity of hits with viral contigs/bins of VC was ≈70%. vSAGs not listed in the table showed an uncertain assignment

Supplementary Table 4. Pairwise BLASTp comparison of vSAG with the closest virus in the global marine viral clusters (VCs) based on protein-sharing network analysis.

vSAG	vSAG (contig)* - Closest virus in VC	No. of shared proteins	No. of total vSAG genes	%Pairwise	Putative new species (NS) or new genera (NG)[β]
vSAG-17-C23	GOV_bin_5106_contig-100_0	25	116	48.60	NS
vSAG-17-D16	GOV_bin_1735_contig-100_0	15	19	62.56	NS
vSAG-17-D19	Contig 1- Tp1_123_SUR_0-0d2_scaffold29973_1 Contig 2- Tp1_123_DCM_0-0d2_scaffold46460_2	8 11	11 16	55.00 56.45	NS
vSAG-17-E11	GOV_bin_2164_contig-100_0	3	11	56.00	NS
vSAG-17-E15	GOV_bin_4005_contig-100_0	10	35	38.70	NS
vSAG-17-F13	GOV_bin_870_contig-100_1	11	14	56.69	NS
vSAG-17-F19	Contig 1-Tp1_30_DCM_0-0d2_scaffold60669_1 Contig 2-GOV_bin_534_contig-100_2 Contig 3-*No Closest*	16 5 0	20 5 3	99.73 56.96 ---	NS
vSAG-17-G23	Contig 1-Tp1_23_DCM_0-0d2_scaffold128056_1 Contig 2-Tp1_23_DCM_0-0d2_scaffold112175_1	7 11	10 13	59.93 52.85	NS
vSAG-30-E13	GOV_bin_636_contig-100_5	6	31	41.50	NS
vSAG-30-J17	GOV_bin_8033_contig-100_1	7	11	56.00	NS
vSAG-37-D17	GOV_bin_3340_contig-100_6	8	11	67.36	NG
vSAG-37-F16	vSAG-41-H4-contig2	15	54	69.67	NS
vSAG-37-F6	SAG AAA164-I21-contig 5	18	24	65.16	NS
vSAG-37-G23	GOV_bin_4091_contig-100_8	14	18	60.30	NS
vSAG-37-H5	Contig 1-GOV_bin_1874_contig-100_1 Contig 2-Tp1_30_DCM_0-0d2_scaffold21665_1	19 16	36 27	56.07 61.41	NS
vSAG-37-I21	Tp1_82_SUR_0-0d2_scaffold12183_1	18	35	47.69	NS
vSAG-37-J6	Contig 1-Tp1_36_DCM_0-0d2_scaffold99746_1 Contig 2-GOV_bin_3099_contig-100_0	18 6	34 6	69.97 37.58	NS
vSAG-37-K11	Tp1_102_SUR_0-0d2_scaffold55818_1	5	17	72.44	NS
vSAG-37-K7	Contig 1- *No Closest* Contig 2- GOV_bin_5817_contig-100_0 Contig 3- GOV_bin_4362_contig-100_0 Contig 4- Tp1_32_SUR_0-0d2_scaffold63617_1	0 5 8 5	11 6 11 12	--- 42.08 64.80 61.26	NG
vSAG-37-L15	Contig 1-GOV_bin_3005_contig-100_2 Contig 2-Uncultured_Mediterranean_phage_uvMED_AP014493 Contig 3-*No Closest*	5 10 0	37 20 2	52.64 55.71 ---	NS
vSAG-37-M19	GOV_bin_2674_contig-100_1	27	37	79.50	NS

vSAG-37-M8	Tp1_100_DCM_0-0d2_scaffold6111_1	14	22	74.10	NS
vSAG-37-P14	Tp1_123_DCM_0-0d2_scaffold44431_1	6	6	46.58	NG
vSAG-40-A23	Tp1_111_DCM_0-0d2_scaffold17799_1	8	10	70.46	NS
vSAG-40-B17	Tp1_111_DCM_0-0d2_scaffold53353_1	13	15	75.85	NG
vSAG-40-B18	Tp1_31_SUR_0-0d2_scaffold205369_1	21	29	61.56	NS
vSAG-40-D19	GOV_bin_4866_contig-100_1	14	36	53.90	NS
vSAG-40-H15	Uncultured_Mediterranean_phage_uvMED_AP014348	7	8	62.63	NS
vSAG-40-J13	GOV_bin_8324_contig-100_4	5	10	88.68	NS
vSAG-40-L14	vSAG-17-D19-contig1	8	12	53.43	NS
vSAG-40-P19	Tp1_124_SUR_0-0d2_scaffold12109_4	4	18	65.23	NS
vSAG-41-A4	Contig 1-GOV_bin_4626_contig-100_1 Contig 2- GOV_bin_2910_contig-100_1	22 17	34 29	55.80 49.59	NS
vSAG-41-D13	GOV_bin_6709_contig-100_0	7	14	60.84	NG
vSAG-41-D7	Contig 1-GOV_bin_2729_contig-100_2 Contig 2- GOV_bin_7344_contig-100_5	14 10	31 20	56.44 67.00	NS
vSAG-41-H16	Tp1_125_DCM_0-0d2_scaffold6988_1	7	7	58.06	NS
vSAG-41-H17	Uncultured_Mediterranean_phage_uvMED_AP014380	13	19	65.05	NS
vSAG-41-H4	Contig 1-GOV_bin_3401_contig-100_0 Contig 2-vSAG-37-F16 Contig 3- GOV_bin_5740_contig-100_6	20 15 9	39 20 14	56.89 68.81 55.29	NS
vSAG-41-I14	Tp1_102_DCM_0-0d2_scaffold2867_3	24	47	70.58	NS
vSAG-41-I16	GOV_bin_3340_contig-100_6	5	9	55.43	NS
vSAG-41-I18	Contig 1-Tp1_22_SUR_0-0d2_scaffold30721_1 Contig 2- GOV_bin_3845_contig-100_3	5 5	10 10	45.92 78.06	NG
vSAG-41-I9	Tp1_66_SUR_0-0d2_scaffold28495_4	4	4	68.88	NS
vSAG-41-O11	GOV_bin_4674_contig-100_0	14	27	58.72	NS
vSAG-80-3-I13	GOV_bin_2729_contig-100_2	16	22	58.86	NS
vSAG-88-3-L14	Tp1_25_DCM_0-0d2_scaffold2249_3	5	15	54.28	NG
MEAN		**11.29**	**20.73**	**60.38**	

*In case two or more genome fragments (viral contig) were obtained from the vSAG, the closest viral genome in database is indicate

[β] Although application of viral taxonomy criteria to define viral species and genera remains complicated to uncultured viruses, in this study we have used the following criteria based on a previous study[4]. New genera are defined when the vSAGs presented weaker connections with closest viral relatives within the global marine viral network, as previously described[4]. New viral species are defined when ≤95% of nucleotide identity was obtained with the closest viral relative.

Supplementary Table 5. Ranking of the first most recruiter viruses at different cut-off identities (70 and 95%) in different oceanic regions[7,11,15,16] for each viral datasets (single-viruses, fosmids[10], virus isolates (Supplementary Table 9), viruses from microbial single amplified genomes (SAGs) cells[9], viral genomes reconstructed by viromics from *Tara* Ocean Viromes (TOV)[7] and Global Ocean Viromes (GOV)[11])

Viral genome dataset[±]	vSAG 37-F6[£]		vSAG		SAGs		Fosmids		Isolates		TOV		GOV	
ID %	70	95	70	95	70	95	70	95	70	95	70	95	70	95
VIROME*														
SS	**1**	55	**1**	14	67	652	5	7	8	6	7	**1**	2	3
POV	3	15	3	15	8	14	**1**	**1**	20	18	10	2	11	26
BBMO	24	99	**1**	7	134	268	3	**1**	18	18	122	24	2	12
CP109	6	18	6	17	76	172	10	24	205	140	32	2	**1**	**1**
MS018	66	369	66	91	145	398	**1**	**1**	14	59	25	9	113	74
MS022	7	62	7	58	55	358	**1**	4	16	29	11	3	10	**1**
MS025	**1**	2	**1**	2	10	115	5	**1**	32	65	38	14	4	3
RS031	**1**	7	**1**	7	61	839	2	4	87	196	9	**1**	5	2
RS032	**1**	18	**1**	18	83	823	3	14	49	36	5	2	2	**1**
RS034	6	26	6	26	38	115	8	3	**1**	**1**	37	13	2	2
NAS036	238	631	238	631	35	128	9	26	2	10	7	3	**1**	**1**
IM038	41	215	41	67	45	292	**1**	**1**	16	18	26	6	18	12
IM039	39	111	39	63	121	665	**1**	**1**	55	51	72	30	60	34
IM041	**1**	2	**1**	2	30	158	3	**1**	130	112	10	8	7	10
IM042	**1**	2	**1**	2	38	216	2	**1**	171	96	19	3	9	29
IM046	**1**	10	**1**	10	79	597	2	3	161	235	36	5	9	**1**
EA064	**1**	2	**1**	**1**	29	551	5	3	16	4	9	6	4	7
EA065	8	58	8	29	160	733	**1**	**1**	37	15	67	4	9	43
BC066	**1**	5	**1**	5	7	55	10	36	51	81	5	2	2	**1**
BC067	81	688	16	55	9	17	**1**	10	49	47	3	**1**	43	20
SA068	**1**	**1**	**1**	**1**	15	356	6	3	52	234	40	5	4	2
SA070	**1**	3	**1**	3	40	347	3	8	30	31	28	5	6	**1**
SA072	**1**	6	**1**	5	30	477	4	20	168	185	10	**1**	5	2
SA076	**1**	3	**1**	3	24	514	7	19	42	118	5	**1**	4	14

[£]Two first columns are for the vSAG 37-F6, which is the most recruiter virus in 13 of the 24 viromes and in the global marine virome. *Viromes used are abbreviated as: Pacific Ocean (POV), Chile-Peru oceanic region (CP), South Atlantic (SS), Red Sea (RS), Mediterranean Sea (MS), Northwest Arabian Sea upwelling (NAS), Indian Monsoon gyre province (IM), Eastern Africa Coastal Province (EA), Benguela Current (BC), and Sargassos Sea (SS), and the Blanes Bay Microbial Observatory Virome (BBMO) which was constructed in this study. [±]Viral genomic dataset used were: 40 marine surface vSAGs (this study), SAGs: 20 viral genomes from uncultured single bacterial cells; Isolates: 180 reference marine virus isolates (Supplementary Table 9), Fosmids: 1148 viral fosmids; TOV: 5466 viral contigs from the *Tara* expedition; and GOV: 3594 sequences from the cosmopolitan viral clusters previously described (VCs 2,3,5,6,8 and 9)[11].

Supplementary Table 6. Comparison by BLASTn of genome of vSAG 37-F6 with the previously described viral cluster 8 (VC_8; in this study VC_2)[11]*

Name	Bit-Score	Pairwise Identity	E Value	Hit end	Hit start	Query end	Query start
unknown_gi_486908286 (SAG AAA164-I21)	1353.81	70	0	612	3610	13588	10602
unknown_gi_486908286 (SAG AAA164-I21)	1142.82	76	0	8279	9887	5065	3480
Flavobacteriia_gi_487372893 (SAG AAA160-P02)	1092.32	72	0	32034	29947	12683	10605
GOV_bin_5468_contig-100_39	966.089	71	0	4638	2613	12620	10604
GOV_bin_2346_contig-100_4	933.628	71	0	1790	3825	12620	10603
GOV_bin_2164_contig-100_0	904.774	70	0	4841	6998	12975	10824
Flavobacteriia_gi_487372893 (SAG AAA160-P02)	839.853	72	0	25190	23594	5070	3479
GOV_bin_4626_contig-100_1	791.162	72	0	7594	6024	5082	3517
GOV_bin_2346_contig-100_4	751.488	71	0	8610	10209	5078	3483

*Only top ten best hits are shown

Supplementary Table 7. Comparison of metaproteomic data from the Oregon coast bacterioplankton[13] to our surface vSAG.

Peptide name[α]	Amino acid sequence	vSAG[β]
8431	YTVYKNPYMTENVILMGYK	37-F16
6640	TAMEGDFDTGNVR	37-F6
6420	SQLVKELEPGLNALFGLEYK	37-F6
5051	MIIPSELQFTAER	37-F6
4982	MFNRAPLTTAMEGDFDTGNVR	37-F6
1627	ELEPGLNALFGLEYK	37-F6
6422	SQLVKELEPGLNALFGLEYKR	37-F6
2780	QLVKELEPGLNALFGLEYK	37-F6
6706	TETYRDPDSFADIVR	37-H5 contig 2
7662	VLLCDEFATPAVSK	37-I21
4739	LSGEIGQVFGSR	37-I21
4493	LISQSYLGNETEEDAIMPILPLIR	37-I21
4022	KLISQSYLGNETEEDAIMPILPLIR	37-I21
3356	IGFTDLIDGATSK	37-I21
2454	GIENAILAGDDADGVYGTSGAAFEGLLHLAR	37-I21
1336	DIENELVLAPLFR	37-I21
5495	NLDKQGAIEENMLFLSR	37-J6 contig 1
5295	MVGAEMPMTSDQVIWSEQNR	37-J6 contig 1
4530	LLDEQNIPEEGR	37-K7 contig 3
4739	LSGEIGQVFGSR	37-M19
6387	SPIKTSMEGDFDTGNVR	41-A4 contig 1
5608	NQLVKELEPGLNALFGLEY	41-A4 contig 1
2780	QLVKELEPGLNALFGLEY	41-A4 contig 1
1627	ELEPGLNALFGLEY	41-A4 contig 1
912	QLVKELEPGLNALFGLEY	41-A4 contig 1
3786	ITGFADMIQLTHLK	41-D7 contig 1
2932	GVIVPAGTSTVYDQQLGK	41-D7 contig 1
6666	TASGISMLMSAANGSIR	41-H16
8431	YTVYKNPYMTENVILMGYK	41-H4 contig 2

[β]tBLASTx comparison was done and only those peptides matching 100% identity and coverage were considered
[α]Peptide name nomenclature was as in the original article[13]. A total of 7151 distinct peptide sequences were obtained in that study.

Supplementary Table 8. Primers of vSAG 37-F6.

Primer pair	Name	Sequence	Minimum	Maximum	Length	Direction	Expected size
1	37F6_78 F	ACGGGTCCAACTGAACATCC	78	97	20	forward	639
1	37F6_716 R	TAGCAGAGGATGGGTCAGCT	697	716	20	reverse	
2	37F6_697 F	AGCTGACCCATCCTCTGCTA	697	716	20	forward	1062
2	37F6_1,758 R	TGTGGTTTCGGGTGATGGAG	1,739	1,758	20	reverse	
3	37F6_697 F	AGCTGACCCATCCTCTGCTA	697	716	20	forward	1166
3	37F6_1,862 R	TGGTAATGCAGGCGTCCTTT	1,843	1,862	20	reverse	
4	37F6_4,647 F	GCATCCTCTGATCCTGCTCC	4,647	4,666	20	forward	788
4	37F6_5,434 R	AGAACACAGGCTGAACCGAG	5,415	5,434	20	reverse	
5	37F6_6,849 F	TCCGACTGTATCACTCGGGT	6,849	6,868	20	forward	818
5	37F6_7,666 R	AGGTGGTGGACTGTGCAAAA	7,647	7,666	20	reverse	

Supplementary Table 9. Marine virus isolates used for fragment recruitment analyses. Genomes were obtained from Joint Genome Institute. All viruses labelled as marine origin were considered (as of date 21st, January, 2016).

Genome name IMG-JGI / Genbank ID	Number of genes	Sequence Length (bp)
Bacteriophage 11b: NC_006356	65	36012
Bacteriophage K139: NC_003313	44	33106
Bacteriophage S-PM2 virion: NC_006820	264	196280
Bacteriophage Syn9 virus: NC_008296	235	176847
Bacteriophage VfO3K6: NC_002362	10	8784
Bacteriophage VfO4K68: NC_002363	8	6891
Cellulophaga phage phi10:1 / NC_021802	108	53664
Cellulophaga phage phi12:1 / NC_021791	64	39148
Cellulophaga phage phi12:2 / NC_021797	13	6453
Cellulophaga phage phi12a:1 / NC_021805	13	6478
Cellulophaga phage phi13:2 / NC_021803	128	72369
Cellulophaga phage phi14:2 / NC_021806	133	100418
Cellulophaga phage phi17:1 / NC_021795	65	38776
Cellulophaga phage phi17:2 / NC_021798	221	145343
Cellulophaga phage phi18:1 / NC_021790	65	39189
Cellulophaga phage phi18:3 / NC_021794	123	71443
Cellulophaga phage phi19:1 / NC_021799	118	57447
Cellulophaga phage phi3:1 / Ga0039577_11	36	22893
Cellulophaga phage phi38:1 / NC_021796	117	72534
Cellulophaga phage phi39:1 / NC_021804	48	28760
Cellulophaga phage phi4:1 / NC_021788	221	145865
Cellulophaga phage phi46:1 / NC_021800	54	34844
Cellulophaga phage phi46:3 / NC_021792	121	72961
Cellulophaga phage phi47:1 / HQ670749	81	60552
Cellulophaga phage phi48:2 / NC_021793	29	11703
Cellulophaga phage phiSM / HQ317392	59	44557
Cellulophaga phage phiST / Ga0040773_11	109	79114
Cyanophage 9515-10a / Ga0034026_11	62	47055
Cyanophage KBS-P-1A / Ga0032521_11	63	45730
Cyanophage KBS-S-1A / Ga0032522_11	60	32402
Cyanophage KBS-S-2A / Ga0039582_11	62	40658
Cyanophage MED4-117 / Ga0039388_11	66	38834
Cyanophage NATL1A-7 / Ga0034027_gi310005689.1	74	47741
Cyanophage NATL2A-133 / Ga0034029_gi310005755.1	73	47536
Cyanophage P60: NC_003390	80	47872
Cyanophage PP / NC_022751	41	42480
Cyanophage P-RSM1 / HQ634175	215	177211
Cyanophage P-RSM3 / HQ634176	211	178750

Cyanophage P-RSM6 / Ga0040776_11	229	192497
Cyanophage P-SS1 / Ga0040801_11	223	178284
Cyanophage PSS2 / GU071090	122	105532
Cyanophage PSS2: NC_013021	131	107530
Cyanophage P-SSM2: NC_006883	330	252401
Cyanophage P-SSM4: NC_006884	198	178249
Cyanophage P-SSP2 / Ga0034028_gi310005818.1	59	45890
Cyanophage P-SSP7: NC_006882	53	44970
Cyanophage SS120-1 / HQ316584	53	46997
Cyanophage S-SSM2 / Ga0032571_11	209	179980
Cyanophage S-SSM6a / HQ317391	311	232883
Cyanophage S-SSM6b / HQ316603	221	182368
Cyanophage S-TIM5 / NC_019516	190	161440
Cyanophage Syn10 / Ga0040497_11	219	177103
Cyanophage Syn2 / Ga0032453_11	218	175596
Cyanophage Syn30 / Ga0032525_11	225	178807
Cyanophage Syn5: NC_009531	61	46214
Emiliania huxleyi virus 86	477	407339
Flavobacterium phage 6H / NC_021867	63	46978
Marine bacteriophage RNA virus SOG	3	4449
Marine birnavirus - AY-98 VP1 / AY123970.1	1	2778
Marine gokushovirus	6	4129
Marine RNA virus JP-A	2	9236
Marine RNA virus JP-B	2	8926
Marinomonas phage P12026	54	31766
Ostreococcus lucimarinus virus OlV1	255	194022
Ostreococcus lucimarinus virus OlV3	265	191242
Ostreococcus lucimarinus virus OlV5	265	186468
Ostreococcus tauri virus 1	232	191761
Ostreococcus tauri virus 2	237	184409
Ostreococcus virus OsV5	269	185373
Paracoccus phage vB_PmaS_IMEP1 / Ga0062596_vB_PmaS_IMEP1.1	55	42093
Pelagibacter phage HTVC008M / NC_020484	198	147284
Pelagibacter phage HTVC010P / NC_020481	64	34892
Pelagibacter phage HTVC011P / NC_020482	45	39921
Pelagibacter phage HTVC019P / NC_020483	59	42084
Prochlorococcus phage MED4-184 / Ga0032523_11	65	38327
Prochlorococcus phage MED4-213 / HQ634174	218	180977
Prochlorococcus phage P-GSP1 / HQ332140	53	44945
Prochlorococcus phage P-HM1: NC_015280	241	181044
Prochlorococcus phage P-HM2: NC_015284	242	183806
Prochlorococcus phage P-RSM4: NC_015283	242	176428

Prochlorococcus phage P-RSP2 / HQ332139	48	42257
Prochlorococcus phage P-SSM2 / GU071092	332	252407
Prochlorococcus phage P-SSM3 / Ga0032395_11	231	179063
Prochlorococcus phage P-SSM5 / HQ632825	331	252013
Prochlorococcus phage P-SSM7: NC_015290	241	182180
Prochlorococcus phage P-SSP10 / Ga0039583_11	61	47325
Prochlorococcus phage P-SSP3 / HQ332137	56	46198
Prochlorococcus phage P-SSP7 / GU071093	52	45135
Prochlorococcus phage Syn1: NC_015288	240	191195
Prochlorococcus phage Syn33: NC_015285	232	174285
Pseudoalteromonas phage PSA-HS4 (complete) / Ga0074570_11	68	38739
Puniceispirillum phage HMO-2011	43	52512
Roseobacter phage RDJL Phi 1: NC_015466	87	62668
Roseophage SIO1: NC_002519	34	39898
Synechococcus phage KBS-M-1A / Ga0039581_11	226	171744
Synechococcus phage metaG-MbCM1 / NC_019443	234	172879
Synechococcus phage S-CAM1 / HQ634177	241	198013
Synechococcus phage S-CAM8 / Ga0039739_11	277	222057
Synechococcus phage S-CAM8 / HQ634178	209	171407
Synechococcus phage S-CBM2 / HQ633061	212	180892
Synechococcus phage S-CBP2 / Ga0032396_11	137	92473
Synechococcus phage S-CBP3 / HQ633062	57	47375
Synechococcus phage S-CBP4 / Ga0039743_11	57	41824
Synechococcus phage S-CBS1 / Ga0035795_11	47	30332
Synechococcus phage S-CBS2: NC_015463	102	72332
Synechococcus phage S-CBS3: NC_015465	46	33004
Synechococcus phage S-CBS4 / Ga0035827_gi374531742.1	108	69420
Synechococcus phage S-CBS4 / HQ634148	167	105580
Synechococcus phage S-CRM01: NC_015569	330	178563
Synechococcus phage S-IOM18 / HQ317383	219	171797
Synechococcus phage S-MbCM6 / NC_019444	225	176043
Synechococcus phage S-RIM2 R1_1999 / HQ317292	216	175430
Synechococcus phage S-RIM2 R21_2007 / HQ317290	214	175430
Synechococcus phage S-RIM2 R9_2006 / HQ317291	217	175419
Synechococcus phage S-RIM8 A.HR1 / Ga0039740_gi375918176.1	225	171211
Synechococcus phage S-RIM8 A.HR3 / Ga0032513_gi375919032.1	225	171211
Synechococcus phage S-RIM8 A.HR5 / HQ317385	211	168327
Synechococcus phage S-RIP1 / HQ317388	61	44892
Synechococcus phage S-RIP2 / HQ317389	57	45728
Synechococcus phage S-RSM4: NC_013085	249	194454
Synechococcus phage S-ShM2: NC_015281	231	179563

Synechococcus phage S-SKS1 / HQ633071	302	208007
Synechococcus phage S-SM1: NC_015282	240	174079
Synechococcus phage S-SM2: NC_015279	278	190789
Synechococcus phage S-SSM4 / HQ316583	223	182801
Synechococcus phage S-SSM5: NC_015289	229	176184
Synechococcus phage S-SSM7: NC_015287	324	232878
Synechococcus phage Syn19: NC_015286	221	175230
Vibrio cholerae filamentous bacteriophage fs-2: NC_001956	9	8651
Vibrio cholerae O139 fs1 phage: NC_004306	15	6340
Vibrio cholerae phage KSF-1phi virus: NC_006294	12	7107
Vibrio cholerae phage VGJphi virion: NC_004736	13	7542
Vibrio harveyi bacteriophage VHML: NC_004456	57	43198
Vibrio phage 11895-B1 / Ga0040774_11	206	126434
Vibrio phage CP-T1 / NC_019457	70	44492
Vibrio phage CTX chromosome I: NC_015209	13	10638
Vibrio phage douglas 12A4 / HQ316580	75	57611
Vibrio phage eugene 12A10 / HQ634195	253	138234
Vibrio phage helene 12B3 / HQ316579	265	135982
Vibrio phage henriette 12B8 / HQ316582	156	107218
Vibrio phage ICP1: NC_015157	230	125956
Vibrio phage ICP2: NC_015158	72	49675
Vibrio phage ICP3: NC_015159	54	39162
Vibrio phage JA-1 / NC_021540	80	69278
Vibrio phage jenny 12G5 / HQ632860	75	40557
Vibrio phage kappa: NC_010275	45	33134
Vibrio phage KVP40: NC_005083	410	244834
Vibrio phage martha 12B12 / HQ316581	51	33277
Vibrio phage N4: NC_013651	47	38497
Vibrio phage nt-1 / HQ317393	405	247511
Vibrio phage pVp-1 / NC_019529	157	111506
Vibrio phage PWH3a-P1 / Ga0039735_11	216	129155
Vibrio phage pYD21-A / Ga0032403_11	75	46917
Vibrio phage pYD38-A / Ga0032404_11	76	47552
Vibrio phage pYD38-B / Ga0040529_11	60	37324
Vibrio phage SIO-2 / HQ316604	116	81184
Vibrio phage vB_VchM-138 / NC_019518	67	44485
Vibrio phage vB_VpaM_MAR / NC_019722	62	41351
Vibrio phage vB_VpaS_MAR10 / NC_019713	107	78751
Vibrio phage VBM1 / HQ317386	56	38374
Vibrio phage VBP32 / Ga0032561_11	117	76718
Vibrio phage VBP47 / Ga0040770_11	119	76705
Vibrio phage VBpm10 / Ga0039578_11	62	33314

Vibrio phage VCY-phi / Ga0036010_11	11	7103
Vibrio phage VD1 / Ga0032407_11	116	81013
Vibrio phage VEJphi: NC_012757	11	6842
Vibrio phage Vf12: NC_005949	7	7965
Vibrio phage Vf33: NC_005948	7	7965
Vibrio phage VFJ / NC_021562	12	8555
Vibrio phage VP882: NC_009016	71	38197
Vibrio phage VP93: NC_012662	44	43931
Vibrio phage VPMS1 / NC_021776	53	42313
Vibrio phage VPUSM 8 / NC_022747	43	34145
Vibrio phage VSK: NC_003327	14	6882
Vibriophage VP2: NC_005879	47	39853
Vibriophage VP4: NC_007149	31	39503
Vibriophage VP5: NC_005891	48	39786
Vibriophage VpV262: NC_003907	67	46012
Yellowtail ascites virus strain AY-98 segment A / AY283785	2	3092

Supplementary Notes

Supplementary Note 1: Fluorescence activated virus sorting (FAVS) and whole genome amplification (WGA): some technical considerations

Viruses are sorted at random, which means that the more abundant a virus is in the sample the higher is the probability to be sorted and deposited in a 384-well plate, and thus, is directly proportional to its abundance. Assuming that the treatment to break capsids is effective to most naturally co-occurring viruses, in theory, with a low sequencing effort, SVGs guarantees the recovering of genetic information of prevalent viral components. Furthermore, as sequencing costs has dropped dramatically in the last five years along with new inexpensive multiplexed libraries strategies[17] and the fact that the sequencing coverage for a virus is significantly less than for a single-cell, genome recovery of low abundant viruses by increasing the number of positive vSAGs selected for sequencing should be feasible.

Supplementary Note 2: Evaluation of free DNA content in microdroplets from seawater

Initially, the interference of free DNA present in seawater that could be co-sorted along with single-viruses and amplified during WGA was assessed (see methods), but data indicated that its potential contribution was negligent (Supplementary Fig. 4d-e) since only two wells from a 384-well plate yielded positive amplification.

Supplementary Note 3: Gene-content based network analysis of marine vSAGs

Of the 61 marine vSAG sequences, 57 were retained in the network and 4 (17-C23-contig2, 17-F19-contig3, 37-K7-contig1, 37-L15-contig3) were excluded, due to few significant similarities to other sequences in the dataset. In cases where a vSAG consisted of several sequences (e.g. 17-F19, 37-K7, 41-H4), vSAG fragments were mostly associated within the same viral clusters (VCs) in GOV[11], expect in some cases where small contigs were obtained along with the large genome fragment, such as the vSAG 17-F19-contig1 (15,706 bp) and contig2 (2,525 bp) that were related to members of VC13, whereas contig3 (2,236 bp) was not found within that network. In cases where disagreements exist, it is highly likely that each sequence fragment carries a different set of gene sequences less related to genes on its sister fragment than to genes present on sequences in separate VCs. The 57 sequences were related to a total of 31 VCs. The VCs ranged in size from 2 (VC_733) to 1090 (VC_0), with most vSAGs associated with large (>100 sequence) VCs. The 19 vSAGs identified through comparison using BLASTn (Supplementary Table 4) covered 14 of the GOV-associated VCs. Disagreements between the BLASTn and network analysis could arise from the differences in approaches, where BLASTn tends to reveal highly related sequences though pairwise relationships whereas the gene-based method allows for sequences to associate with multiple others, with sequences sharing the greatest proportion of genes being placed within the same cluster. In general, the larger the VC the more likely it contained a GOV-associated VC and agreed with BLAST. Due to the inclusion of archaeal and bacterial viruses from NCBI RefSeq, preliminary taxonomic predictions could be made in the context of reference sequences within each VC. Tentative affiliations could only be made for 24 of the 57 sequences (21 vSAGs) due to the lack of any reference sequence within

the VCs (Supplementary Table 3). All taxonomic predictions were of the *Caudovirales*, with 18 sequences (15 vSAGs) classified in the *Podoviridae* family, 3 sequences (3 vSAGs) as *Myoviridae* and 3 sequences (3 vSAGs) as *Siphoviridae*. The overall prediction quality of all but 2 sequences (17-C23-contig1, 30-E13) were low, as most of the VCs containing reference sequences were supported by 1-2 references within VCs containing 130 to over 200 sequences. The strongest support was for vSAG 17-C23-contig1 and 30-E13, both members of VC_78 and likely T5-like viruses.

Supplementary Note 4: Virome recruitment of marine single amplified viral genomes (vSAGs)

In this study, with 44 surface vSAGs that added up to ≈1 Mb of genomic assembled dataset (<5 million raw reads), we have unveiled the genome of superabundant uncultured viruses with very high virome recruitment frequencies. In the *Tara* virome survey[7], with 5,476 viral contigs (109 Mb of assembled genome data and 2,16 billion raw reads) recruited up to 9.97%[7]. However, after normalization of recruitment rate according to total assembled genomic data, 1 Mb of single-virus genomic data would recruit ≈3.5-fold more than data obtained by viromics (Supplementary Fig. 13). Finally, the overall sequencing effort carried out here to deliver 44 reference genomes compared to previous viromic surveys[7] was significantly less, at least a 3-fold decrease.

Supplementary Note 5: Structure of marine viral populations. Microdiversity matters for metagenomic assembly: the diversity curves

The diversity curves that represent the relative distribution of recruited reads at different nucleotide identities for a given viral reference genome in a virome informs about the structure and (micro)-diversity of a particular viral population at the species and genus level. In general, for most vSAGs and reference virus isolates showed a unimodal pattern in the diversity curve with a recruitment peak of recruited read frequency near 90% of identity and no recruitment was observed below 75% of identity. To summarize, we propose a model based on our obtained diversity curves that is depicted in Supplementary Fig 10c:

1) In general, the more (micro-) diverse is a viral population, the lower is the height of the curve (value H), and the higher is the width of the curve (value W) (Supplementary Fig 10c). In contrast, in a scenario where an abundant virus has no viral relatives co-existing in the same population (no microdiversity), the pattern of its viral population structure would be a narrow sharp curve, such as the metagenomic contigs depicted in Fig. 6b.

2) Recruited reads with identity values around 95% or higher were likely from our reference vSAG and/or close viral relatives belonging mostly to the same population at species-level.

3) Recruited reads with identity values under the observed empirical peak around 90% are from viral relatives belonging mostly to the same population at the genus or sub-family levels.

As shown in Fig. 6a, single-virus genomic approach can uncover the reference genome of uncultured viral populations regardless of the accumulated microdiversity since the complexity in terms of genome reconstruction is simplified. For viromics, in

general (Fig. 6a), we have observed that the species-specific recruitment patterns for many of the most abundant assembled genomes (viral contigs) in their own *Tara* viromes lacked of microdiversity. We analyzed over 50 abundant viral species (Fig. 6a; for convenience only 12 are shown in that panel) obtained from *Tara dataset* in different oceanic regions, and overall, the obtained pattern suggested a lack of microdiversity in these viral species populations at the sampling site where they were generated. This likely means, as we demonstrated in our simulated viromes (Fig. 6c, Supplementary Fig 20), that the assembler resolved successfully the genome reconstruction only for those populations mostly when the microdiversity scenario was low and there was sufficient sequencing coverage to be assembled; in other words, overall fairly abundant in the viral community and very dominant within its population. In turn, for those highly microdiverse and diverse populations, despite they are abundant, the assembler yielded small genome fragments and a very partial reconstruction. In the case of the *Tara* expedition[32], where MOCAT assembler was used, all obtained diversity curves for assembled viral contigs that were abundant in the corresponding viral assemblages lacked of microdiversity, except in two viral contigs (22SUR_22922 and 64SUR_1238) where the observed species-specific recruitment pattern indicated low microdiversity. In our study, with our virome from Blanes, we have observed that with IDBA_UD and SPAdes assemblers, in some cases, they delivered viral contigs representing viral populations with moderate microdiversity. Thus, the selection of the metagenomic assembler could have a negative impact on the genomic reconstruction, biasing thus the biological conclusions. We suggest from our analyses, that SPAdes could outperform other programs in terms of resolving the genome reconstruction from microdiverse viral populations.

Finally, it is important to remark that nearly all diversity curves obtained for the tested reference viral isolates, fosmids, vSAGs and viruses found in single-cells for all studied viromes (Supplementary Fig 10) showed that viral populations in general tend to be structured accumulating diversity and microdiversity. Therefore, the fact of finding diversity curves lacking of microdiversity when a viral contig "X" is compared against its own virome "X", shows:

1) that virus "X" clearly bloomed in that specific virome "X" dominating its population over other viral relatives belonging to same population (e.g. kill the winner scenario)

2) the inability of the assembler in general to resolve the assembly from highly microdiverse and diverse viral populations regardless the abundance. In fact, for many cases where a particular viral contig in its own virome showed a diversity curve lacking of microdiversity (e.g. above case of virus "X"), when it was computed for other viromes (Y, Z, etc…), the curve revealed the existing microdiversity of that population, indicating likely that in these other virome samples, that particular virus "X" was not dominating the population. However, we hypothesize that from the later virome sample (virome Y or Z), where dominance of the virus X was not observed; likely the genome of virus X would not be reconstructed by assemblers such as MOCAT.

Supplementary Methods

Simulation of natural viromes with different degrees of microdiversity

Firstly, we selected the *Tara* virome MS022[7] from the Mediterranean Sea for our simulation as a model since we previously demonstrated by fragment recruitment and diversity curves the presence of the highly microdiverse population of vSAG 37-F6. It is worth noting that in a previous study[7], from this natural virome dataset, MOCAT assembler was unable to reconstruct the genome of virus vSAG 37-F6 despite its abundance. Later, with the same dataset, by using IDBA_UD, which in principle outperforms MOCAT assembler, combined with genome binning[11] failed on the genome reconstruction of virus 37-F6. From that *Tara* virome MS022 dataset, we subtracted the raw reads corresponding with 37-F6 virus population. For that, we mapped the whole *Tara* virome MS022 against reference virus vSAG 37-F6 and a total of 74,278 reads were removed from the dataset. Geneious bioinformatic program[18] was used to map and subtract the reads with the parameters previously used for fragment recruitment (identity >70% and mean coverage >90%). Supplementary Fig. 20d shows that no reads belonging to 37-F6 population remained in the dataset. The trimming tool Trimmomatic version 0.36 was used to ensure that all remained reads in the virome were in the paired-end format for the metagenomic assembly after removing reads corresponding to vSAG 37-F6 population. Then, taking the reference genome vSAG 37-F6, we simulated three scenarios with different populations, A, B and C with different degrees of microdiversity and diversity (Supplementary Fig. 20b). Population A has no microdiversity with two simulated genomes (genome of vSAG 37-F6 and a simulated genome 1 with >99.9% nucleotide identity) and only 20 SNPs of difference. Population B is a low microdiverse population with 5 simulated genomes with approximately ≥95% nucleotide genome identity along all genome including in the hypervariable genome island (Fig. 4 and Supplementary Fig. 14). This is likely a simplistic scenario since in many cases even close viral relatives have a large variability in the hypervariable genomic island[19]. Population C is a medium-high microdiverse population with 10 simulated genomes. Eight of which had approximately ≥90% nucleotide genome identity along all genome, except in the genomic island, where higher genetic variability was introduced among the simulated genomes with <50% nucleotide identity in that region. The global nucleotide identity value of 90% was taken from the empirical peak observed in the resulting diversity curves for the natural population of vSAG 37-F6 in *Tara* MS022 virome (Supplementary Fig. 10). The value of 50% of identity for the genomic island has been taken according to the recruitment plot obtained for vSAG 37-F6 in different viromes where very high variability was observed. In addition, existing data on the co-existence of several virus isolate strains with high global genome identity but high variability in the genomic islands are described[19]. The remaining two simulated genomes (no. 7 and 9) were genetically more distant with the rest of genomes, approximately 80% identity value. The genomes were simulated with the publicly available bioinformatic tool at the following link: http://www.bioinformatics.org/sms2/mutate_dna.html. Then, with these simulated genomes for each population and assuming equal abundance of each genome within the population, we generated approximately a total of 74,278 Illumina reads for each population by using the program Art[20] that can simulate the same Illumina error rate

for the HiSeq 2000 platform previously used to sequence the *Tara* virome dataset. The parameters used were art_illumina -ss HS20 -sam -p -l 100 -s 10 -o paired_dat. (Supplementary Fig. 20c). Those simulated reads from each one of the populations were merged with the *Tara* MS022 virome where reads of 37-F6 were removed (Supplementary Fig. 20d). So, three different *Tara* MS022 viromes were finally constructed with different and controlled degrees of microdiversity, (Supplementary Fig. 20e) in which the reference genomes forming that population were known. Finally, these three simulated natural viromes were assembled by IDBA_UD with the same parameters previously used (--mink 20 –maxk 100 –step 20 –min_contig 1000) and described for that virome reconstruction[11]. In addition, SPAdes[21] version 3.9 was used with the following parameters for metagenomic assembly: "metaspades.py -k 33,55,77,99". Obtained contigs were mapped against the simulated reference genomes for each one of the population with the following cut-off parameters: ≥95% of identity value and ≥80% of contig coverage.

Supplementary References

1. Brussaard, C. P. D. Optimization of Procedures for Counting Viruses by Flow Cytometry. *Appl. Environ. Microbiol.* **70,** 1506–1513 (2004).

2. Tennessen, K. *et al.* ProDeGe: a computational protocol for fully automated decontamination of genomes. *ISME J.* **10,** 269–272 (2015).

3. Mills, R., Rozanov, M., Lomsadze, A., Tatusova, T. & Borodovsky, M. Improving gene annotation of complete viral genomes. *Nucleic Acids Res.* **31,** 7041–7055 (2003).

4. Besemer, J. & Borodovsky, M. GeneMark: Web software for gene finding in prokaryotes, eukaryotes and viruses. *Nucleic Acids Res.* **33,** 451–454 (2005).

5. Mizuno, C. M., Ghai, R., Saghaï, A., López-García, P. & Rodriguez-Valera, F. Genomes of abundant and widespread viruses from the deep ocean. *MBio* **7,** e00805-16 (2016).

6. Marchler-Bauer, A. *et al.* CDD: a Conserved Domain Database for the functional annotation of proteins. *Nucleic Acids Res.* **39,** D225-9 (2011).

7. Brum, J. R. *et al.* Ocean plankton. Patterns and ecological drivers of ocean viral communities. *Science* **348,** 1261498 (2015).

8. Caro-quintero, A. & Konstantinidis, K. T. Bacterial species may exist, metagenomics reveal. *Environ. Microbiol.* **14,** 347–55 (2012).

9. Labonté, J. M. *et al.* Single-cell genomics-based analysis of virus-host interactions in marine surface bacterioplankton. *ISME J.* **9,** 2386–2399 (2015).

10. Mizuno, C. M., Rodriguez-Valera, F., Kimes, N. E. & Ghai, R. Expanding the marine virosphere using metagenomics. *PLoS Genet.* **9,** e1003987 (2013).

11. Roux, S. *et al.* Ecogenomics and potential biogeochemical impacts of globally abundant ocean viruses. *Nature* **537,** 689–693 (2016).

12. Brum, J. R. *et al.* Illuminating structural proteins in viral 'dark matter' with metaproteomics. *Proc. Natl. Acad. Sci. U. S. A.* **113,** 2436–2441 (2016).

13. Sowell, S. M. *et al.* Environmental proteomics of microbial plankton in a highly productive coastal upwelling system. *ISME J.* **5,** 856–65 (2011).

14. Zhao, Y. *et al.* Abundant SAR11 viruses in the ocean. *Nature* **494,** 357–360 (2013).

15. Hurwitz, B. L. & Sullivan, M. B. The Pacific Ocean Virome (POV): a marine viral metagenomic dataset and associated protein clusters for quantitative viral ecology.

PLoS One **8,** (2013).

16. Angly, F. E. *et al.* The marine viromes of four oceanic regions. *PLoS Biol.* **4,** e368 (2006).

17. Baym, M. *et al.* Inexpensive multiplexed library preparation for megabase-sized genomes. *PLoS One* **10,** 1–15 (2015).

18. Kearse, M. *et al.* Geneious Basic: an integrated and extendable desktop software platform for the organization and analysis of sequence data. *Bioinformatics* **28,** 1647–9 (2012).

19. Mizuno, C. M., Ghai, R. & Rodriguez-Valera, F. Evidence for metaviromic islands in marine phages. *Front. Microbiol.* **5,** (2014).

20. Huang, W., Li, L., Myers, J. R. & Marth, G. T. ART: a next-generation sequencing read simulator. *Bioinformatics* **28,** 593–4 (2012).

21. Bankevich, A. *et al.* SPAdes: a new genome assembly algorithm and its applications to single-cell sequencing. *J. Comput. Biol.* **19,** 455–77 (2012).